The Pennsylvania State University

The Graduate School

College of Engineering

KINETICS OF OZONE REACTION WITH LOW-MOLECULAR WEIGHT ANTIOXIDANTS AT PHYSIOLOGICALLY RELEVANT CONDITIONS

A Thesis in

Chemical Engineering

by

Sanaz Kermani

Submitted in Partial Fulfillment
of the Requirements
for the Degree of

Doctor of Philosophy

May 2007

The thesis of Sanaz Kermani was reviewed and approved* by the following:

James S. Ultman
Professor Emeritus of Chemical Engineering
Thesis Advisor
Co-Chair of Committee

Abdellaziz Ben-Jebria
Professor of Chemical Engineering
Co-Chair of Committee

Ali Borhan
Professor of Chemical Engineering

Michael Pishko
Distinguished Professor of Chemical Engineering

Anne M. Andrews
Assistant Professor of Molecular Toxicology

Andrew L. Zydney
Professor of Chemical Engineering
Head of the Department of Chemical Engineering

*Signatures are on file in the Graduate School

ABSTRACT

Ozone (O_3), a major component of photochemical smog is a highly reactive gas that causes a decrement in lung function and lung inflammation upon inhalation. Respiratory tract lining fluid (RTLF) contains natural antioxidants such as uric acid (UA), ascorbic acid (AH_2), and glutathione (GSH) that protect the underlying epithelium from toxic gases such as O_3. The purpose of this study was to better understand and quantify the reaction kinetics between O_3 and these antioxidants under conditions that are similar to those encountered when polluted air is inhaled into the respiratory system. To achieve this objective, we developed a semi-batch reactor in which a 300 to 800 ml/min flow of air containing 1-5 parts per million by volume (ppm) of O_3 contacted 3 ml of a well-stirred test solution. The concentration of O_3 at the outlet of the reactor and the concentration of antioxidant in the aqueous solution were measured at reaction times of 5, 10 and 15 minutes, allowing the simultaneous determination of O_3 absorbed and antioxidant consumed.

Data was collected on test solutions consisting of single-component, binary and ternary mixtures of 50-200 μM UA, AH_2 and GSH. Kinetic parameters were determined using a mathematical model in which the squared-error between the observed amounts of O_3 absorbed and antioxidant consumed and their simulated values was minimized. The results obtained in single-component solutions of the antioxidants indicated that: 1) mass transfer resistances in the gas and liquid phases were negligible; 2) the reaction of O_3 with UA or with AH_2 has a one-to-one (1:1) stoichiometry; 3) the reaction of O_3 with GSH has a 1:2.5 stoichiometry; and 4) the reactivity between O_3 and these antioxidants is

in the following order: UA ≈ AH_2 > GSH. The rate constants estimated from these data for O_3 reaction with UA, AH_2, and GSH were $5.8\times10^4\ M^{-1}\ sec^{-1}$, $5.5\times10^4\ M^{-1}\ sec^{-1}$ and $57.5\ M^{-0.75}\ sec^{-1}$, respectively. Comparing the previous studies with the current investigation indicates: 1) with the exception of one study, all the previously-reported rate constants of UA and AH_2 with O_3 are two to three orders of magnitude larger than our values; 2) all the reported data agree with our conclusion that the reaction of O_3 with UA or with AH_2 is first-order with respect to O_3, as well as the antioxidant; 3) our study is the only one that provides clear evidence of a non-first-order reaction between O_3 and GSH.

For binary and ternary mixtures of the antioxidants, we found that: 1) the consumption of UA and AH_2 are decreased in the presence of one another. Numerical simulations verified that this protective effect is mostly due to the competitive reaction of UA and AH_2 toward O_3; 2) both UA and AH_2 can attenuate the consumption of GSH in the binary mixtures whereas GSH does not have the same effect on UA and AH_2. It was necessary to employ an interaction parameter in the numerical simulation in order to account for this; and 3) the presence of UA and AH_2 simultaneously in the mixture also diminished GSH consumption.

We also studied the kinetics of reaction between O_3 and albumin. Concentrations of tryptophan residues in albumin ranged from 6 to 20 μM. By employing a procedure similar to the one used for the antioxidants we found a stoichiometry of 1.5:1.0 and an optimal rate constant of $1.22\times10^8\ M^{-1.5}\ sec^{-1}$ for reaction between O_3 and a tryptophan residue in albumin. The effectiveness of GSH for protecting tryptophan groups from O_3

oxidation was examined in binary solutions of GSH and albumin. The Concentrations of GSH in the solutions ranged from 0 to 200 μM, whereas equivalent tryptophan concentrations were varied from 0 to 20 μM. The results indicated that GSH and tryptophan groups can attenuate the consumption of one other. However, the changes in GSH consumption caused by tryptophan residues were not as drastic as the changes in tryptophan consumption caused by GSH. Therefore, GSH is more effective in protecting tryptophan residues in albumin from O_3 oxidation than tryptophan groups are in inhibiting GSH reaction.

Finally, we studied the reaction of O_3 with nasal lavage samples obtained from healthy human subjects. The results indicated that: 1) approximately 50% of the total O_3 absorption in nasal lavage is due to UA. This demonstrates that UA is an effective scavenger of ozone; and 2) half of the UA is spared by other substrates such as albumin and mucin that successfully compete for half of the O_3 with a non-unity stoichiometry.

TABLE OF CONTENTS

LIST OF FIGURES

LIST OF TABLES

ACKNOWLEDGEMENTS

I have many people to thank for all their help, guidance, and support during my graduate studies here at Penn State. First and foremost, I would like to thank my advisor, Dr. James S. Ultman for his guidance, patience, and support. I am extremely appreciative of all the time he spent discussing this research with me, helping me see things from new perspectives, reviewing my papers and dissertation drafts, and offering advice and encouragement that helped me overcome the many obstacles I encountered along the way. Without his support and wisdom, the completion of this work would not have been possible. It was an honor and a great experience to work for him.

I would also like to thank Dr. Aziz Ben-Jebria for his advice, support and insightful suggestions on how to improve this dissertation. His help and guidance have been invaluable. Additionally, I would like to thank Dr. Anne M. Andrews and Dr. Michael Pishko for serving on my committee and reviewing this thesis.

I would like to express my sincere gratitude to Dr. Ali Borhan for all his valuable guidance, help, and support throughout the past few years, and also for serving on my committee.

Special thanks to all my friends here at Penn state, especially Sharareh Zolghadr, Shamila Mokhtari, and Banafsheh Keshavarzi who made the last few years an enjoyable experience.

I would not be where I am today without the love and support of my family. To my mom and dad, Nasrin and Behrooz: thank you for your unconditional love, for giving so much of yourselves, for always believing in my abilities and for teaching me to strive

for the highest levels of excellence in all aspects of my life. To my sister and brother, Elnaz and Behnood: thanks for all your love and support.

Finally, my love and thanks to my husband, Reza, for his understanding and encouragement, and for always believing in me and being there for me. Thank you for your love, help, and support. Your patient love enabled me to complete this work. I dedicate this thesis to you.

Chapter 1

INTRODUCTION

Ozone (O_3) is an oxidative air pollutant formed in the troposphere mainly by the photochemical reaction of oxygen catalyzed by automobile emissions (Mudway and Kelly, 2000; Mustafa, 1990). O_3 is a highly reactive gas that is capable of oxidizing biological molecules such as lipids and proteins, both of which are critical components of cell membranes (Pryor, 1992; Krishna et al., 1996). Oxidative damage to membrane lipids via lipid peroxidation is widely recognized as a mechanism of O_3 toxicity in the lung (Mudway and Kelly, 2000; Mustafa, 1990). Fortunately, the conducting airways are lined by a protective thin layer of mucous that contains low molecular weight antioxidants including uric acid (UA), ascorbic acid (AH_2) and glutathione (GSH) (Cross et al., 1994; Van Der Vliet et al., 1999). This so-called Respiratory tract lining fluid (RTLF), which forms a barrier between the underlying cells and the external environment, is considered to be the first line of defense against toxic pollutants such as O_3 (Cross et al., 1992 and 1994). Therefore, understanding the nature of the RTLF interactions with O_3 is critical to elucidating the mechanisms governing the health effects of O_3 toxicity in humans.

There have been several previous studies of the individual reactivities of UA, AH_2 and GSH with O_3 (Giamalva et al., 1985, Kanofsky and Sima, 1995, Mudway et al., 1996, and 1999, Mudway and Kelly, 1998, Pryor et al., 1984, and Housley et al., 1995). These studies employed different types of reactors (i.e., interfacial exposure of an

antioxidant solution by an impinging ozonated air stream or by ozonated air bubbles; and rapid mixing of an O_3-containing water stream with an antioxidant solution) and various model solutions (i.e., pure antioxidant solutions, blood plasma, nasal lavage fluid, and broncho-alveolar lavage fluid). Most of these studies depended on the measurement of O_3 depletion alone to characterize reaction rates. Moreover, O_3 levels supplied to the reactors were far greater than those expected in the lung. The hierarchy of the observed reactivities of UA, AH_2 and GSH was not consistent among these studies.

The purpose of the present work was to better quantify the reaction between O_3 and biological substrates in RTLF under conditions that are similar to those encountered when polluted air is inhaled into the respiratory system. An interfacial reactor in which a flow of ozonated air continuously contacted a well-mixed substrate solution was developed. Because diffusion resistances were absent in both the gas and the liquid phases, we could apply a straightforward mathematical model to obtain the reaction stoichiometry and rate constant from dynamic measurements of O_3 and substrate concentrations. The specific aims of this work were to use the interfacial reactor system and the mathematical model to:

1. Measure the reaction kinetics of O_3 with single antioxidant solutions of UA, AH_2, and GSH.
2. Study the interaction of these three antioxidants in binary and ternary solutions with O_3.
3. Quantify the kinetics of O_3 reaction with tryptophan residues in albumin and observe the effectiveness of GSH in sparing this amino acid from oxidation by O_3.

4. Determine what kinetic information can be obtained by studying a biological sample -nasal lavage- in the interfacial reactor.

The thesis is structured in the following way. Chapter 2 provides background information relevant to the research to be presented. Chapter 3 describes the interfacial reaction system, as well as the assays employed to quantify the substrate concentrations. In Chapter 4, the mathematical model and associated numerical algorithms employed to predict the kinetic parameters are presented. Chapter 5 describes the experimental data and mathematical simulations when O_3 reacts with either UA, AH_2 or GSH. In Chapter 6, interaction effects in mixtures of these three antioxidants are presented. Kinetic parameters of O_3 reaction with tryptophan, as well as the effectiveness of GSH in protecting tryptophan against oxidation caused by O_3 are presented in Chapter 7. Chapter 8 describes the kinetic information obtained from experiments with samples of nasal washings. Finally, a summary of the results from these studies, as well as suggestions for future work are presented in Chapter 9.

Chapter 2

BACKGROUND

2.1 Introduction

Ozone (O_3) is a highly reactive, poorly water soluble gas and is the major oxidant present in photochemical smog. O_3 also occurs as a natural component of the atmosphere. While it is a source of protection in the upper atmosphere (stratosphere), O_3 is a health risk when it is present in the lower atmosphere (troposphere) (Mudway and Kelly, 2000). The "ozone layer" located in the stratosphere, which lies between 10 and 50 kilometers above the surface of the earth, inhibits harmful ultraviolet radiation from reaching the surface of the earth, and thus prevents adverse effects such as skin cancer and suppression of immune response on human health (Mustafa, 1990). O_3 present within the lower troposphere, located between ground level and 10 km above the surface of the earth, is a secondary air pollutant formed through a complex photochemical reaction sequence involving primary pollutants--nitrogen dioxide (NO_2) and unburned hydrocarbons—and sunlight (Equation **2.1**) (Lippmann, 1991; and Wright et al., 1990).

$$\begin{aligned} NO_2 &\xrightarrow{\text{uv light}} NO + O^{\bullet} \\ O^{\bullet} + O_2 &\rightarrow O_3 \\ 2NO + O_2 &\xrightarrow{\text{hydrocarbons}} 2NO_2 \end{aligned} \qquad (\mathbf{2.1})$$

In contrast to stratospheric O_3, humans are directly in contact with tropospheric O_3 that causes deleterious responses and injury when inhaled (Mudway and Kelly, 2000).

A small proportion of protective stratospheric ozone reaches the earth's surface, but the majority of tropospheric O_3 arises from photochemical reactions dependent on pollutants from vehicle emissions, weather conditions, and on the strength of sun's radiation (Mudway and Kelly, 2000). Baseline concentrations of O_3 occurring naturally in the troposphere fluctuate between 20 and 40 parts per billion (ppb) depending on seasonal and geographical factors. During the summer, due to the increase in the intensity of the sun's radiation, this level can be elevated to 200 ppb (Mudway and Kelly, 2000; Mustafa, 1990). The United States Environmental Protection Agency (EPA) has classified O_3 as a criteria pollutant and has established a National Ambient Air Quality Standard (NAAQS) of 0.12 parts per million (ppm) averaged over a period of one hour, not to be exceeded more than three times in 3 years (Committee of the Environmental and Occupational Health Assembly of the American Thoracic Society, 1996). However, environmental O_3 levels in urban areas frequently exceed this limit. In southern California, O_3 levels remain at 0.1-0.2 ppm almost year-round, and in the summer, the levels reach 0.3-0.4 ppm. In other US cities, the levels of O_3 can reach 0.1-0.3 ppm frequently (Mustafa, 1990).

O_3 is a highly reactive gas that is capable of oxidizing biological molecules such as lipids and proteins, both of which are critical components of cell membranes (Pryor, 1992; Krishna et al., 1996). Consequently, O_3 has been found to have adverse health effects when inhaled. Short-term exposure of humans to ozone result in acute respiratory symptoms including coughing, shortness of breath, nose and throat irritation, discomfort

or pain upon breathing deeply, lung function impairment, airway inflammation, as well as tissue injury with altered airway permeability (Krishna, et al; 1996; Mudway and Kelly,2000).

It is becoming clear that there are long-term chronic consequences of O_3 exposure in the severity of lung disease and in lung development during childhood. In 1997, Devlin and co-workers suggested that long-term human exposure to O_3 could result in sustained lung function decrements (Devlin et al., 1997). An intermittent exposure of 7-month-old male monkeys to 0.25 ppm O_3 for 18 months resulted in lung disease caused by obliterative bronchiolitis (Tyler, et al., 1988). Lung growth was also reported to be abnormal. Nasal tissue damage has been detected in people who are exposed daily to high levels of O_3 (up to 300 ppb) in Mexico City (Valverde et al., 1997). A study on 520 freshmen at Yale University who never smoked, demonstrated that living for 4 or more years in regions of the country with high levels of ozone and related copollutants is associated with diminished lung function and more frequent reports of respiratory symptoms (Galizia and Kinney, 1999). Furthermore, Frischer and colleagues (1999) followed a cohort of 1,150 primary school children for 3 years in nine regions of Austria with contrasting pollution levels to investigate the long-term effects of ambient ozone. Children were selected because they are considered to be at higher risk than adults to possible damage caused by air pollution, since they spend more time outdoors, are more active and their growing lungs might be more susceptible. Their findings indicated that O_3 might negatively influence lung function growth. Thus, ozone would constitute a risk factor for premature respiratory morbidity later in life (Frischer et al., 1999).

It is generally believed that the biological damage produced by O_3 is imputable to its ability to cause oxidative destruction of biomolecules (Mustafa, 1990). Although O_3, is not a radical species itself (O — O ═ O), many of its toxic effects are mediated through free radical reactions. This is attained either directly by the oxidation of biomolecules to give classical radical species such as hydroxyl radical ($^{\bullet}OH$), or by driving radical-dependent production of cytotoxic, non-radical species such as aldehydes and ozonides (Kelly et al., 1995; Mustafa, 1990; Pryor, 1994).

2.2 Respiratory Tract Lining Fluid (RTLF)

Because inhalation is the main route by which air pollutants enter the body, the respiratory system is the first region that comes in contact with inspired O_3. The surface of the respiratory tract is lined with a heterogeneous thin aqueous layer, the respiratory tract lining fluid (RTLF), which extends from the nasal cavity to the alveoli. RTLF forms a barrier between the underlying cells and the external environment, and therefore, is considered as a first line of defense against toxic gases such as O_3 and NO_2.

The RTLF in conducting airways is composed of two layers, the surface mucus (or gel) layer and a deeper aqueous (or serous) sol layer in which the base of the cilia is located (Kaliner, 1991; Hatch, 1992). The gel layer is 5 to 10 μm deep, composed of products of the mucous glands and goblet cells, and rides on the tips of the cilia (Kaulbach et al., 1993). Particles can be trapped in the gel layer and transported by mucociliary action to the posterior pharynx and then swallowed (Kaliner, 1991). The sol layer, which is a watery fluid bathing the cilia is 5 to 8 μm deep and originates from

serous glands or transudates from the cells lining the airways (Kaliner, 1991; Kaulbach et al., 1993). RTLF components are heterogeneously distributed between these two layers (Hatch, 1992).

Different regions of the respiratory tract have different layer thicknesses. For example, the thickness of RTLF in the upper respiratory tract ranges from 1-10 μm compared to 0.2-0.5 μm in the alveolar regions (Cross et al., 1994). Table **2-1** compares the different layer thicknesses in different regions of the respiratory tract.

Table **2-1**: Human RTLF's Thickness. Reproduced from Cross et al., 1994

region	Thickness (μm)	Surface area (cm^2)	Volume (ml)
Nasal	5-10	180	0.15
Airways	1-10	4500	3.5
Alveoli	0.2-0.5	885000	9

The uptake of O_3 is governed directly by reactions with substrates present in the RTLF, a process termed "reactive absorption" by Langford et al. (1995).

Several kinds of substrates present in the RTLF can react with O_3, including:

- **Low molecular weight antioxidants** such as uric acid (UA), ascorbic acid or vitamin C (AH_2), and reduced glutathione (GSH) (Cross et. al, 1994; Hatch, 1992).

- **Proteins** such as albumin, cerruloplasmin, transferrin, lysozyme, and lactorferrin (Davis and Pacht, 1991; Hatch, 1992)
- **Lipids:** Lipids represent 20% of the solids found in tracheobronchial surface layer. The major phospholipids present in the RTLF are phosphatidylcholine, phosphatidylglycerol, and phosphatidylethanoalmine, where phosphatidylcholine is the principal lipid (Pryor et al., 1995a, 1995b). Palmitoleic, oleic, linoleic, and arachidonic acids are the unsaturated fatty acid groups (UFA) present in the phospholipids. UFA's are a primary target for O_3 oxidation. They react with O_3 via a Criegee mechanism in which O_3 adds to a carbon-carbon double bond, yielding aldehydes, hydroxyhydroperoxides, and Criegee ozonide (Pryor et al., 1990; Pryor, 1994).
- **High molecular weight glycoconjugates (HMG)** such as mucus glycoproteins mainly mucin and proteoglycans. HMGs are the major contributors to the high viscosity and stringy, gel-like characteristic of mucus (Hatch, 1992). Mucins have a molecular weight of 200,000 to 400,000 Da and are composed of 70-80% carbohydrate, 20% protein, and 1-2% sulfate (Kaliner, 1991). Mucins effectively scavenge hydroxyl radial, hence, may represent a major antioxidant in the upper RTLF (Cross et al., 1994).

There are differences in antioxidant concentrations between different regions of the respiratory tract, as illustrated in Table **2-2**. It can be observed that uric acid is by far the most predominant antioxidant in the upper RTLF. Antioxidant compositions in RTLF have not been well characterized, because they are obtained from nasal and bronchoalveolar lavage (NL and BAL), which produces a dilution of the RTLFs that is

not precisely known (Cross et al., 1994). Assuming that urea diffuses so rapidly that its concentration in blood and RTLF is identical, researchers have estimated the dilution factor as the ratio of the urea concentrations in blood and in lavage. These estimates range between 10 and 100 (Van der Vliet et al., 1999; Santiago, 2001).

Oxidative damage to proteins and membrane lipids are widely recognized as a mechanism of O_3 toxicity in the lung (Mudway and Kelly, 2000; Mustafa, 1990; Pryor, 1992). As mentioned before, these toxic effects are produced through protein oxidation and lipid peroxidation directly and/or by free radical chain reactions. Antioxidants can limit cellular injury by offering protection against free radical formation by preventing the propagation of chain reactions. Figure **2-1** shows the mechanism of O_3 toxicity in the respiratory system (Kelly et al., 1995).

Table **2-2**: Concentrations (μM) of Substrates in the RTLF Within the Respiratory Tract. Source: Mudway and Kelly, 2000, except *: Source: Cross et al., 1994.

	Nasal RTLF	Proximal RTLF	Distal RTLF
Uric Acid	100-400	100-300	150-300
Ascorbic Acid	10-50	20-45	10-35
Glutathione	5-10	50-200	70-225
Albumin-SH*	10	No data	70

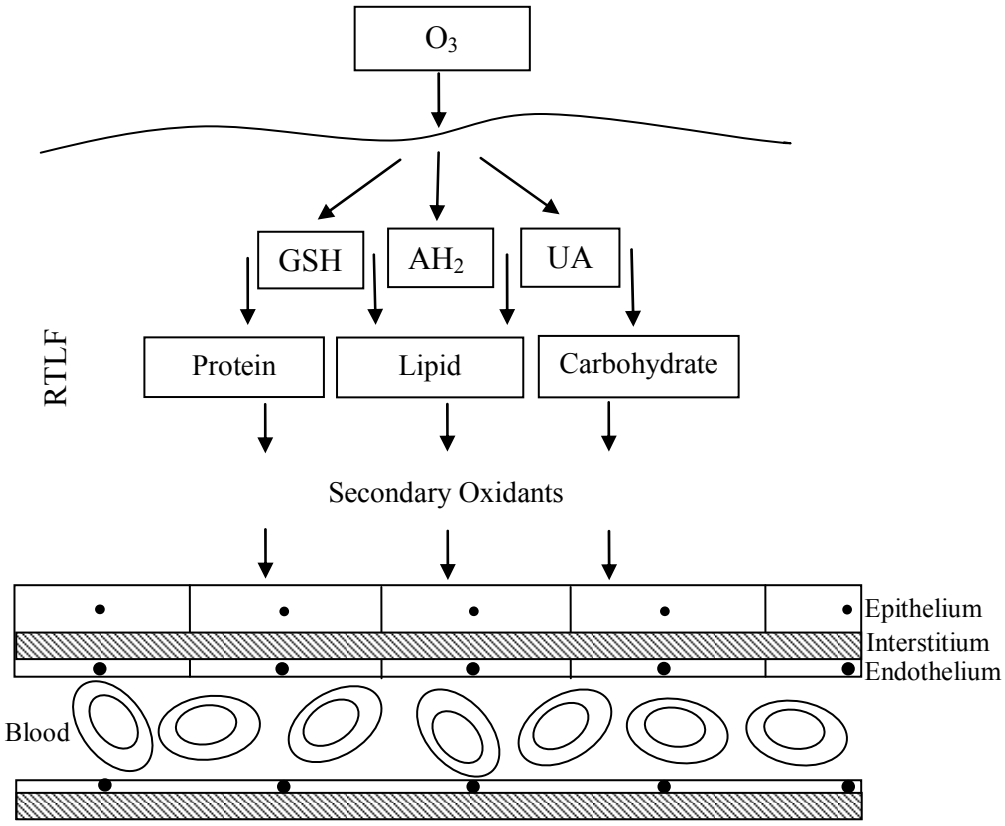

Figure **2-1**: Proposed Mechanism of O_3 Toxicity in the Respiratory System. (Adopted from Kelly et al., 1995)

2.2.1 Uric Acid

Uric acid (UA) is a water-soluble compound with a molecular weight of 168.1 Da. It is exclusively derived from adenine- and guanine- based purine compounds (Becker, 1993). UA is produced by the oxidation of hypoxanthine and xanthine by xanthine oxidase and dehydrogenase enzymes (Halliwell, 1996). In contrast to most mammals that excrete allantoin and urea as the major nitrogen-containing metabolites of purines, uric acid is an end-product of purine metabolism in man. This is due to the fact that the enzyme uricase (urate oxidase), which is responsible for transforming uric acid to allantoin, is not expressed in humans (Becker, 1993). Although the liver appears to be the major site of uric acid formation in man, because xanthine oxidase activity has been detected in the mucosa of the small intestine, the kidney, heart, spleen, and skeletal muscle, it is likely that uric acid is also produced in tissues throughout the body and is available at many sites (Meadows and Smith, 1985).

Uric acid has been identified as a major antioxidant in the upper RTLF (Peden et al., 1990, 1993). Peden et al. (1990) demonstrated that uric acid in the upper airways is derived, at least in part from glandular secretion. There is considerable evidence for a protective action of urate against oxidative damage of enzymes, lipids, nucleobases, and cells in vitro. Uric acid attenuates oxidation of plasma lipids and unsaturated fatty acids (linolenic acid) caused by O_3 (Cross et al., 1992; Meadows et al., 1986). Urate protects erythrocyte ghosts against lipid peroxidation and peroxidative damage leading to lysis (Ames et al., 1981). Meadows and Smith (1986) investigated the effect of uric acid on nucleobase degradation caused by O_3. Their findings demonstrate that uric acid protects

thymine, guanine, and uracil from degradation by O_3, with allantoin and urea being identified as degradation products.

The antioxidant properties of uric acid discussed above involve urate oxidation via classical scavenger mechanisms. Earlier studies reported that uric acid is oxidized to products such as allantoin, urea, oxonic acid, and parabonic acid, where allantoin is the prevalent product in the scavenging of hydroxyl radicals ($^{\bullet}OH$) (Ames et al,. 1981; Kaur and Halliwell, 1990; Howell and Wyngaarden, 1960), singlet molelcular oxygen (Ames et al,. 1981), and oxo-haem oxidant (Howell and Wyngaarden, 1960; Ames et al,. 1981). The structure of uric acid and its oxidation products are shown in Figure **2-2** . Because in neutral media uric acid has a single negative charge (Simic and Jovanovic, 1989), the reaction of these radicals ($R^{\bullet}$) with the monoanion urate (UH^{-}) would follow the general electron transfer as:

$$UH^{-} + R^{\bullet} \rightarrow U^{\bullet -} + RH \qquad (\mathbf{2.2})$$

The loss of an electron from uric acid was assumed to take place at O^8 because this hydroxy group was the strongest acid (Simic and Jovanovic, 1989). Alternatively, Maples and Mason (1988) placed the radical character at N^9 and N^7 (Figure **2-3**).

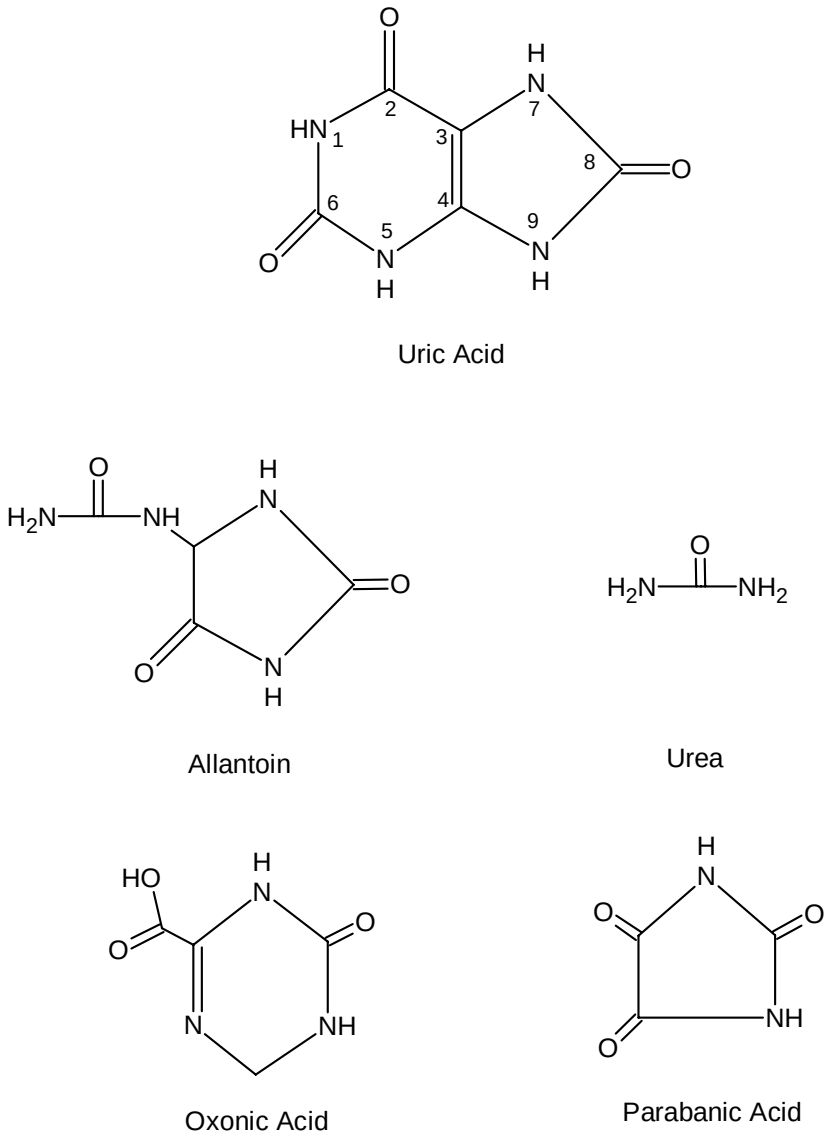

Figure **2-2**: Structure of Uric Acid and its Oxidation Products

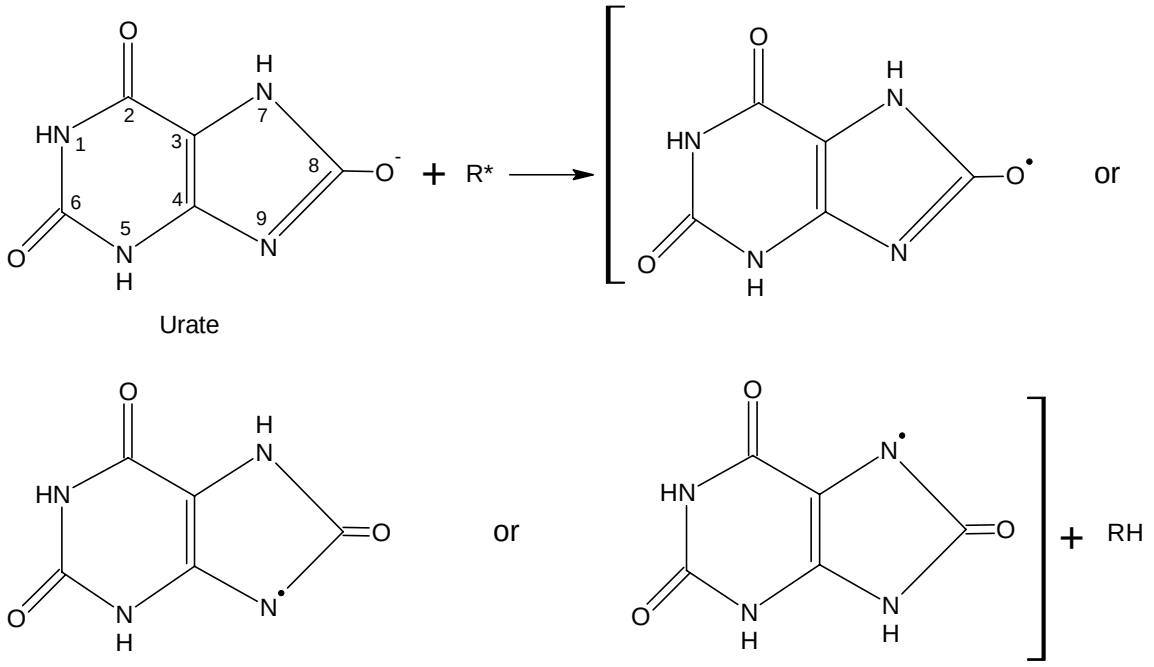

Figure **2-3**: Formation of Urate Radical

The radical form of uric acid decays to stable inert molecular products such as allantoin (Ames et al., 1981). The urate radical is relatively stable compared to oxygen radicals such as ($^{\bullet}$OH), and does not react with oxygen (Simic and Jovanovic, 1989). This accounts for the radical chain-breaking action of urate. Howell and Wyngaarden (1960) showed that uric acid scavenges hydroxyl radicals produced by hydrogen peroxide and suggested that oxidation of uric acid is a two-electron, one proton oxidation, in which the urate radical obtained via dehydrohgenation, is then hydroxylated by a hydroxyl radical. The intermediate is then hydrated with one molecule of water and rearranges to form allantoin.

Previous studies in which pure uric acid or plasma and bronchoalveolar lavage fluids were exposed to O_3, indicated that uric acid is an important scavenger of O_3 and it is consumed in a dose and time dependent manner by O_3 (Cross et al., 1992; Mudway and Kelly, 1998; Mudway et al., 1996).

Uric acid ozonation products have not been investigated in detail. As mentioned earlier, Meadows and Smith (1986) studied protective effects of uric acid on nucleobases from O_3 oxidation and reported that allantoin and urea are the major products of uric acid ozonation. However, the exact mechanism by which uric acid ozonation occurs has not been determined. The decomposition of O_3 in aqueous solutions with pH above 5 or 6 is known to produce hydroxyl radical (Byvoet et al., 1995). Therefore, uric acid can react directly with O_3, or it can react with hydroxyl radicals produced from decomposition of O_3 in aqueous solution.

2.2.2 Ascorbic Acid

Ascorbic acid (vitamin C) is a white crystalline solid that is very soluble in water and has a molecular weight of 175.1 Da. Plants and many animals synthesize ascorbic acid from glucose, but humans, other primates, and guinea pigs are unable to synthesize ascorbate and hence, require it to be present in their diets as vitamin C (Brown and Jones, 1996). As a consequence of its high solubility in water, ascorbic acid is widely distributed throughout the aqueous compartments of the body (Kelly et al., 2003). As this antioxidant is freely diffusible, dietary intake of vitamin C may play an important role in dictating RTLF ascorbic acid concentrations (Kelly et al., 2003). At physiological pH of 7.4, 99.9% of ascorbic acid is present as the monoanion (Buettner and Jurkiewicz, 1996). The most striking chemical property of ascorbate is its ability to act as a reducing agent. It can scavenge a variety of free radicals and oxidants, including hydrogen peroxide, hypochlorous acid, superoxide and peroxide and hydroxyl radicals, and singlet oxygen (Mudway and Kelly, 2000; Buettner and Jurkiewicz, 1996). During this antioxidant action, ascorbate readily undergoes two consecutive, reversible, one electron oxidation to form dehydroascorbate, with the intermediate formation of semidehydroascorbate radical (Buettner and Jurkiewicz, 1996). The fact that the intermediate radical is relatively unrecative, makes ascorbate a superior biological donor antioxidant (Mudway and Kelly, 2000). Figure **2-4** shows structures of ascorbic acid and its oxidation products.

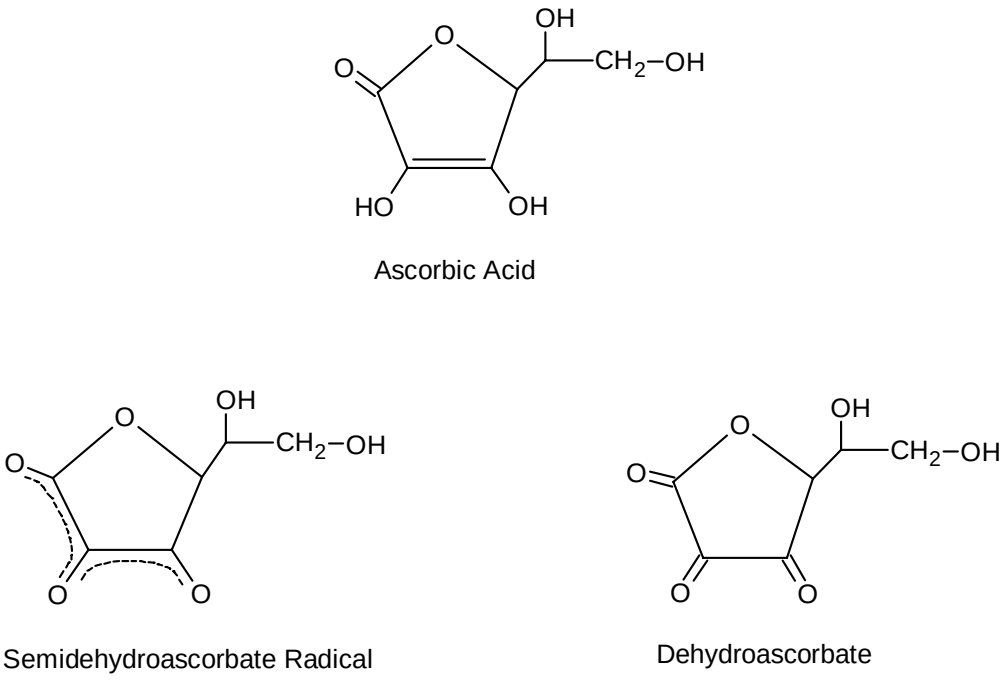

Figure **2-4**: Structures of Ascorbic Acid and its Oxidation Products.

In addition to a direct scavenging action, ascorbate also acts indirectly to prevent lipid peroxidation through its reaction with membrane tocopherol (vitamin E) (Mudway and Kelly, 2000). Perhaps this involvement in the electron transfer-mediated recovery of vitamin E radical (Equation **2.3**), thereby restoring the scavenging ability of this important lipid antioxidant is the most salient feature of ascorbic acid in connection with its antioxidant activity (Packer et al., 1979).

$$\alpha T - O^{\bullet} + AH^{-} \rightarrow \alpha T - OH + A^{\bullet -} \qquad (\mathbf{2.3})$$

where $\alpha T - O^{\bullet}$, AH^{-}, $\alpha T - OH$, and $A^{\bullet -}$ are vitamin E radical, ascorbate, vitamin E, and ascorbate radical, respectively. This synergistic action of ascorbate that has been clearly demonstrated in vitro has not been reported in vivo (Mudway and Kelly, 2000).

Both in vivo and in vitro studies with human lavage fluid have shown that ascorbic acid is an important scavenger of O_3 and it is consumed in a O_3 concentration and time-dependent manner (Kelly et al., 1995).

Decreased ascorbic acid levels in cigarette smokers appear to be mainly caused by increased RTLF ascorbic acid utilization subsequent to its oxidation by oxidants contained in the cigarette smoke (Lykkesfeldt et al., 2000). This was compensated by moderate supplementation. Ascorbic acid was also significantly reduced in nonsmokers regularly exposed to environmental tobacco smoke. This observation supports an antioxidant role of ascorbic acid in the RTLF.

2.2.3 Glutathione

Glutathione (γ-L-glutamyl, L-cysteinglycine), is a tripeptide of the amino acids glutamate, cysteine, and glycine (Shaw, 1998). It is a white, crystalline solid with a molecular weight of 307.3 Da that dissolves easily in water. The glutathione molecule has two peptide bonds, two carboxylic acid groups, one thiol group, and one amino group (Shaw, 1998). The high water solubility of GSH is due to the large number of hydrophilic functional groups combined with a low molecular weight. Glutathione is a submajor component of all cells and is almost always the major non-protein thiol compound present in cells (Kosower, 1976). This biological antioxidant occurs in rather high concentrations (0.1-10 mM) in the cytosol of many types of cells (Larson, 1997). Prolonged failure to maintain a sufficient intracellular supply is detrimental to the survival of the cell (Kosower, 1976).

The thiol group (-SH) is the most important chemically reactive group present in the glutathione molecule (Kosower, 1976). Glutathione has a very important role in protection against free radical damage. Like other antioxidants, glutathione is readily oxidized. It reacts rapidly with many one-electron oxidants including hydroxyl radical, peroxide, superoxide, hypochlorous acid, and singlet oxygen to form thiyl radical ($GS^{\bullet}$), which can subsequently be converted to oxidized glutathione (GSSG) (Larson, 1997) . GSH and GSSG are interconvertible (Shaw, 1998). The structure of glutathione and its oxidization product oxidized glutathione are shown in Figure **2-5**. The reaction of glutathione (GSH) with free radicals ($R^{\bullet}$) follows a general electron transfer as:

$$GSH + R^{\bullet} \rightarrow GS^{\bullet} + RH \qquad (\mathbf{2.4})$$

$$2GS^{\bullet} \rightarrow GSSG \qquad (\mathbf{2.5})$$

Due to their reduction potentials, thiyl radicals can be reduced by ascorbate and urate as follows (Ford et al., 2002; Buettner and Jurkiewicz, 1996):

$$\begin{aligned} UH^{-} + GS^{\bullet} &\rightarrow U^{\bullet -} + GSH \\ AH^{-} + GS^{\bullet} &\rightarrow A^{\bullet -} + GSH \end{aligned} \qquad (\mathbf{2.6})$$

RTLF from the lower airways contains high concentrations of reduced glutathione, which is approximately 100 times that present in plasma (Kelly and Mudway, 2003). Studies with pure glutathione solution and human lavage fluid have shown that glutathione is an important scavenger of O_3 (Mudway et al., 1996; Mudway and Kelly, 1998; Kanofsky and Sima, 1995). O_3 reacts with glutathione, oxidizing it to $GS^{\bullet}$ and subsequently GSSG, through a radical transfer process, the details of which are not fully understood (Kelly et al., 1995). Several conditions connected to inflammatory airways responses such as cigarette smoking, asthma, and experimental exposure to O_3, are associated with high levels of RTLF glutathione. Increased glutathione has been interpreted as an adaptive response to chronic oxidant stress (Cross et al., 1994; Davis and Pacht, 1991).

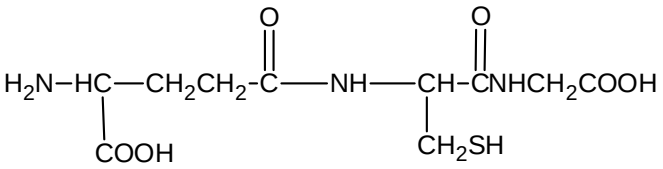

GSH

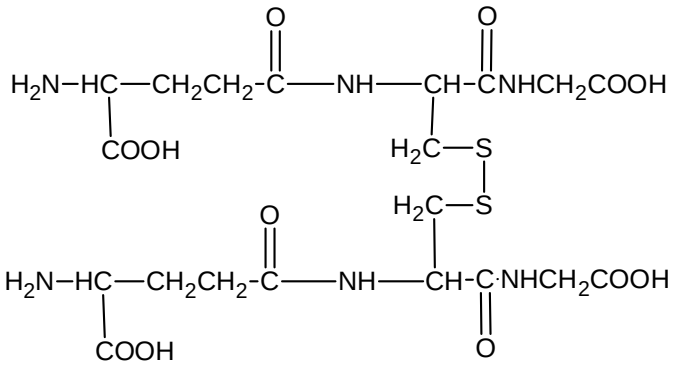

GSSG

Figure **2-5**: Structures of Glutathione and its Oxidation Product Oxidized Glutathione.

2.2.4 Albumin

Albumin, with a molecular weight of 68,000 Da, is the principle protein constituent in both upper and lower RTLF, comprising about 50% of total protein in this fluid (Davis and Pacht, 1991, Hatch, 1992). The liver is the major site of albumin synthesis in the body (Hatch, 1992).

O_3 can react with many proteins including albumin. The reaction of O_3 with proteins is often evaluated by the loss of enzymatic or other functional activity of the protein (Pryor and Uppa, 1993; Mudway and Kelly, 2000). Proteins contain a variety of amino acid residues, and O_3 is particularly reactive towards a limited number of them including cysteine, tryptophan, methionine, tyrosine, and histidine (Pryor et al., 1984; Pryor and Uppa, 1993; Berlett et al., 1996; Kelly et al., 1995; Mudd et al., 1969). The basis of the damage that O_3 inflicts upon proteins is the result of its ability to directly or through free radical mediated reactions, oxidize a range of functional groups including sulphydryls, amines, alcohol, and aldehydes (Kelly ate al., 1995; Mudway and Kelly, 2000). The oxidation of proteins by O_3 can be determined by changes in the concentration and/or the appearance of products of a single amino acid residue (Pryor and Uppa, 1993).

Albumin contains two tryptophan residues per molecule (Berlett et al., 1996; Pryor and Uppa, 1993). Tryptophan is the only amino acid that contains an indole group (Figure **2-6**). The indole group of tryptophan was shown to be particularly susceptible to free radical and oxidative attack by a number of agents including ozone (Mudd et al., 1969). Goldstein and McDonagh (1975) demonstrated that a loss in cell membrane

protein fluorescence is a subtle parameter related to the effects of ozone in comparison to other known indicators of ozone-induced cell membrane toxicity. Native protein fluorescence is predominantly due to tryptophan content and in particular, to its indole group (Goldstein and McDonagh, 1975; Meiners et al., 1977).

Studies on the reaction of tryptophan with O_3 identified kynurenine and N-formylkynurenine as major reaction products (Dooley and Mudd, 1982; Knight and Mudd, 1984). Pryor and Uppa (1993) investigated the reaction of O_3 with tryptophan using a panel of 11 tryptophan containing proteins (albumin, carbonic anhydrase, β-casein, α-chymotrypsin, α-lactalbumin, β-lactoglobulin, lysozyme, papain, ribonuclease A, apotransferrin and trypsin) solubilized in reverse micelles. Their findings indicated that O_3 reacts directly with tryptophan via a Criegee ozonation mechanism in which all three oxygen atoms of O are incorporated (Figure **2-7**). Thus, the product was suggested to be Criegee ozonide and not N-formylkynurenine. Because these investigators detected only trace amounts of H_2O_2 (0.07 mol/mol tryptophan), which is neither destroyed nor consumed during the reaction, they suggested that it is more likely that intermediates III and IV convert to VII instead of V and VI. Although they have not investigated the chemical nature of the product, they suggested that during this process VII can also give rise to kynurenine (X).

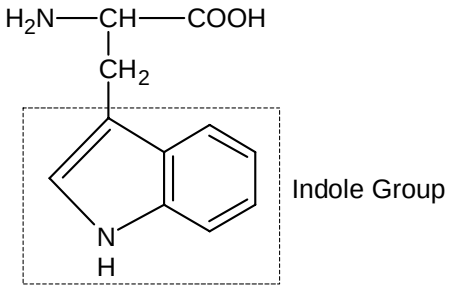

Figure **2-6**: Structure of Tryptophan Molecule

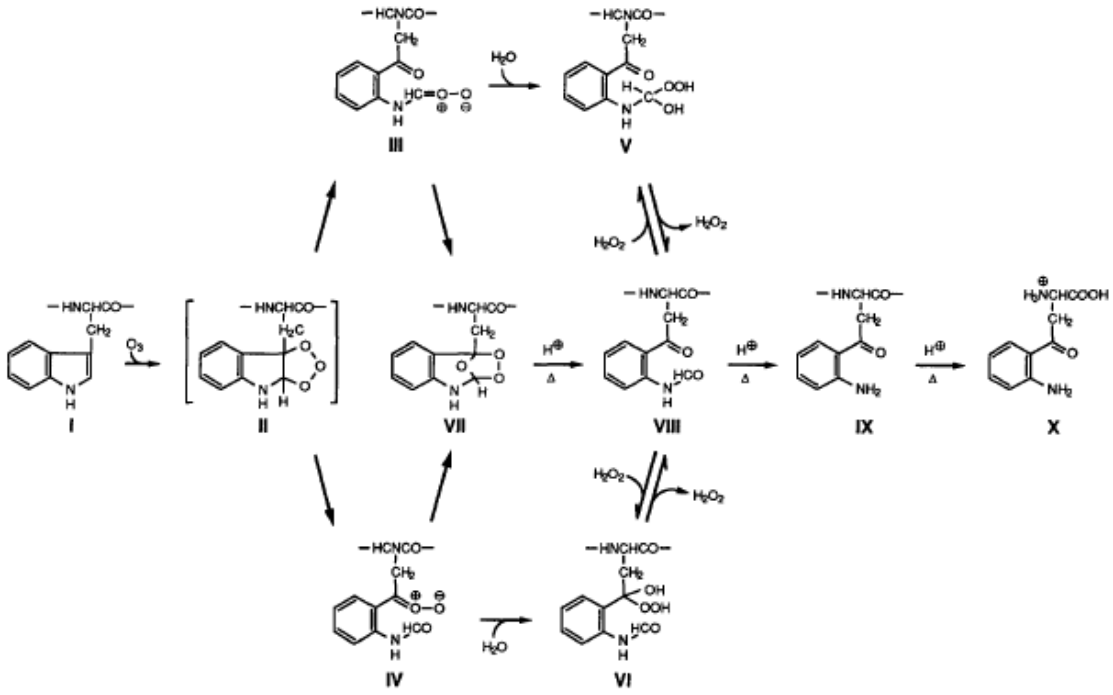

Figure **2-7**: Schematic Representation of Formation of Criegee Ozonides of Protein-Bound Tryptophan and Hydrogen Peroxide During Ozonation of Proteins and Occurrence of Kynurenine in Amino Acid Hydrolysates of Ozonide Proteins (Adopted from Pryor and Uppa, 1993)

2.3 Kinetics of Antioxidants Reaction with O_3

Due to ozone's high chemical reactivity with RTLF substrates and also due to its low aqueous solubility, it is unlikely that unreacted O_3 reaches the underlying epithelium (Pryor, 1992). This indicates that antioxidants in RTLF have a major role to protect the underlying cells against damage caused by ozone.

Several approaches have been taken to study the reaction of O_3 with uric acid, ascorbic acid, and glutathione (Giamalva et al., 1985, Kanofsky and Sima, 1995, Mudway et al., 1996, and 1999, Mudway and Kelly, 1998, Pryor et al., 1984, and Housley et al., 1995). These investigators were interested in determining the relative reactivity of antioxidants toward O_3, and evaluating the rate constants of the reactions between O_3 and these antioxidants. These studies employed different types of reactors (*i.e.*, interfacial exposure of an antioxidant solution by an impinging ozonated air stream or by ozonated air bubbles; and rapid mixing of an O_3-containing water stream with an antioxidant solution) and also various model solutions (*i.e.*, pure antioxidant solutions, blood plasma, nasal lavage fluid, and broncho-alveolar lavage fluid). The hierarchy of the observed reactivities of UA, AH_2 and GSH was not consistent among these studies. From the rate constants reported by Pryor et al. (1984) and Giamalva et al. (1985), a reaction hierarchy of GSH > AH_2 > UA was predicted. Such a hierarchy was not found however in models examined by Mudway and Kelly (1998) ($AH_2 \approx$ UA > GSH) and Kanofsky and Sima (1995) (AH_2> GSH). Table **2-3** summarizes the rate constants of O_3 reaction with uric acid, ascorbic acid, and glutathione that have been reported in the literature. The

factors that might have caused the inconsistencies in data in this table will be discussed in greater detail in the discussion sections of Chapters 5 to 8.

Table **2-3**: Reported Rate Constants of O_3 Reaction with UA, AH_2, and GSH.

k_r	UA	$1.18\times10^4\ M^{-1}s^{-1}$	---	$1.4\times10^6\ M^{-1}s^{-1}$	---
	AH_2	$1.36\times10^4\ M^{-1}s^{-1}$	$4.8\times10^7\ M^{-1}s^{-1}$	$6.0\times10^7\ M^{-1}s^{-1}$	---
	GSH	$4.94\ M^{-0.75}s^{-1}$	$2.5\times10^6\ M^{-1}s^{-1}$	---	$7.0\times10^8\ M^{-1}s^{-1}$
Reference		Mudway & Kelly , 1998*	Kanofsky& Sima, 1995	Giamalva, *et al.*, 1985	Pryor, *et al., 1984*
O_3 (ppm)		0.1-1.5	20-40	Extremely High	Extremely High
Antioxidant (μM)		200-400	5,000-100,000	Not Given	Not Given
Reactor Type		1 ml multiwell plates in a 5.6L chamber on an orbital shaker with 3 Lpm flow of ozonated air	Stagnant liquid contacted with ozonated air through an impinging jet.	Liquid-liquid reaction in stopped flow apparatus	Liquid-liquid reaction in stopped flow apparatus

* k_r values have been estimated from the data of Mudway and Kelly (Mudway and Kelly, 1998) (see APPENDIX E for details).

Chapter 3

EXPERIMENTAL METHODS

This chapter describes the experimental system developed to study the kinetic parameters of the reactions between ozone and biological substrates. Equipments and methods employed to determine substrate concentrations are also described.

3.1 Materials

UA (2, 6, 8- trihyroxy purine), GSH (L-glutathione reduced), 5, 5', 7, 7- indigo trisulfonic acid (ITS), albumin (from bovine serum), and sodium phosphate monobasic were purchased from Sigma Aldrich. AH_2 (L (+) ascorbic acid sodium salt) and potassium phosphate monobasic were purchased from Fluka and Fisher Scientific, respectively. Saline (Respiratory therapy solution, 0.9% sodium chloride inhalation solution) was purchased from Baxter.

3.2 Substrate Solutions

Solutions of UA, AH_2, GSH and albumin were prepared using physiological saline containing 0.02 M sodium phosphate buffer. The pH of the final solution was adjusted to 7.4 using 1 M solutions of hydrochloric acid and sodium hydroxide.

3.3 Substrate Assays

3.3.1 Quantitation of Uric Acid, Ascorbic Acid, and Glutathione Using HPLC

Antioxidant concentrations in aqueous solutions were determined using reversed phase-high performance liquid chromatography (Model HP 1100, Agilent Technologies) with a diode array detector (Model G1315A, Agilent Technologies, Palo Alto, CA) and an LC-18 column (Model 58230-U, 15 cm × 4.6 mm, 5 μ particle size, Supelco, Bellefonte, PA). A 0.2 M KH_2PO_4 solution adjusted to a pH of 2.1 was used as the mobile phase at a flow rate of 1 ml/min. Subsequent to injecting ten microliters of sample into the chromatographic system, chromatograms were recorded for up to 10 minutes. Each solution was sampled and analyzed in triplicate.

In HPLC, substrates in a sample are separated into bands based on their partitioning between a polar mobile phase (flowing buffer) and a non-polar stationary phase (column). Therefore, non-polar compounds are retained longer on the column compared to polar compounds, which have higher affinities for the polar mobile phase. Separated bands of the analytes exit the column and pass through the diode array detector, whose signal is recorded by a computer and displayed as absorbance. Figures **3-1** and **3-2** show the breakthrough curves and spectra, respectively, for UA (top), AH_2 (middle) and GSH (bottom) after injecting samples of single-components solutions.

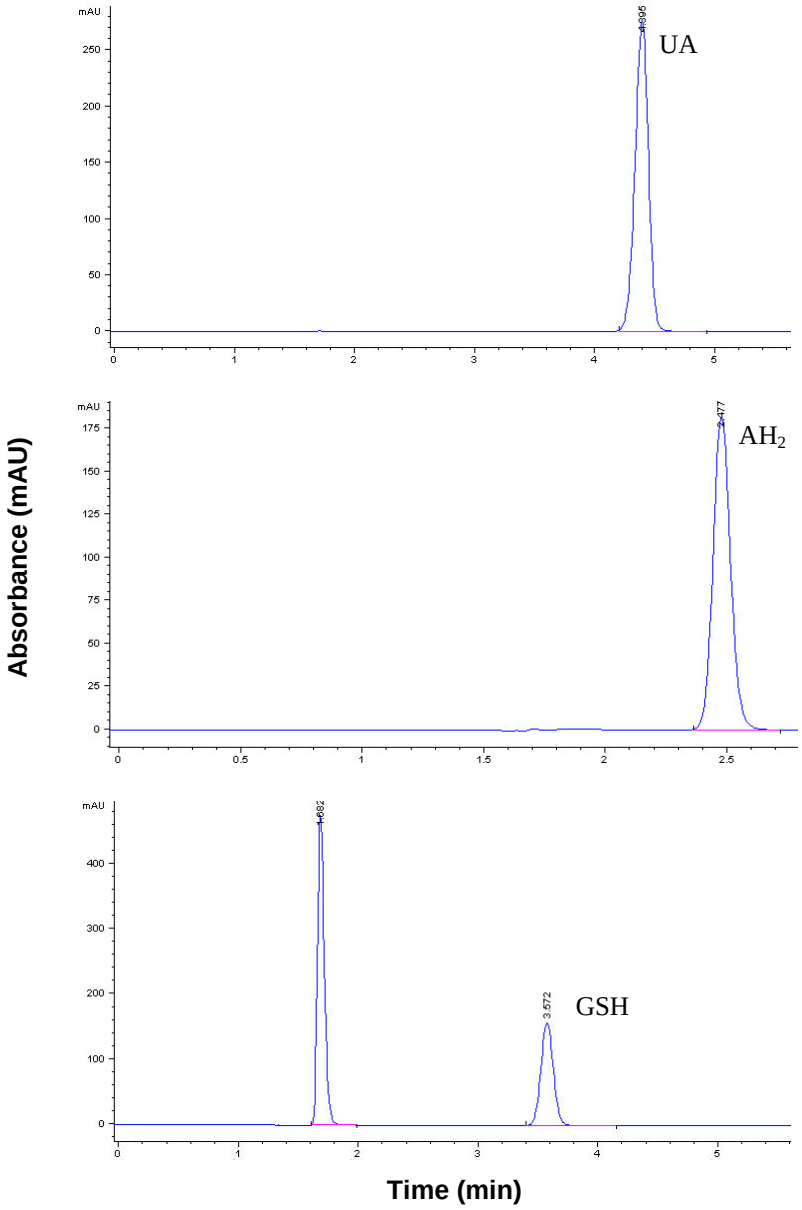

Figure **3-1**: Breakthrough Curves Obtained from the Diode Array Detector for Single-Components UA (top), AH_2 (middle) and GSH (bottom) Solutions.

Ten microliters of saline solution containing 200 µM of UA, AH_2 and GSH were injected into the HPLC. Retention times for UA, AH_2, and GSH were 4.395, 2.477, and 3.572 minutes, respectively.

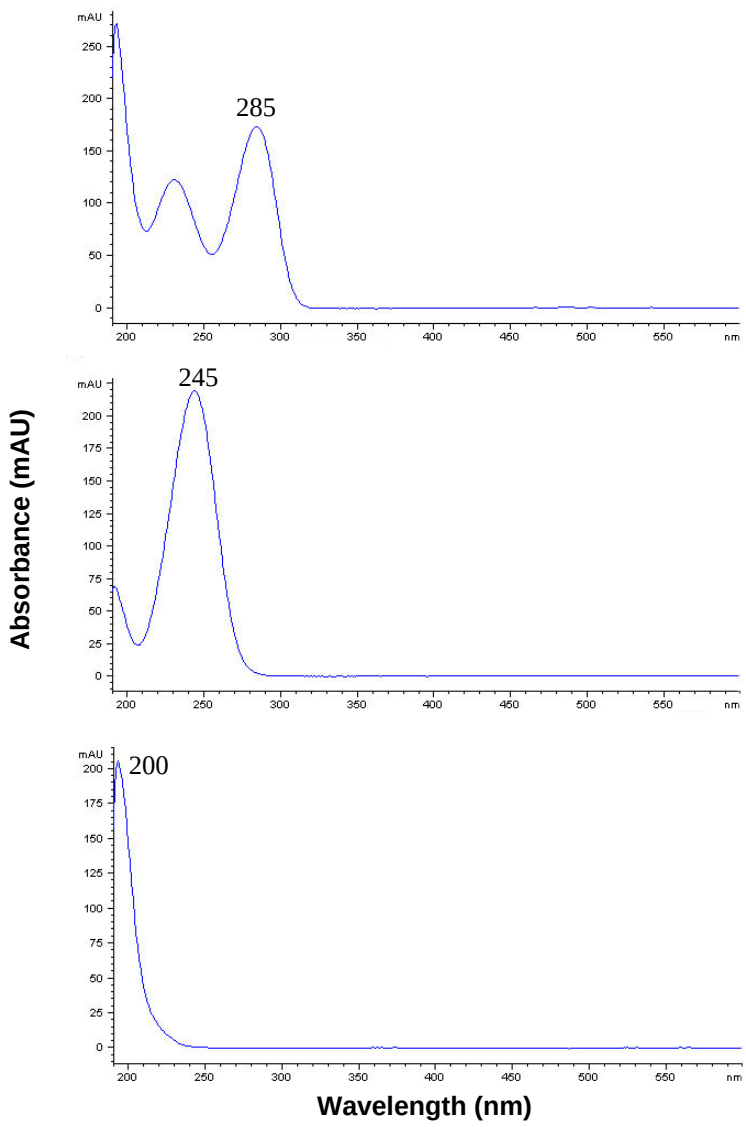

Figure **3-2**: Spectra of Absorption of UA (top), AH_2 (middle), and GSH (bottom).

The wavelengths of maximum absorption for each compound are indicated.

The peaks corresponding to UA, AH_2 and GSH were identified in binary and ternary solutions by comparing retention times and absorption spectra to those obtained from single-component solutions. Figure **3-3** shows the chromatograms obtained from binary solutions of UA and AH_2 (top), UA and GSH (middle), and AH_2 and GSH (bottom) using diode array detector. The identity of each peak is indicated in the chromatograms.

The area under the curve (AUC) of each peak is directly proportional to the concentration of given substances in the sample. Unknown concentrations of UA, AH_2, and GSH were determined from standard curves developed from the HPLC analyses of standard solutions. Each standard curve was constructed by obtaining the breakthrough curves of a series of single-component solutions containing known antioxidant concentrations from 0 to 200 μM. AUCs at the wavelength of maximum absorption (i.e., 285 nm for UA, 245 nm for AH, and 200 nm for GSH) were regressed against antioxidant concentrations, resulting in a linear relationship with $R^2>0.9999$ for each of three antioxidants. Figure **3-4** illustrates the representative standard curves for UA (top), AH_2 (middle) and GSH (bottom).

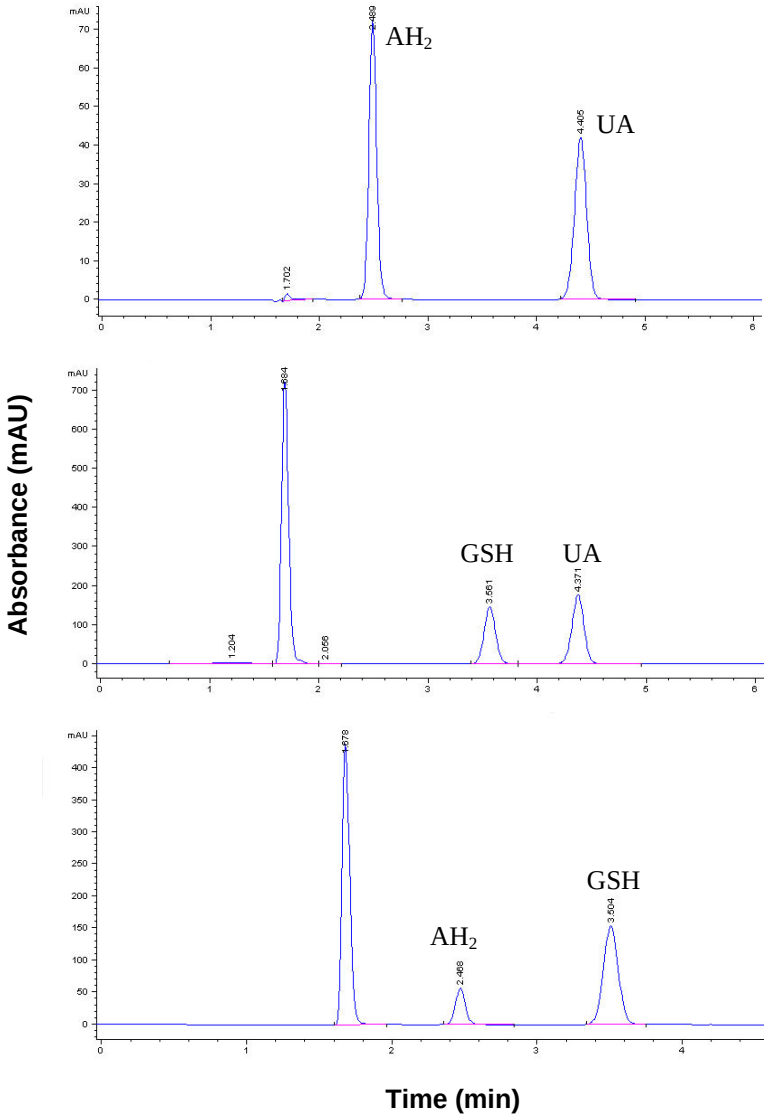

Figure **3-3**: Chromatograms of Binary Solutions Obtained from the Diode Array Detector for Binary Solutions of UA and AH_2 (top), UA and GSH (middle), and AH_2 and GSH (bottom).

The peaks corresponding to UA, AH_2 and GSH are identified.

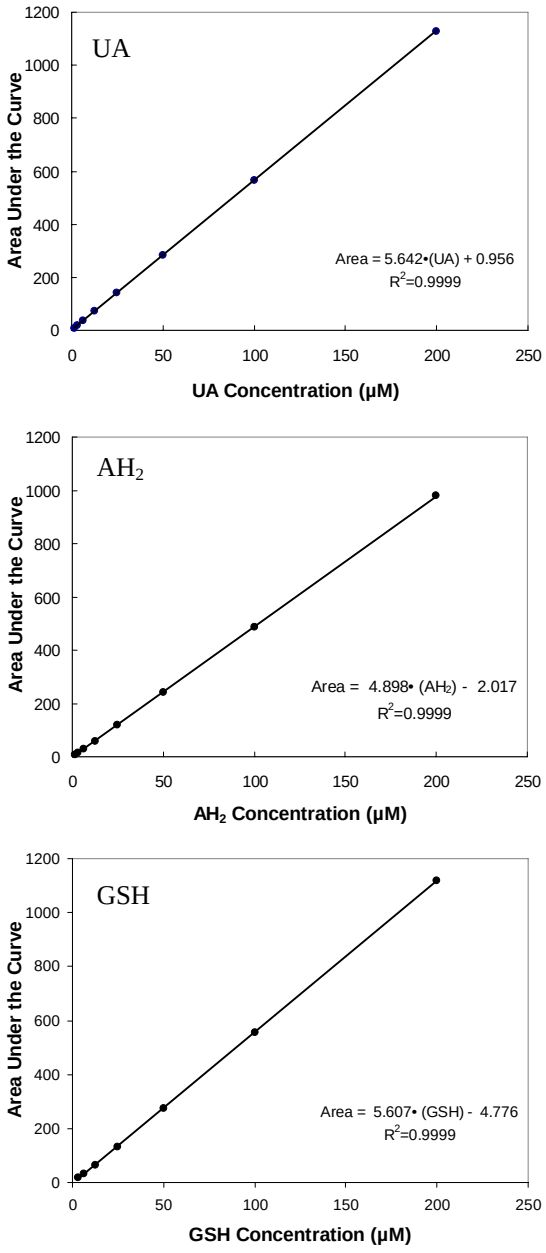

Figure **3-4**: Standard Curves for UA (top), AH_2 (middle), and GSH (bottom).

Each point represented in the graphs illustrates an average value from triplicate measurements.

3.3.2 Quantitation of Tryptophan (Albumin) Using Spectrofluorometry

Albumin contains two tryptophan residues per molecule (Berlett et al., 1996; Pryor and Uppa, 1993). Concentrations of albumin were determined by analyzing the native fluorescence of tryptophan using a spectro-fluorometer (Model SPEX Fluorolog-3, HORIBA JOBIN YVON). The spectro-fluorometer is an instrument that takes advantage of the fluorescent properties of some compounds to provide information regarding their concentration. The reported excitation peak of tryptophan is 280 nm and the emission peak is 330 nm. Under these conditions, fluorescence is predominantly due to the excitation of the indole group of tryptophan, an amino acid present in albumin (Goldstein and McDonagh, 1975). From a wavelength scan, the excitation and emission peaks on our instrument were established to be 280 nm and 343 nm, respectively. The intensity of the emission peak is directly proportional to the concentration of tryptophan in the sample.

Unknown concentrations of tryptophan in a sample were determined from a standard curve constructed from the fluorescence analyses of standard solutions. To construct a standard curve, 200 μL of an albumin solution containing a known tryptophan concentration from 0 to 20 μM was inserted into the cuvette (Cat. No: 16-10F-Q-10/z 15, Starna cells, Inc). The cuvette was then placed in the sampler shutter and the intensity of the fluorescence emission peak was determined. Figure **3-5** illustrates the standard curve with each data point representing the average of triplicate values and the line indicating a linear regression for which R^2>0.999. Buffered saline solution was used as the blank in these determinations.

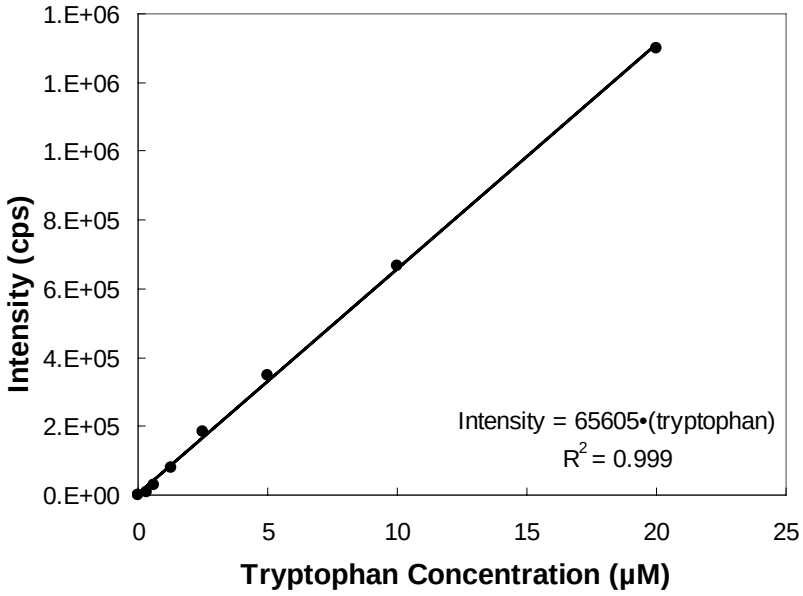

Figure **3-5**: Representative Standard Curve for Tryptophan Using Fluorescence Measurements. Each point represented in the graph illustrates an average value from triplicate measurements.

3.3.3 Quantitation of Indigo Trisulfonic Acid (ITS) Using Spectrophotometer

Concentrations of ITS were determined using a spectrophotometer (DU 520 Spectrophotometer, Beckman Instruments, Fullerton, CA). Unknown concentrations of ITS in a sample were determined from linear standard curves constructed from the spectrophotometer analyses of standard solutions. Solutions containing known concentrations of 0 to 0.1 mM of ITS were prepared in filtered, distilled water and pipetted into 1-cm path length, disposable cuvettes. Distilled water was used as a blank. The absorbance of these samples was determined at 600 nm and graphed against ITS concentration. The resulting standard curve shown in Figure **3-6** has a slope of 21,804 M^{-1}. After taking into account the 65% purity of the sample, this slope corresponds to an absorptivity of 21,804 $M^{-1}cm^{-1}$ which is within 8% of the published molar absorptivity of 23,800 $M^{-1}cm^{-1}$ reported by Bader and Hoigne (1981). This discrepancy was probably due to uncertainty in the purity value specified by the manufacturer.

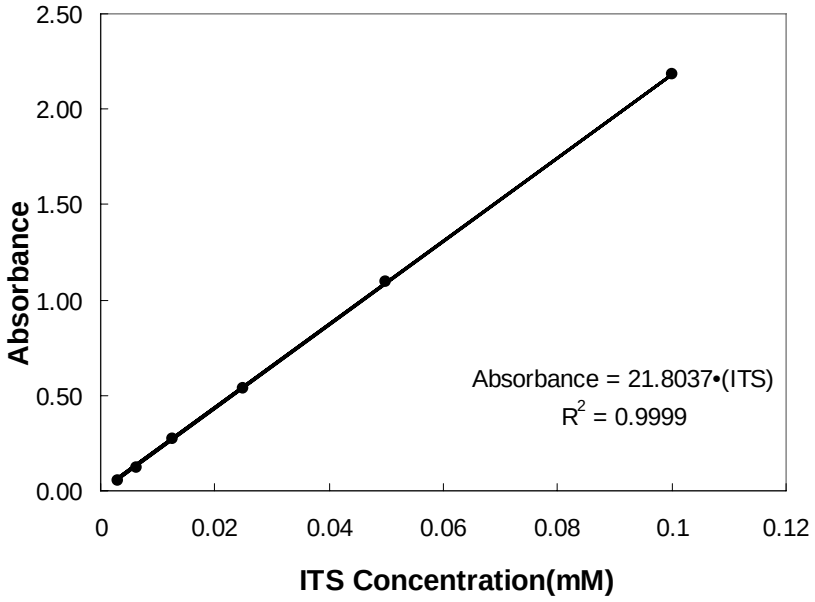

Figure **3-6**: Representative Standard Curve for ITS.

Each point represented in the graphs illustrates an average value from triplicate measurements.

3.4 Interfacial Reactor System

The experimental system consisted of a semi-batch reactor, an O_3 generator, a chemiluminescent O_3 analyzer, a rotometer, and a data acquisition system (Figure **3-7**). All components that came in contact with O_3 were made of teflon, glass or stainless steel.

Ozonated air generated by ultraviolet radiation (Model 165C, Thermo Environmental Instruments Inc.) (Appendix A) was flowed through a 275 ml reactor (Cat. no: 7538-05, ACE Glass incorporated) where it contacted the surface of a 3 ml antioxidant solution that was about 3.2 mm in depth (Figure **3-8**). A rotometer which was calibrated using a wet test meter, was employed to set the gas flow rate before it entered the reactor. Gas reached the liquid surface through a 25 mm diameter glass tube that terminated with a downward-facing fritted glass disc (model. no: 7538-07, ACE Glass Inc.). The disk was positioned 1.0 cm above the liquid surface, and had a diameter that was slightly less than the inner diameter of the reactor. Thus, the gas was well distributed in the narrow gap between the liquid surface and the surface of the fritted disk.

To reduce the diffusion resistance of the antioxidant solution, it was mixed by a 12.7×3 mm magnetic stirrer bar (Cat. no: 58948.397, VWR Scientific). The reactor had a side port about 1.5 mm below the gas-liquid interface so that small samples of liquid could be withdrawn through a hypodermic needle while O_3 exposure was in progress. A fast- responding, chemiluminescent O_3 analyzer (MacDougal et al., 1998) (Appendix B) in combination with a digital data acquisition system (DAQ-802, Omega Engineering,

Inc.) (Appendix C) was used to continuously record the O_3 concentration in the air stream that exited through the reactor every second.

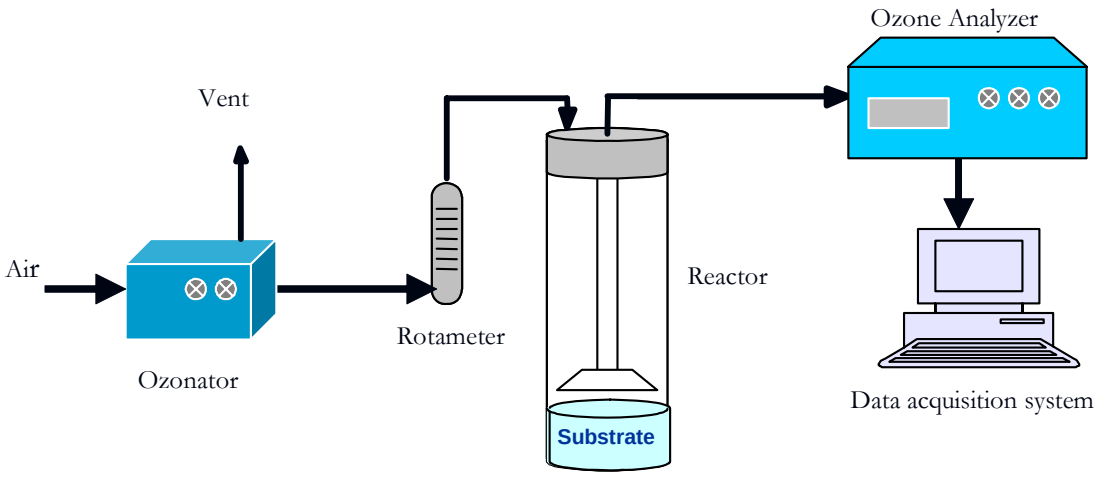

Figure **3-7**: Overview of the Reaction System

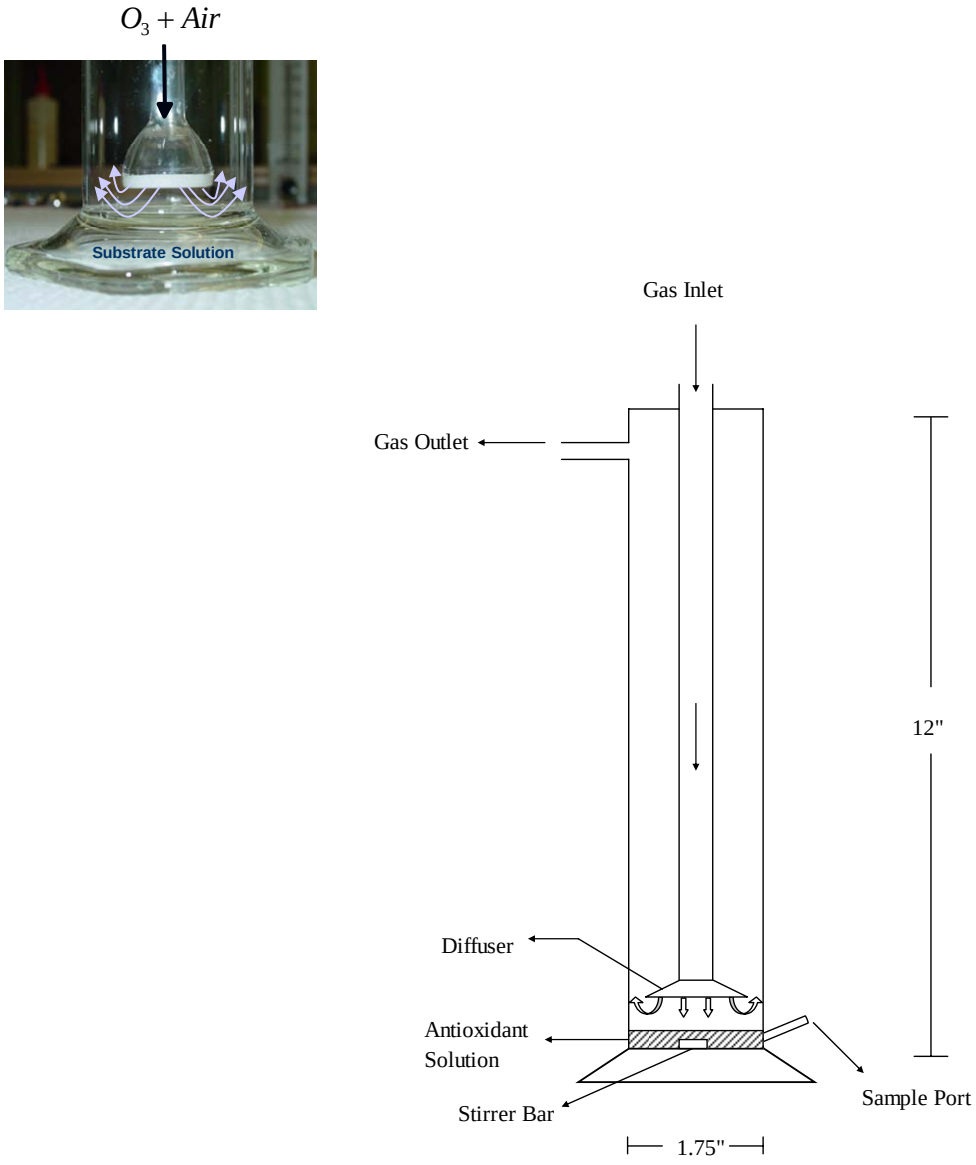

Figure **3-8**: Schematic of the Interfacial Reactor.

The O_3 analyzer was calibrated using ITS, a water-soluble substance whose deep violet color is rapidly bleached upon reaction with O_3. ITS solution was placed in the reactor and was exposed to an ozonated air flow for 15 minutes. Experiments were performed at room temperature ($T = 25 \pm 1\,^{\circ}C$) with inlet O_3 concentrations of approximately 1, 3, and 5 parts per million by volume (ppm) and flow rates of 300, 500 and 800 ml/min. ITS concentrations were determined before and after O_3 exposure, and the output voltage of the O_3 analyzer was continuously recorded. These measurements were repeated for a control experiment in which ozonated air flowed through the reactor containing buffered saline solution free of ITS. Since the reaction between ITS and O_3 has a 1:1 stoichiometry (Bader and Hoigne, 1981), the concentration/voltage calibration constant for the analyzer could be obtained from material balances on the ITS in solution and the O_3 in the gas phase. In particular, the calibration constant was selected so that the moles of ITS consumed in the solution were equal to the moles of O_3 absorbed from the air (see Equations **3.1** and **3.3**). Figure **3-9** shows the calibration curve for the O_3 analyzer obtained from ITS experiments. To correct O_3 concentrations, values obtained from the O_3 analyzer were divided by the calibration constant.

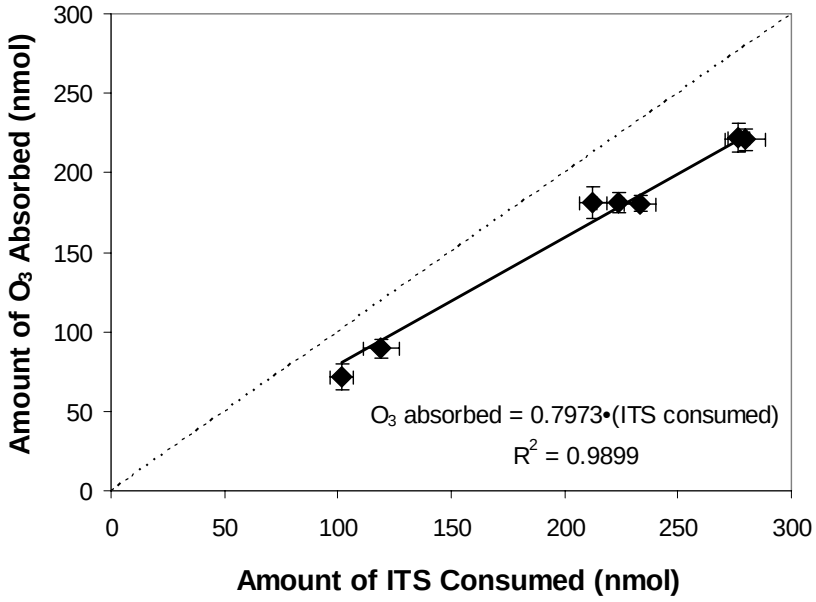

Figure **3-9**: Representative Calibration Curve for O_3 Analyzer Obtained from ITS Experiments.

Each point represented in the graph illustrates a mean value from three measurements and the bars represent the standard error of the mean. To correct O_3 concentrations, values obtained from the O_3 analyzer must be divided by the calibration constant.

3.5 Protocol

Experiments were conducted at room temperature ($T = 25 \pm 1\,^{\circ}C$) with inlet O_3 concentrations of 1-5 parts per million by volume (ppm). Gas flow and magnetic stirrer speed were progressively increased until O_3 absorption reached an upper limit, indicating that both gas-phase and liquid-phase diffusion resistances were negligible. Thereafter, a single gas flow and stirrer speed was used in each experiment. Various solutions of UA, AH_2, GSH, and albumin (tryptophan) were employed as a liquid phase in the reactor.

To begin an experiment, a substrate solution was charged to reactor, the magnetic stirrer was turned on, and the O_3 generator was set to produce the O_3 concentration of interest. The outlet O_3 concentration was then monitored for a 15-minute interval. The concentration of substrate or substrates in the test solution were always evaluated at the beginning (0 min) and at the end (15 min) of the O_3 exposure. In some experiments, small samples of the solution were also withdrawn at 5 and 10 minute time points. A control experiment in which the reactor was charged with buffered saline, free of substrates, was performed at each O_3 concentration of interest. To evaluate the effect of evaporation, another control experiment was performed in which the reactor was charged with a substrate solution but was exposed to clean air rather than ozonated air. In that case, the substrate concentration increased by less than 4%, and therefore evaporation was ignored in all experiments. In addition, to examine autooxidation in the absence of O_3, changes in antioxidant concentrations were monitored in solutions stored at room temperature for varying periods of time. It was observed that concentrations of AH_2, GSH, and albumin were decreased by less than 1% and 10% after 15 minutes (the period

of the usual experiment) and 3 hours, respectively. UA concentrations did not change even after 3 days. To avoid autooxidation occurring over longer time periods, solutions of AH_2, GSH, and albumin were prepared fresh before each experiment.

The amount of substrate that was depleted at any time t relative to the start of the reaction at t=0 was computed from a material balance on the liquid phase.

$$A_S(t) = V_L[C_S(0) - C_S(t)] \qquad \textbf{(3.1)}$$

where the V_L is the volume of the solution in the reactor and C_S is the molar concentration of substrate in the solution. The absorption rate of ozone into the substrate solution at a particular t, was computed from a material balance on the gas phase.

$$\dot{A}_{O3} = \dot{V}(C_{O3,2} - \tilde{C}_{O3,2}) \qquad \textbf{(3.2)}$$

where $\dot{V}$ is the volumetric flow rate of air entering the reactor, and $C_{O3,2}$ and $\tilde{C}_{O3,2}$ are the O_3 concentrations exiting the reactor during the actual and the control experiments, respectively. In order to obtain the total amount of O_3 absorbed from the beginning of exposure to a time t, the O_3 concentration data were numerically integrated according to the following equation:

$$A_{O3} = \int_0^t \dot{A}_{O3}dt = \int_0^t \dot{V}(C_{O3,2} - \tilde{C}_{O3,2})dt \qquad \textbf{(3.3)}$$

Chapter 4

MATHEMATICAL MODEL

This chapter describes a mathematical model developed to predict kinetic parameters of the reaction between O_3 and biological substrates. The chapter also explains the numerical solutions including an optimization program employed to solve the model.

A spatially-lumped model of the semi-batch reactor consisted of three well-mixed compartments is shown in Figure **4-1**. The liquid phase compartment is composed of the test solution, gas phase compartment I consists of the gas located within the narrow gap between the diffuser and the liquid surface, and gas phase II contains the gas outside of this gap.

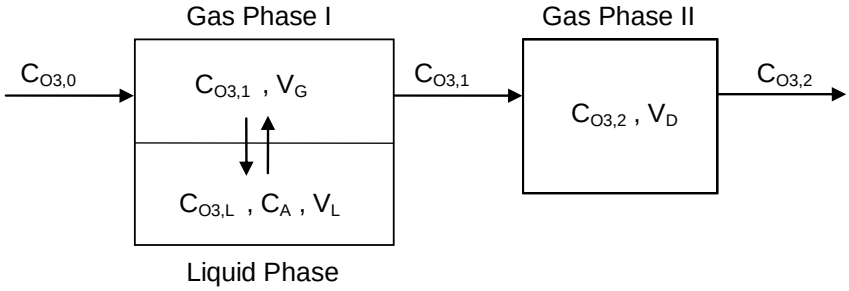

Figure **4-1**: Diagram of the Mathematical Model for the Semi-Batch Reactor Consisting of Three Well-Mixed Compartments.

The liquid phase compartment is composed of the test solution, gas phase compartment I consists of the gas between the diffuser and the liquid surface, and gas phase II contains the remaining gas.

A material balance on the substrate that is only present in the liquid phase can be formulated as:

$$Accumulation = Input - Output \pm Reaction$$

$$\frac{dC_S}{dt} = -\dot{R}_S \qquad (\mathbf{4.1})$$

where $\dot{R}_S$ is the rate of consumption of substrate by chemical reaction per unit volume of the liquid. For multicomponent solutions, Equation **4.1** can be written for each substrate that is present in the liquid phase.

A material balance for O_3 in the gas phase I can be written as follows:

$$V_G \frac{dC_{O3,1}}{dt} = \dot{V}\,(C_{O3,0} - C_{O3,1}) - N_{O3}A \qquad (\mathbf{4.2})$$

where $\dot{V}$ is the volumetric flow rate of air entering the reactor, V_G is the volume of the gas phase, and $C_{O3,0}$ and $C_{O3,1}$ are O_3 concentrations entering and exiting gas phase I, N_{O3} is the flux of ozone from the gas phase I into the liquid phase, and A is the interfacial area.

The material balance for O_3 in the liquid phase is as follows:

$$V_L \frac{dC_{O3,L}}{dt} = N_{O3}A - V_L\dot{R}_{O3} \qquad (\mathbf{4.3})$$

where V_L is the volume of the liquid phase, $C_{O3,L}$ is O_3 concentration in the liquid phase, and $\dot{R}_{O3}$ is the molar rate of depletion of O_3 by chemical reaction per unit volume of the liquid phase.

Using Equations **4.2** and **4.3**, a material balance can be formulated for O_3 in gas phase I and the liquid phase combined.

$$\frac{d(C_{O3,1}V_G + C_{O3,L}V_L)}{dt} = \dot{V}(C_{O3,0} - C_{O3,1}) - V_L\dot{R}_{O3} \qquad (\mathbf{4.4})$$

Assuming that the mechanical stirring of the liquid phase and the high-velocity stagnation flow in gas phase I insured interfacial equilibrium between these two compartments, we may write

$$C_{O3,l} = \lambda_{O3}^{G,L} C_{O3,L} \qquad (\mathbf{4.5})$$

where $\lambda_{O3}^{G,L}$ is the gas:liquid partition coefficient of O_3 at interfacial equilibrium. Recognizing that the reaction rate of O_3 with a substrate usually occurs at a fixed stoichiometric ratio, we may also stipulate that

$$\dot{R}_{O3} = \eta^{O3,S}\dot{R}_S \qquad (\mathbf{4.6})$$

where $\eta^{O3,S}$ is the moles of O_3 that reacts with each mole of substrate.

For multicomponent solutions, Equation **4.6** must be separately applied to each substrate S_i so that the overall rate of O_3 consumption is given as

$$\dot{R}_{O3} = \sum_i \eta^{O3,S_i} \dot{R}_{S_i} \qquad (\mathbf{4.7})$$

Combining Equations **4.4- 4.7** results in the final material balance for O_3 in the combined liquid-gas phase I compartment.

$$V_G' \frac{dC_{O3,1}}{dt} = \dot{V}(C_{O3,0} - C_{O3,1}) - V_L \sum_i \eta^{O3,S_i} \dot{R}_{S_i} \qquad (\mathbf{4.8})$$

where V_G' is the combined volume of the liquid phase and gas phase I compartments as if they were an equivalent single gas phase compartment.

$$V_G' = V_G + \frac{V_L}{\lambda_{O3}^{G,L}} \qquad (\mathbf{4.9})$$

To arrive at a prediction of the outlet concentration $C_{O3,2}$, we must account for the washout of O_3 through the gas phase II compartment, the relatively large volume of gas located outside of the narrow gap from which O_3 absorption occurs. We assume that the O_3 entering this "dead space" region, V_D, at a concentration $C_{O3,1}$ is ideally backmixed with residual gas so that its exiting concentration $C_{O3,2}$ can be predicted by the following material balance.

$$\frac{dC_{O3,2}}{dt} = \frac{\dot{V}}{V_D}(C_{O3,1} - C_{O3,2}) \qquad \textbf{(4.10)}$$

Note that it is $C_{O3,2}$ which is actually monitored by the O_3 analyzer in the experiments.

To complete the formulation of the model, $\dot{R}_S$ must be supplied as a function of C_S and $C_{O3,1}$. Though the exact form of $\dot{R}_S$ depends on the mechanism of the reaction, a formula that has wide applicability is given by

$$\dot{R}_S = k_r C_{O3,1}^m C_S^n \qquad \textbf{(4.11)}$$

where k_r is the reaction rate constant, and m and n are the reaction orders with respect to O_3 and substrate, respectively.

For the special case of the control experiment, in which substrate was not present in the test solution, $\dot{R}_S = 0$ so that an analytical solution to the model equations can be found.

$$\tilde{C}_{O3,2} = C_{O3,0}\left[1 - \exp(-\frac{\dot{V}}{V_D}t)\right] \qquad \textbf{(4.12)}$$

where it has been assumed that $V_D >> V_G'$. Thus, although the O_3 concentration at the inlet of reactor ($C_{O3,0}$) was never actually measured, it was taken to be the long-time

asymptotic of O_3 concentration at the reactor outlet observed in control experiments ($\tilde{C}_{O3,2}$).

The final model is an initial value problem consisting of four equations (Equations **4.1**, **4.8** , **4.10** , and **4.11**) that contain four dependent variables (C_S, $C_{O3,1}$, $C_{O3,2}$ *and* $\dot{R}_S$) whose initial values were completely specified ($C_{O3,1}(0)=C_{O3,2}(0)=0$; $C_S(0)=C_{S0}$). The model equations also contained five system parameters ($V_G, V_D, V_L, \dot{V}$ *and* $C_{O3,0}$) and four kinetic parameters ($\eta^{O3,S}, k_r, m$ *and* n). The system parameters were obtained by independent volume and flow measurements, whereas the kinetic parameter $\eta^{O3,S}$ was determined from the slope of the measured values of ozone absorption versus substrate consumption. These parameter values were then used in the model simulations to determine k_r, m, and n by fitting the experimental data.

In particular, to determine reaction rate constants in single-component solutions, the amount of substrate consumed and corresponding amount of O_3 absorbed were measured after 5, 10 and 15 minutes at four different substrate concentrations. These twenty four data points were simulated by selecting an initial value of k_r and numerically solving the stiff model equations using Gear's BDF method (IVPAC Subroutine, FORTRAN IMSL Library). The model equations were solved again using a k_r value that was updated with a modified Levenberg-Marquadrt algorithm (Bates and Watts, 1981). This iterative process was continued until the least square error between the twenty four data points and their simulated values was minimized. A copy of the FORTRAN code can be found in Appendix D.

Chapter 5

KINETICS OF OZONE REACTION WITH INDIVIDUAL ANTIOXIDANTS

This chapter contains the experimental data and mathematical simulations used to determine the kinetic parameters of reaction between O_3 and the individual antioxidants UA, AH_2, and GSH in single-component solutions. The chapter describes experimental conditions such as antioxidant concentrations, O_3 concentrations, and gas flow rates. The adequacy of the mathematical model in simulating the experimental data is also described. Finally, the chapter presents the reaction stoichiometry and reaction rate constants for reactions between O_3 and UA, AH_2, and GSH.

5.1 Experimental Design

The preliminary goal of this study was to design and test a bioreactor that could be employed to study the kinetic parameters of reaction of O_3 with biological substrates. In order to do that, it was necessary to examine the effect on O_3 absorption and substrate consumption of several parameters such as inlet gas flow rate, inlet O_3 concentration, initial substrate concentration, and mixing speed in the liquid. Because UA has been identified as the major antioxidant in nasal lining fluid (Peden et al., 1990, 1993), we initially focused on this antioxidant to develop the experimental conditions, along with the mathematical model. Initial UA concentrations of 50, 100, 150, and 200 μM were

employed in our experiments. From Table **2-2** it is observed that these values are within the range of UA concentration in the RTLF.

5.1.1 Effect of Gas Flow Rate and Inlet O_3 Concentration

To understand the effect of gas flow rate and inlet O_3 concentration, ozonated gas entered the reactor at flow rates of 300 to 800 ml/min, while O_3 concentration in the inlet stream and initial UA concentration were varied from 1 to 5 ppm and 100 to 200 μM, respectively. Figure **5-1** and Figure **5-2** summarize the amount of O_3 absorbed and UA utilized during the 15 minutes obtained by applying Equations **3.1** and **3.3** to the O_3 and antioxidant outlet concentration data.

Generally speaking, flow rate has very small effect on total amount of O_3 absorbed and UA consumed, indicating that there is a negligible mass diffusion resistance in the gas phase. On the other hand, Figures **5-1** and **5-2** show that increasing the inlet O_3 concentration causes an increase in both O_3 absorption and UA consumption.

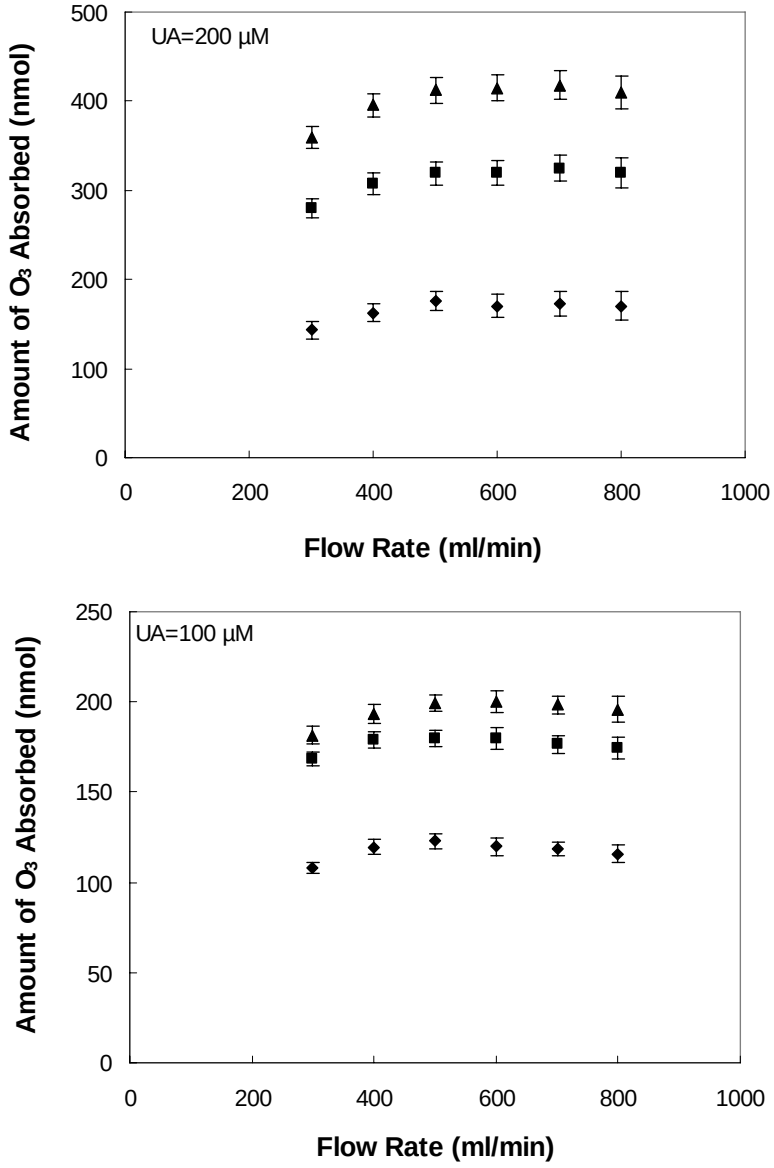

Figure **5-1**: Effect of Flow Rate and Inlet O_3 Concentration on O_3 Absorbed in 15 Minutes.

O_3 concentrations of approximately 1 ppm (♦), 3 ppm (■), and 5 ppm (▲), and gas flow rate of 300-800 ml/min were applied. Top and bottom graphs correspond to initial UA concentration of 200 µM and 100 µM, respectively. Each point represented in the graphs illustrates a mean value from three measurements and the bars represent the standards error around the mean.

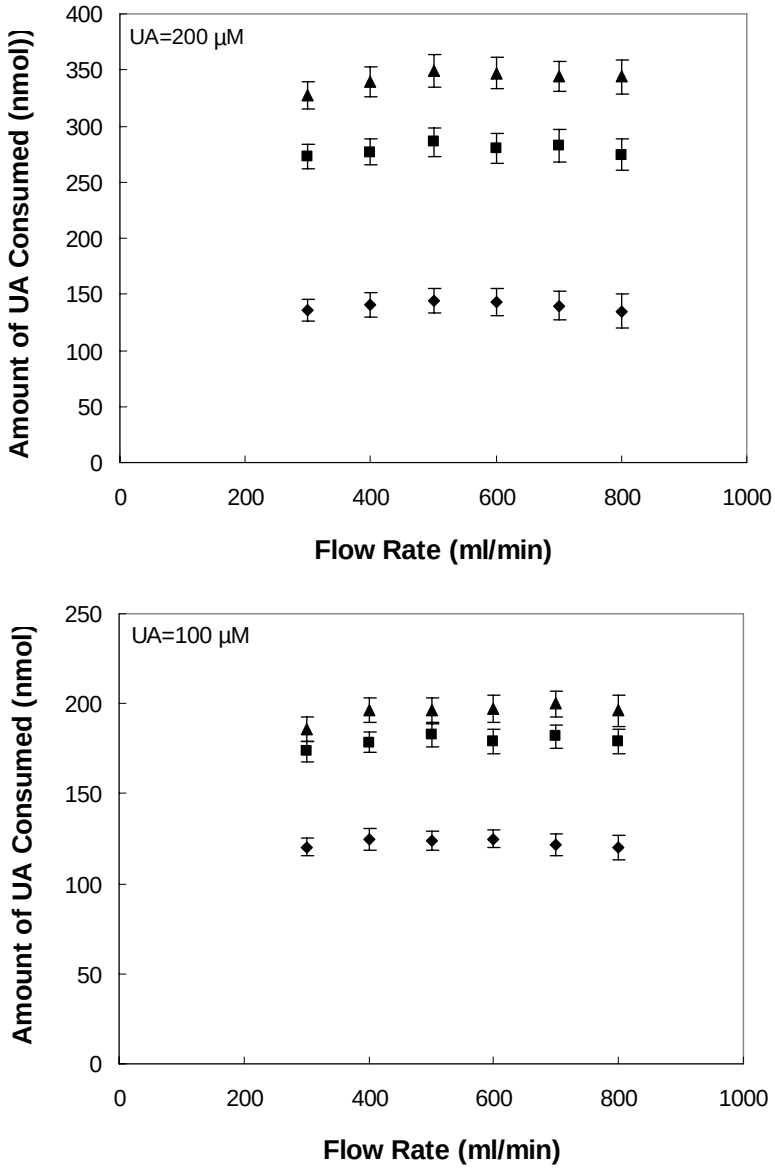

Figure **5-2**: Effect of Flow Rate and Inlet O_3 Concentration on UA Consumed in 15 Minutes.

O_3 concentrations of approximately 1 ppm (♦), 3 ppm (■), and 5 ppm (▲), and gas flow rate of 300-800 ml/min were applied. Top and bottom graphs correspond to initial UA concentration of 200 µM and 100 µM, respectively. Each point represented in the graphs illustrates a mean value from three measurements and the bars represent the standards error around the mean.

5.1.2 Mixing Effect

Several sets of experiments were performed to assess the effect of mixing in the aqueous phase. The liquid phase was agitated with a 12.7×3 mm magnetic stir bar. It was hypothesized that mixing in the solution increases the mass transfer in this liquid phase. Therefore having a well-mixed condition in the solution would cause its mass transfer resistance to be negligible, and hence would cause the reaction to be rate-controlling. Figure **5-3** shows the effect of progressively increasing stirrer speed on the O_3 absorbed and UA consumed in 15 minutes. Notice that the higher is the mixing speed, the greater are O_3 absorption and UA consumption. Once a stirred speed of 750 revolutions per minute (rpm) is reached, however, increasing the mixing speed further does no longer affect O_3 absorption and UA consumption. This upper limit indicates that liquid phase diffusion resistance was unimportant. The fact that there was negligible diffusion resistance in both liquid phase and gas phase justifies the assumption of interfacial equilibrium employed in the mathematical model. A single stirrer speed of 750 rpm was used in future experiments.

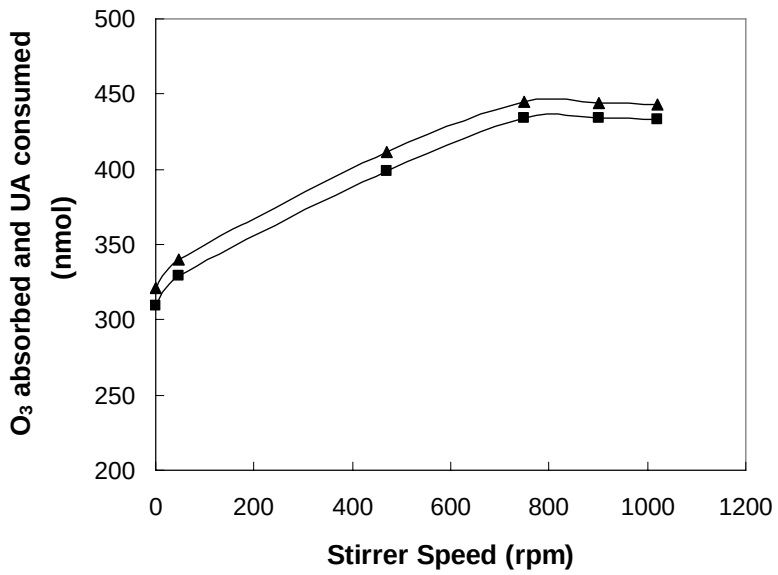

Figure **5-3**: Effect of Mixing speed on the Amounts of O_3 Absorbed and UA Consumed in 15 Minutes.

Gas flow rate of 500 ml/min, inlet O_3 Concentration of 3 ppm and UA Concentration of 200 μM were used. (▲) corresponds to the total amount of O_3 absorbed, whereas (■) corresponds to the total amount of UA consumed.

5.1.3 Experimental Conditions

To Study the kinetic parameters of the reactions between O_3 and UA, AH_2, and GSH, the outlet O_3 concentration and aqueous substrate concentrations were measured over a reaction time of 15 minutes for several inlet O_3 concentrations and antioxidant concentrations. Ozonated gas entered the reactor at flow rate of 500 ml/min while O_3 concentration in the inlet stream varied from 1 to 5 ppm. Initial UA, AH_2, and GSH concentrations of 50, 100, 150 and 200 μM were employed. These are physiologically relevant concentrations. A control experiment in which the reactor was charged with buffered saline, free of antioxidants, was performed at each O_3 concentration of interest.

5.2 Results

5.2.1 **Raw Data**

Representative data of outlet O_3 concentration for UA, AH_2, and GSH are compared to the saline control data in Figures **5-4** to **5-6** , respectively, for a fixed gas flow of 500 ml/min and a fixed inlet O_3 concentration of 3 ppm. Some intermediate data points were omitted in these plots for purposes of visual clarity. Collectively, these plots illustrate six important features of O_3 reaction with these antioxidants.

First, the outlet O_3 concentration in the control experiments reaches a constant value after about 2 minutes of exposure, indicating that O_3 does not react in saline alone.

Second, there is a rapid rise in concentration from an initial value of zero during the first 2 minutes of exposure in both the control and the substrates experiments. This

corresponds to the wash-out of gas phase II (Figure **4-1**) located above the diffuser (Figure **3-8**).

Third, as the time goes on, the outlet concentration of O_3 increases. This is due to the fact that, as the reaction proceeds, less antioxidant remained in the solution to react with O_3. Therefore, more unreacted O_3 appeared in the outlet gas stream.

Fourth, the outlet concentration of O_3 in the antioxidant experiments increases as the initial antioxidant concentration decreases. This can be explained by the fact that a lower concentration of antioxidant in the solution causes a slower reaction with O_3 and therefore less O_3 absorption from the gas phase. Indeed, when the concentration of antioxidants in the solution are 50 μM, the final O_3 concentrations measured in the antioxidant experiments closely approaches those observed in the saline experiments.

Fifth, changes in the UA and AH_2 concentrations appear to have a larger effect on O_3 absorption than the GSH concentration.

Sixth, the separation between the outlet O_3 concentrations for saline and antioxidant solutions becomes smaller and smaller from UA to AH_2 to GSH experiments. This implies that the hierarchy in reactivity between O_3 and these antioxidants is UA>AH_2>GSH.

As mentioned in chapter 3, we also computed the absorption rate of O_3 into the antioxidant solutions using Equation **3.2**. Representative data of O_3 absorption rates for UA, AH_2, and GSH are shown in Figures **5-7** to **5-9**, respectively, for a fixed gas flow of 500 ml/min and a fixed inlet O_3 concentration of 3 ppm. Because outlet O_3 concentrations of GSH were closer to those of the saline compared to what was seen for UA and AH_2, the O_3 absorption rate data were more scattered for GSH. Consistent with the outlet O_3

concentration curves, there is an initial rapid rise in absorption rate due to the wash-out of gas phase II located above the diffuser (Figure **3-8**). The absorption rate remains relatively high until, as time goes on and antioxidant is progressively consumed, the O_3 absorption rate decreases. In fact, at the lowest initial antioxidant concentration of 50 μM, the final O_3 absorption rate approaches zero.

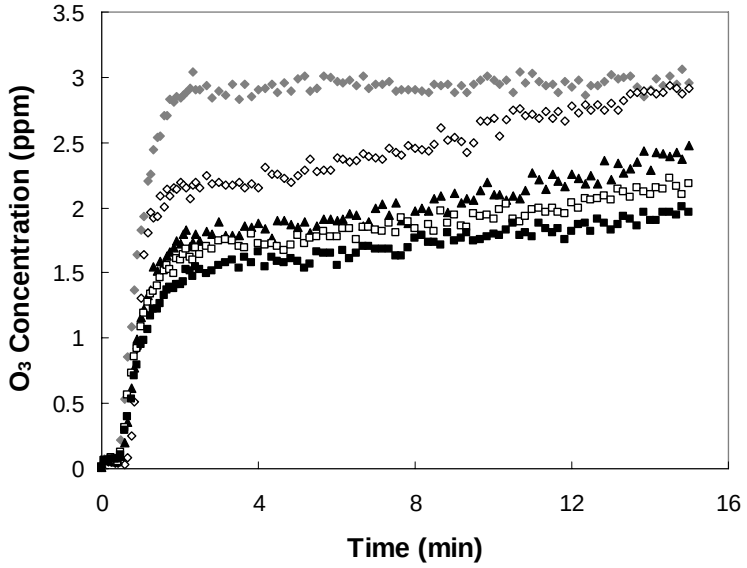

Figure **5-4**: Gas Breakthrough Curves for UA.

Representative data illustrating the O_3 output concentration at a fixed flow of 500 ml/min and a fixed O_3 concentration of 3.0 ppm. Data was collected for saline solution (♦) and initial UA concentrations of 50 µM (◊), 100 µM (▲), 150 µM (□) and 200 µM (■).

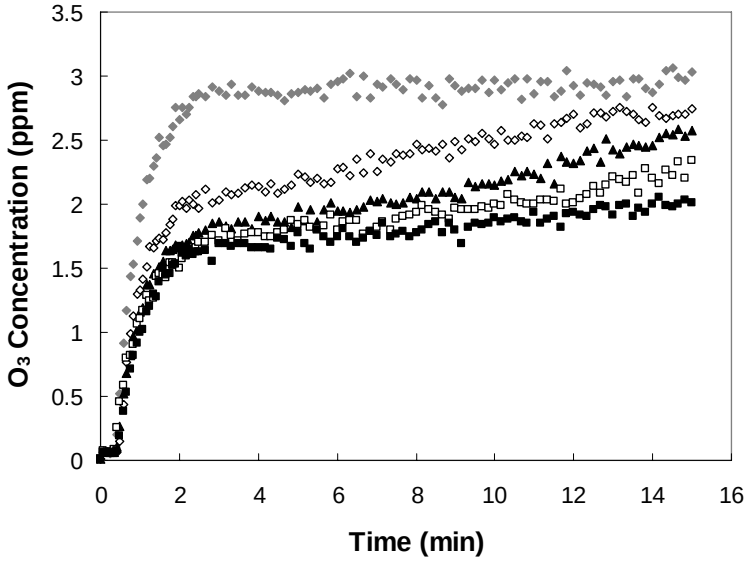

Figure **5-5**: Gas Breakthrough Curves for AH_2.

Representative data illustrating the O_3 output concentration at a fixed flow of 500 ml/min and a fixed O_3 concentration of 3.0 ppm. Data was collected for saline solution (♦) and initial AH_2 concentrations of 50 µM (◊), 100 µM (▲), 150 µM (□) and 200 µM (■).

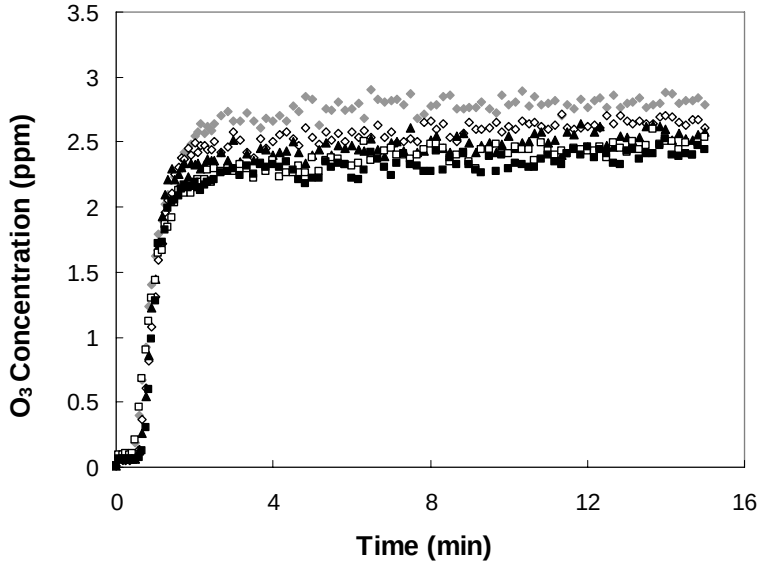

Figure **5-6**: Gas Breakthrough Curves for GSH.

Representative data illustrating the O_3 output concentration at a fixed flow of 500 ml/min and a fixed O_3 concentration of 3.0 ppm. Data was collected for saline solution (♦) and initial GSH concentrations of 50 µM (◊), 100 µM (▲), 150 µM (□) and 200 µM (■).

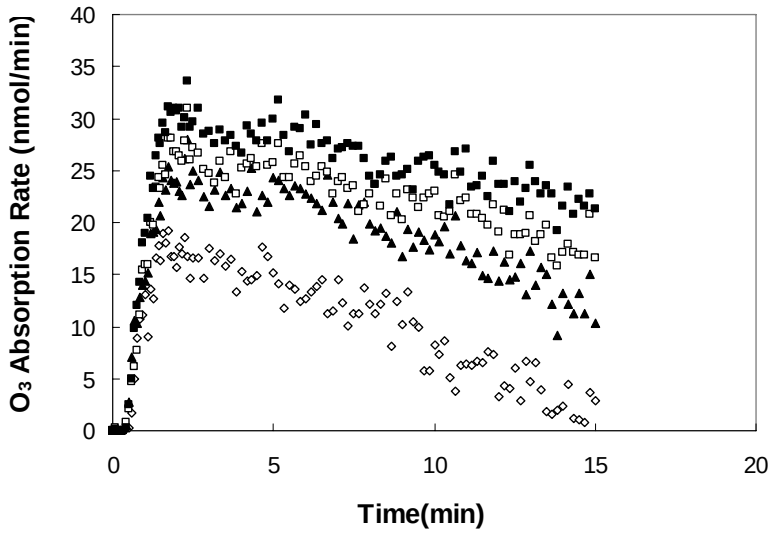

Figure **5-7**: O_3 Absorption Rate Curves for UA.

Representative data illustrating the O_3 absorption rate at a fixed flow of 500 ml/min and a fixed O_3 concentration of 3.0 ppm. Data was collected for initial UA concentrations of 50 µM (◊), 100 µM (▲), 150 µM (□) and 200 µM (■).

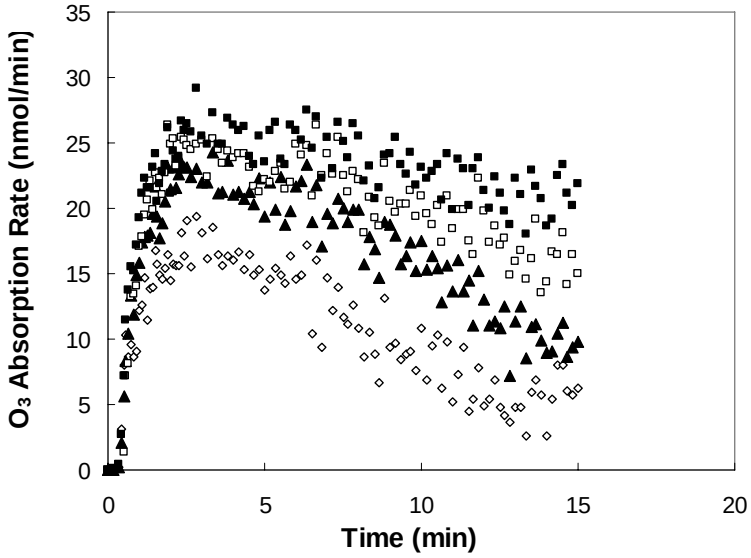

Figure **5-8**: O_3 Absorption Rate Curves for AH_2.

Representative data illustrating the O_3 absorption rate at a fixed flow of 500 ml/min and a fixed O_3 concentration of 3.0 ppm. Data was collected for initial AH_2 concentrations of 50 µM (◊), 100 µM (▲), 150 µM (□) and 200 µM (■).

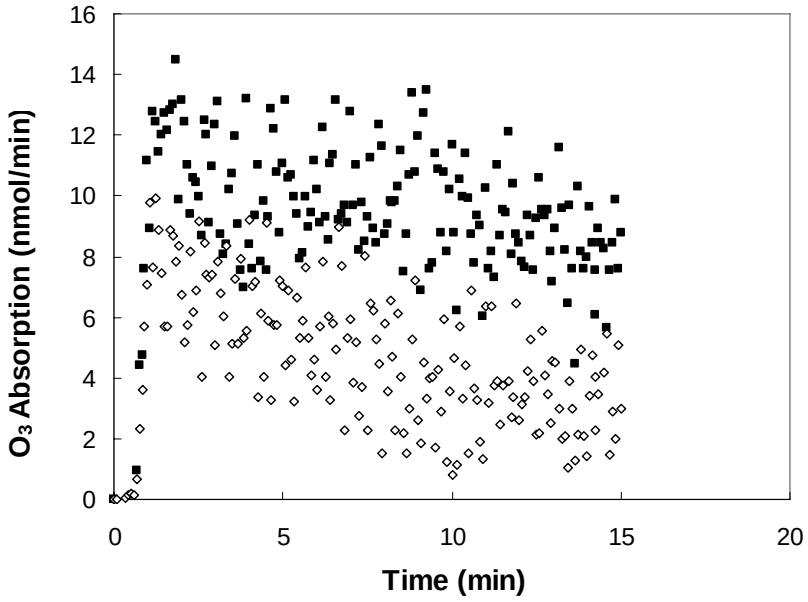

Figure **5-9**: O_3 Absorption Rate Curves for GSH.

Representative data illustrating the O_3 absorption rate at a fixed flow of 500 ml/min and a fixed O_3 concentration of 3.0 ppm. Data was collected for initial GSH concentrations of 100 μM (◊), and 200 μM (■). For clarity, only two concentrations (100 and 200 μM) of GSH are shown.

5.2.2 Reproducibility of the Experimental Data

Experiments were carried out several times for each initial concentration of UA, AH_2, and GSH. Figure **5-10** shows the amounts of UA consumed (top graph) and O_3 absorbed (bottom graph) in UA experiments. Figure **5-11** shows the amount of GSH consumed in GSH experiments (top graph) and amount of AH_2 consumed in AH_2 experiments (bottom graph). As can be observed from these graphs, experimental data obtained from repeated experiments were quite reproducible.

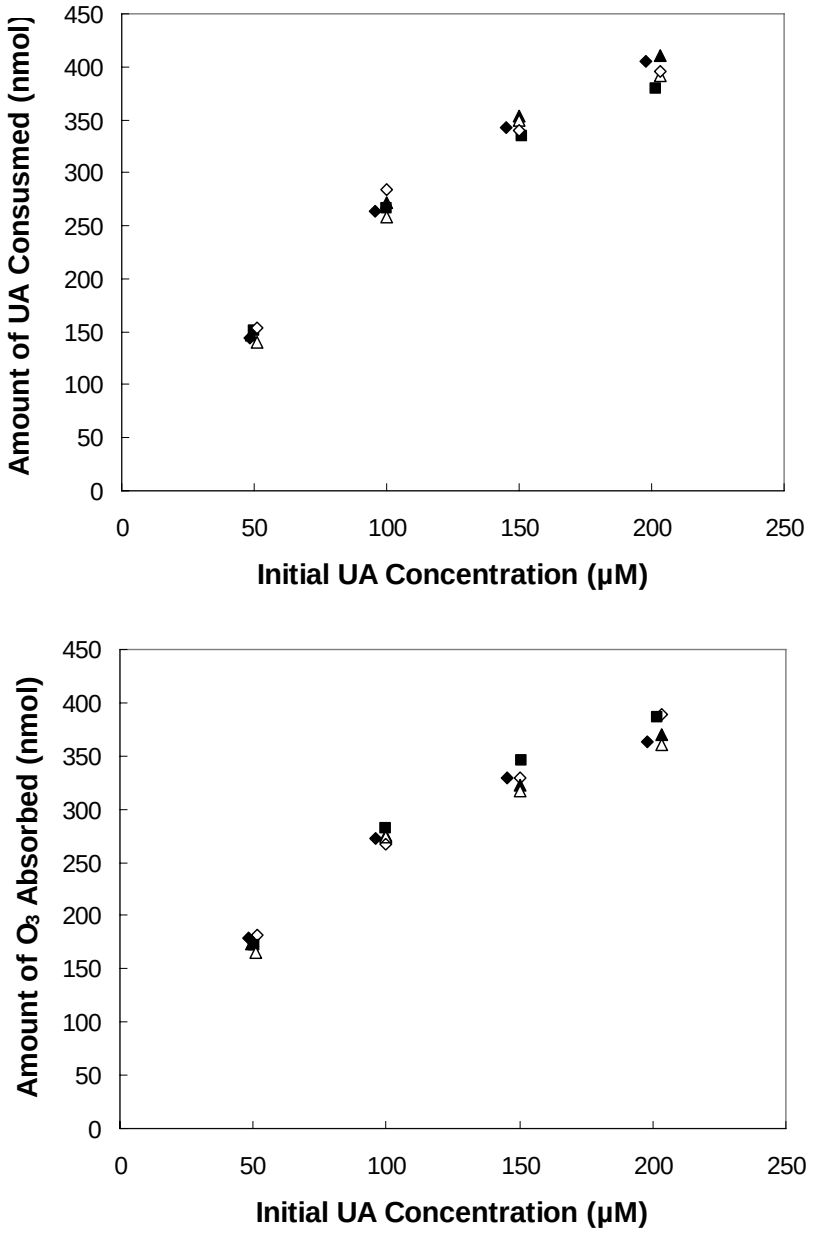

Figure **5-10**: Reproducibility of UA Experiments.

Top graph shows the total Amount of UA Consumed after 15 minutes O_3 exposure for five repeated experiments. Bottom graph shows the total amount of O_3 absorbed after 15 minutes exposure to O_3 for five repeated experiments. Different symbols represent data obtained from repeated experiments for each initial UA concentration.

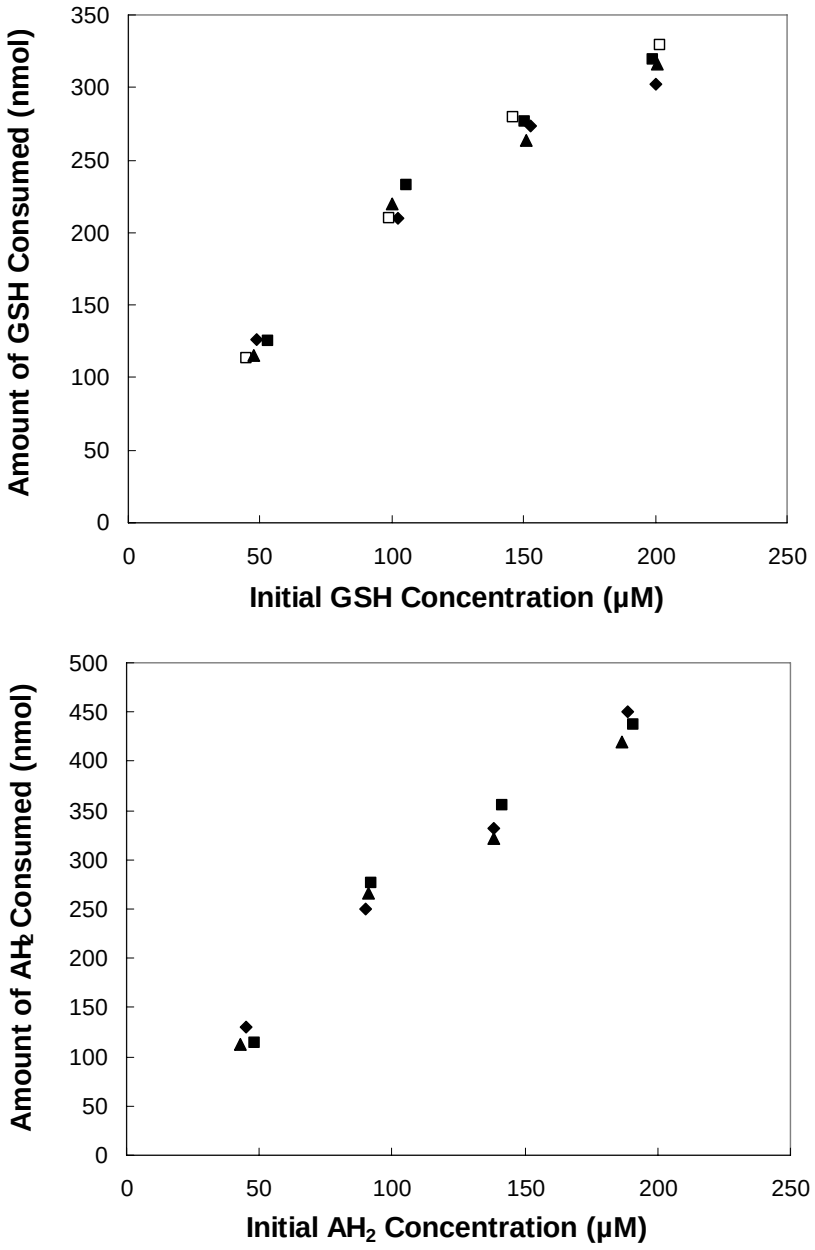

Figure **5-11**: Reproducibility of GSH and AH_2 Experiments.

Top graph shows the total Amount of GSH Consumed after 15 minutes O_3 exposure for four repeated GSH experiments. Bottom graph shows the total amount of O_3 absorbed after 15 minutes exposure to O_3 for three repeated AH_2 experiments. Different symbols represent data obtained from repeated experiments for each initial GSH or AH_2 concentration.

5.2.3 Stoichiometry Analysis

Central to this investigation were the simultaneous, time-dependent measurements of gas and substrates concentrations. Using these data, we computed both the amount of O_3 absorbed (Equation **3.3**) and the amount of substrate consumed (Equation **3.1**) at each time point of each experiment. Figures **5-12** to **5-14** present all the data collected at 5, 10, and 15 minutes of O_3 exposure in experiments with initial antioxidant concentrations of 50, 100, 150 and 200 μM. A least-square linear regression (forced through zero) of O_3 absorbed against antioxidant consumed indicate two key features. First, one mole of O_3 is needed to react with each mole of UA or AH_2, implying that these reactions have a one-to-one (1:1) stoichiometry. Second, for each mole of O_3 absorbed, 2.5 moles of GSH are consumed which suggests that this reaction has a 1.0:2.5 stoichiometry.

In order to evaluate the reaction rate parameters, these stoichiometries were incorporated into the kinetic parameters specified in the mathematical model. That is, when simulating O_3 reaction with UA or with AH_2, we used the following kinetic parameters: $\eta^{O3,S} = m = n = 1.0$. On the other hand, when simulating the reaction of O_3 with GSH, we used the following kinetic parameters: $\eta^{O3,S} = 0.4,\ m = 0.5,\ and\ n = 1.25$. The resulting k_r values were $5.83 \times 10^4\ \mathrm{M}^{-1}\,\mathrm{sec}^{-1}$, $5.5 \times 10^4\ \mathrm{M}^{-1}\,\mathrm{sec}^{-1}$, and $57.5\ \mathrm{M}^{-0.75}\,\mathrm{sec}^{-1}$ for the reaction of O_3 with UA, AH_2, and GSH, respectively. Comparisons between the measured and simulated values of O_3 absorption and substrate consumption obtained by using these optimal k_r values in the simulations are shown in Figures **5-15 - 5-22**.

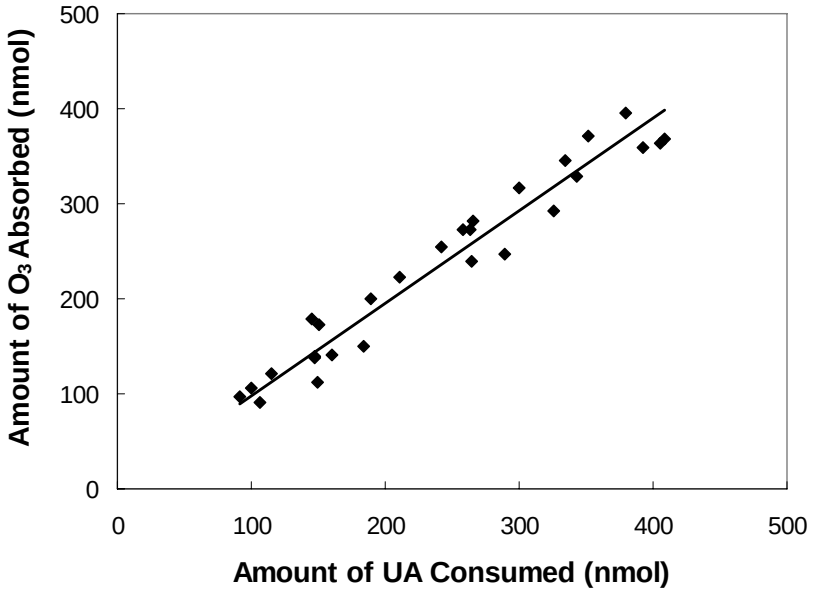

Figure **5-12**: Comparison Between UA Consumed and O_3 Absorbed After 5, 10 and 15 Minutes of O_3 Exposure.

The linear regression shown by the solid line was used to establish the stoichiometry of the reaction between O_3 and UA. Performing a least-squared linear regression analysis results in:

$Y = (0.974 \pm 0.034)\ X$; $R^2 = 0.992$ where ±95% confidence limits have been indicated for the coefficient.

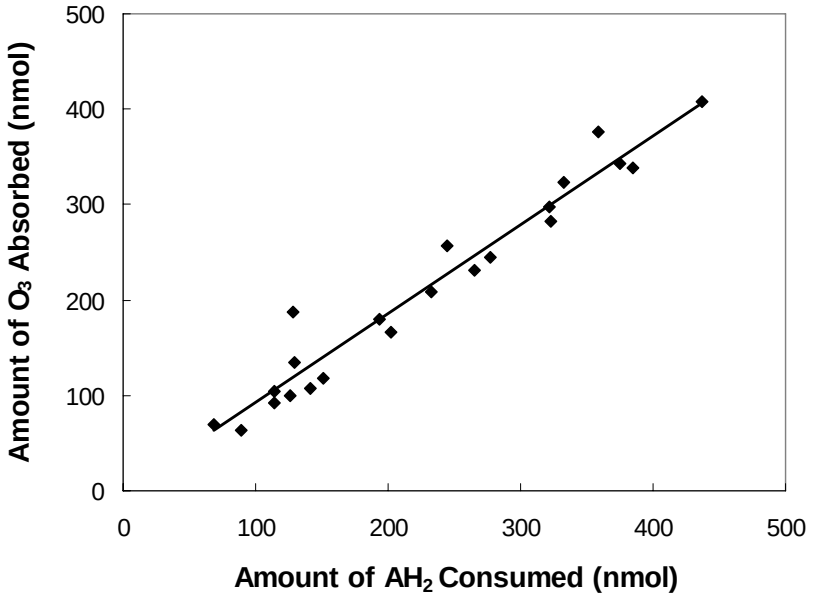

Figure **5-13**: Comparison Between AH_2 Consumed and O_3 Absorbed After 5, 10 and 15 Minutes of O_3 Exposure.

The linear regression shown by the solid line was used to establish the stoichiometry of the reaction between O_3 and AH_2. Performing a least-squared linear regression analysis results in:

$Y = (0.929 \pm 0.041)\ X$; $R^2 = 0.991$ where ±95% confidence limits have been indicated for the coefficient.

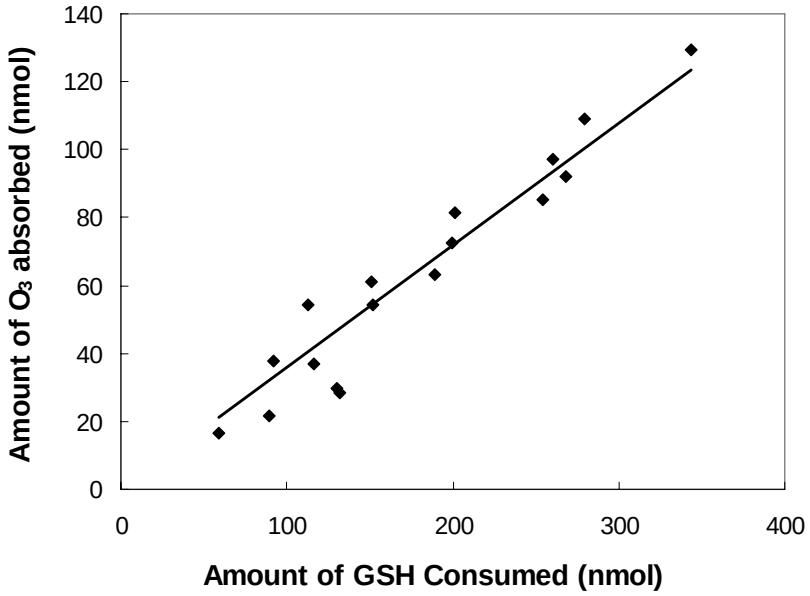

Figure **5-14**: Comparison Between GSH Consumed and O_3 Absorbed After 5, 10 and 15 Minutes of O_3 Exposure.

The linear regression shown by the solid line was used to establish the stoichiometry of the reaction between O_3 and GSH. Performing a least-squared linear regression analysis results in:

$Y = (0.376 \pm 0.025)\ X$; $R^2 = 0.982$ where ±95% confidence limits have been indicated for the coefficient.

5.3 Discussion

In evaluating the health effects of O_3 on the lung, a means of extrapolating from exposure concentration to target tissue dose is needed to improve dose-response relationships. Mathematical diffusion models can be helpful in this regard, but they require reliable data about the intrinsic rate of O_3 reaction with substrates lining the airways. We have chosen to study the kinetics of O_3 reaction with UA, AH_2, and GSH because these antioxidants are abundant in the epithelium lining fluid of the upper (nasal cavity) and proximal airways (tracheo-brochial tree) (Cross et al., 1994; Van der Vliet et al., 1999) and also because they are important scavengers of O_3. A unique aspect of the current research was the measurement of time-dependent changes in both O_3 absorption and substrate consumption. Using this approach, we were able to: 1) verify the closure of the mass balance between the amount of O_3 absorbed and the amount of substrate consumed; and 2) determine the stoichiometry between O_3 and each of the three antioxidants.

To quantify reaction kinetics, we utilized a combination of experimental analyses and numerical simulations. As a first step, we compared the amount of O_3 absorbed to the amount of substrate consumed (Figures **5-12- 5-14**). As discussed in the previous section, this allowed us to identify a 1:1 stoichiometry between O_3 and either UA or AH_2 acid, and a stoichiometry of 1.0:2.5 between O_3 and GSH. For UA and AH_2, in particular, we assumed that their reaction with O_3 are elementary so that a 1:1 stoichiometry implies that m=n=1.0 for both reactions. The assignment of these reaction orders allowed us to determine the corresponding second-order reaction rate constants k_r

from model simulations. Data from the substrate experiments were simulated by numerical solution of the differential mass balance Equations **4.1**, **4.4** , **4.8**, and **4.10**, whereas data from the saline control experiment were predicted by Equation **4.12**.

A comparison of the model simulations to the measurements of O_3 outlet and antioxidant concentrations are shown for the UA and AH_2 experiments in Figures **5-15** and **5-17,** respectively. A comparison between model predictions and experimental observations of the total amounts of O_3 absorbed and antioxidant consumed are shown in Figures **5-16** and **5-18**, respectively. In all cases, the simulations compare favorably to the data. Moreover, for each panel shown in Figures **5-16** and **5-18**, a regression analysis of simulated versus measured values produced lines whose intercepts were not significantly different from zero and whose slopes were not significantly different from 1.0 (see figure legends). In other words, these cross-plots all followed a line of identity. We used a similar procedure to determine the k_r value for the reaction between O_3 and GSH. In this case, the 1.0:2.5 stoichiometry we inferred from the relative consumption of O_3 and GSH was close to the 2:1 stoichiometry reported for the ozonation of GSH to GSSG (Mudway and Kelly, 1998). Results from Mudd and associates (1969) also indicated that for one mole of O_3 absorbed, between 2 to 3 moles of GSH is oxidized. In fitting the mathematical model to the dynamic reaction data, we first assumed reaction orders of m=n=1.0 with a stoichiometry of 1:1, as we had done for UA and AH_2. We then tried alternative reaction orders of m=0.5; n=1.25 and m=1.0; n=2.5, both in keeping with the assumption of elementary reaction and a stoichiometry of 1:2.5.

Figure **5-19** and **5-20** compare the model simulations and experimental data for the time course of outlet O_3 concentration and GSH concentration, respectively. Figure **5-**

21 and Figure **5-22** compare model predictions and experimental data for the total amount of O_3 absorbed and GSH consumed, respectively. As was discussed for UA and AH_2, regression analyses of these cross-plots were performed to determine whether or not they followed the line of identity. As we expected, the slope of the regression was significantly different from 1.0 when m=n=1.0 was assumed. On the other hand, assumptions of m=0.5; n=1.25 or m=1.0; n=2.5 both resulted in regression lines with slopes not significantly different from 1.0 and intercepts that were not significantly different from 0. This indicates that a stoichiometry of 1:2.5 provides a better simulation than does a stoichiometry of 1:1. However, the regression obtained when m=0.5; n=1.25 resulted in the narrower 95% confidence intervals than when m=1.0; n=2.5, indicating that the former set of reaction orders lead to better agreement of simulations and data. The time courses of the simulations in Figures **5-19** and **5-20** are also in somewhat better agreement when m=1.0; n=2.5 than when m=0.5; n=1.25. Determination of the kinetic rate parameters for the reaction of O_3 with constituents of RTLF is not abundant in the literature. Table **5-1** summarizes the values of the rate constants for the three antioxidants found by different research groups and also indicates the experimental conditions that were employed. Several observations can be made by comparing these previous studies to the current investigation: 1) with the exception of Mudway and Kelly (1998), all the previously-reported reaction rate constants of UA or AH_2 with O_3 are two to three orders of magnitude larger than our values; 2) unlike the study of Giamalva and colleagues (Giamalva et al.,1985), the results of Mudway and Kelly (1998) agree with our findings that the reaction rate constant for UA is not much different from the rate constant for AH_2; 3) all the reported data agree with our conclusion that the reaction of

O_3 with UA or with AH_2 is first-order with respect to O_3 as well as the antioxidant; and 4) our study is the only one that provides clear evidence of a non-first-order reaction between O_3 and GSH.

To explain the discrepancies between the values of the reaction rate constants in the current study compared to the much higher values found in some previous studies, one can single out two methodological differences in the experimental designs. First, reactant concentrations employed in most other investigations were larger than those used in the present experiments: antioxidant concentrations were at least 100 times greater and O_3 concentrations were at least 10 times higher in the previous studies. Thus, the difference in rate constants among the studies might be due to a dissimilarity in the rate-determining steps of the reaction process. Second, the experimental conditions under which O_3 and antioxidant solutions were contacted differed markedly from study to study. Pryor and collaborators (Giamalva et al., 1985, and Pryor et al., 1984) utilized a stopped-flow reactor that rapidly mixed antioxidant solution with a high concentration O_3 solution. This is far different than the situation in the respiratory system where O_3 is contacted with mucous at a gas-liquid interface. Kanofsky and Sima (1995) used a 17-gauge stainless steel needle that impinged 1.25 ml/sec of ozonated air on the surface of the antioxidant solution, and interpreted their result in terms of a pure reaction-diffusion model. It is possible that the jetting of gas through the needle may have caused local convection in the liquid that lead to an overestimation of the reaction rate constant. Moreover, Kanofsky and Sima (1995) referenced their reaction rate constants to the published value of the reaction rate constant of methionine with O_3. In other words, they did not actually measure absolute values of reaction rate constants.

Mudway and Kelly (1998) studied the kinetics of O_3 reaction with pulmonary antioxidants by utilizing physiologically-relevant concentrations of UA, AH_2 and GSH (Cross et al., 1994) as well as environmentally relevant concentrations of O_3 (Mustafa, 1990). Similar to the current investigation, they utilized a gas-liquid reactor in which an ozonated air stream flowed over a flat liquid interface. Consistent with our findings, Mudway and Kelly (1998) concluded that GSH is less reactive with O_3 than are UA and AH_2. This relatively low reactivity of GSH is similar to the observation made in a previous study (Ben-Jebria et al., 1998) in which the addition of AH_2 to buffered albumin solution significantly attenuated albumin depletion by NO_2 (another environmental oxidant gas), whereas the addition of GSH provided no protection to the albumin.

The rate constants reported in Table **5-1** for Mudway and Kelly's study (1998) are based on our own interpretation of their raw data, assuming that both gas and liquid phases were well-mixed (APPENDIX E). These estimated rate constants are smaller than (but of the same order of magnitude) the rate constants found in the current study. A possible explanation for this is a lack of adequate mixing by the orbital shaker used by Mudway and Kelly. They demonstrated that the oxidation of potassium iodide by O_3 in their apparatus was not different with the orbital shaker on or off, and concluded that mixing was sufficient to eliminate diffusion limitations in their O_3-antioxidant measurements. However, it is not clear whether or not orbital shaking had any effect on mixing in the gas phase. It is also unclear if potassium iodide is sufficiently reactive with O_3 that it served as an appropriate surrogate for antioxidants in these mixing experiments.

In summary, the reaction between O_3 and UA, AH_2, and GSH were studied in a semi-batch interfacial gas-liquid reactor. To quantify reaction kinetics, we employed a

process that utilized a combination of experimental analyses and numerical simulations. The reactions between O_3 and UA, AH_2, and GSH were found to have 1:1, 1:1 and 1:2.5 stoichiometry, respectively. The reactivity between O_3 and these antioxidants is in the following order: UA $\approx$ AH_2 > GSH. We believe that the reaction stoichiometries and the reaction rate equations that we inferred will prove useful in the future development of physiological models to predict the distribution of O_3 dose to target tissues within the respiratory tract.

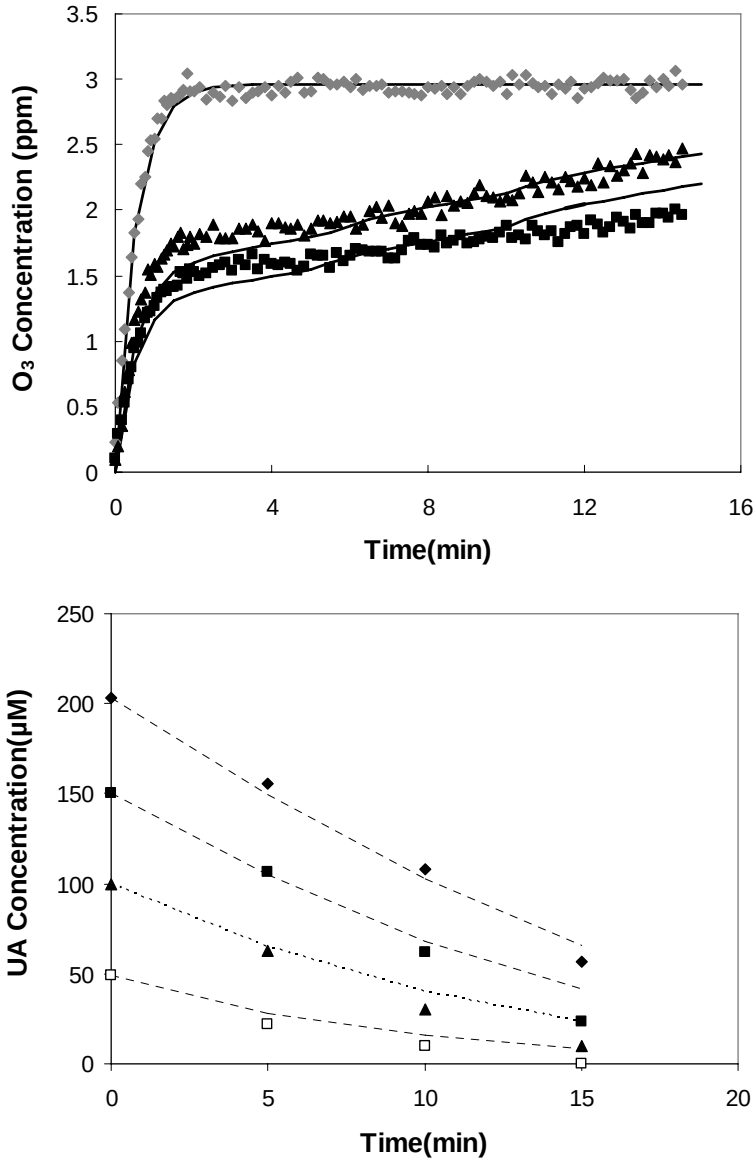

Figure **5-15**: Experimental Data and Model Simulations of O_3 Outlet Concentration and UA Concentration.

Representative data illustrate the model simulations (solid or dashed lines) and experimental data for a fixed flow of 500 ml/min and a fixed O_3 concentration of 3.0 ppm. Top graph shows the time course of O_3 output concentration in saline control experiments (♦) and in experiments with initial UA concentrations of 200 µM (■), 100 µM (▲). For clarity, only two concentrations (100 and 200 µM) of UA are shown. Bottom graph shows the time course of UA concentration in experiments with initial UA concentrations of 200 µM (♦), 150µM (■), 100 µM (▲), and 50 µM (□).

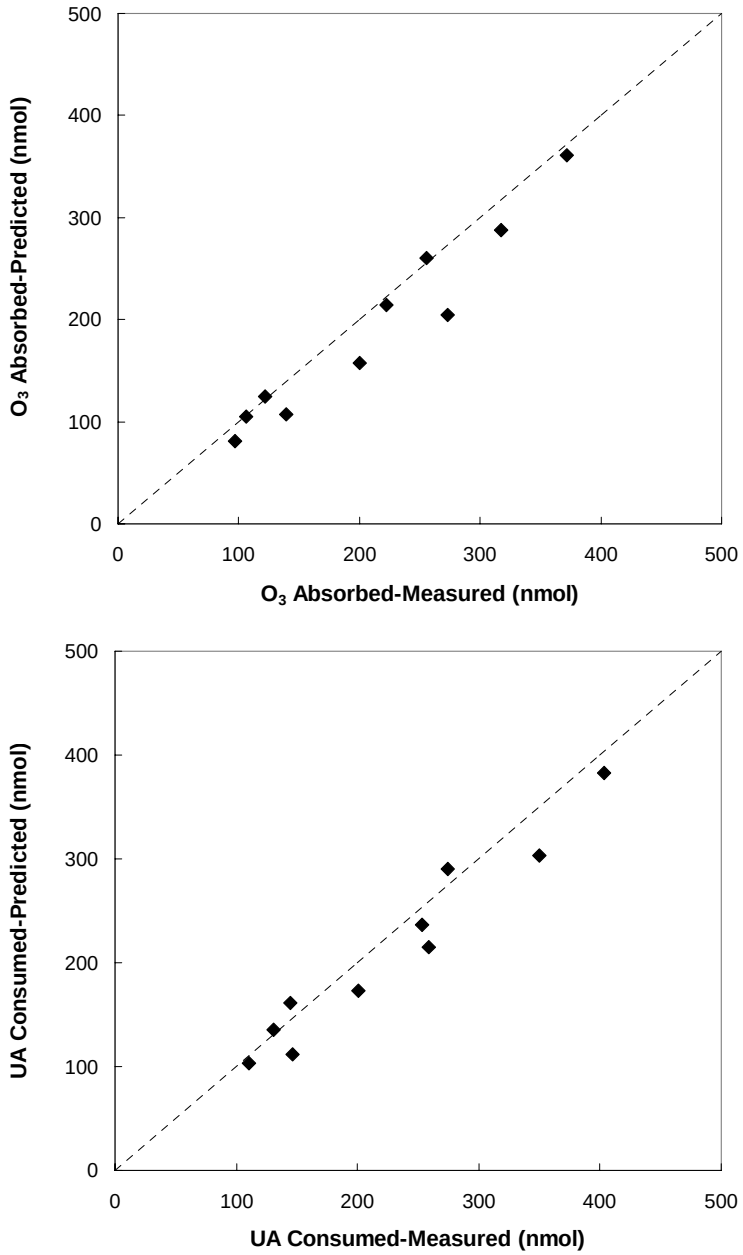

Figure **5-16**: Experimental Data and Corresponding Model Simulations of O_3 Absorbed and UA Consumed after 5, 10, and 15 Minutes.

Top graph illustrates the representative data of total amount of O_3 absorbed after 5,10, and 15 minutes, whereas bottom graph illustrates the total amount of UA consumed after 5, 10, and 15 minutes. Dashed lines represent the line of identity. Performing a least-squared linear regression analysis results in: Top graph: $Y = (0.941 \pm 0.196) X + (-7.554 \pm 44.766)$; Bottom graph: $Y = (0.908 \pm 0.178) X + (4.773 \pm 43.707)$ where ±95% confidence limits have been indicated for each of the coefficients.

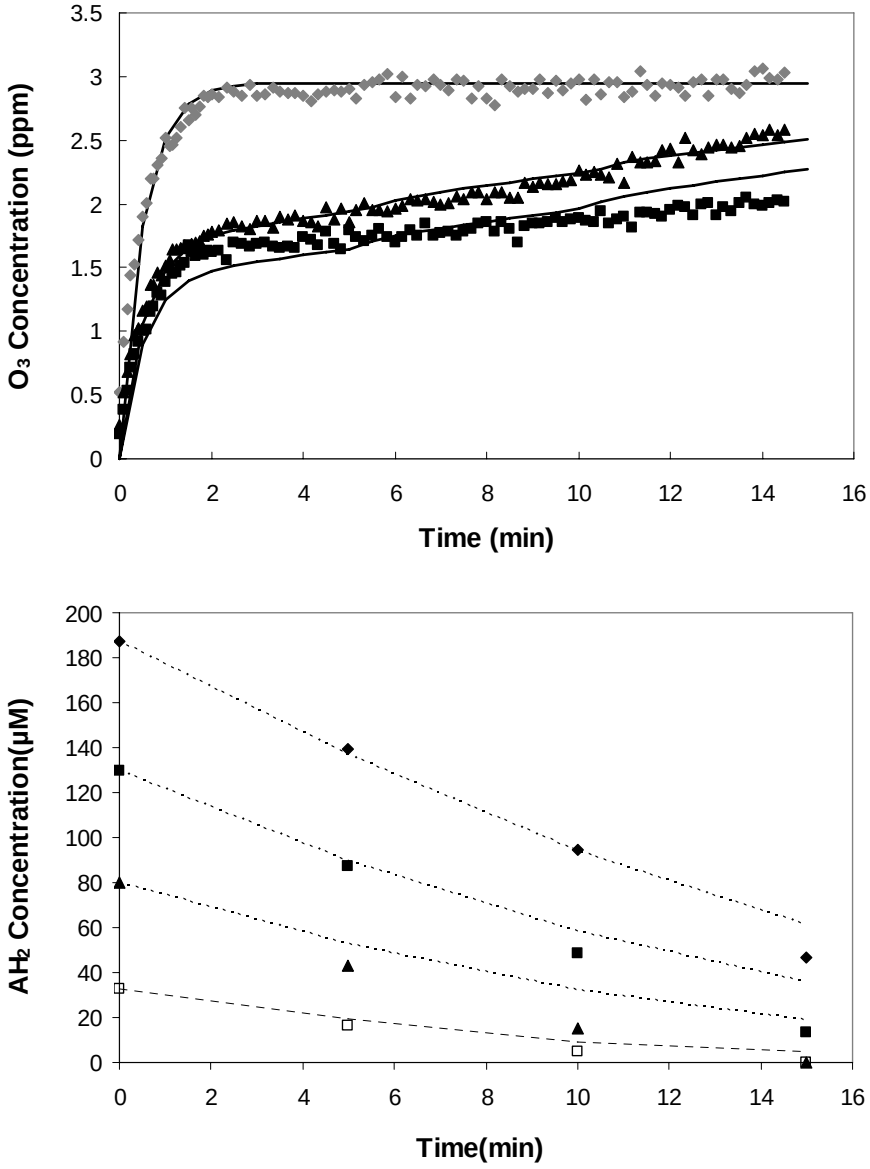

Figure **5-17**: Comparison Between Experimental Data and Corresponding Model Simulations of the Time Course of O_3 Outlet Concentration and AH_2 Concentration.

Representative data illustrate the model simulations (solid or dashed lines) and experimental data for a fixed flow of 500 ml/min and a fixed O_3 concentration of 3.0 ppm. Top graph shows the time course of O_3 output concentration in saline control experiments (♦) and in experiments with initial AH_2 concentrations of 200 µM (■), 100 µM (▲). For clarity, only two concentrations (100 and 200 µM) of AH_2 are shown. Bottom graph shows the time course of AH_2 concentration in experiments with initial AH_2 concentrations of 200 µM (♦), 150µM (■), 100 µM (▲), and 50 µM (□).

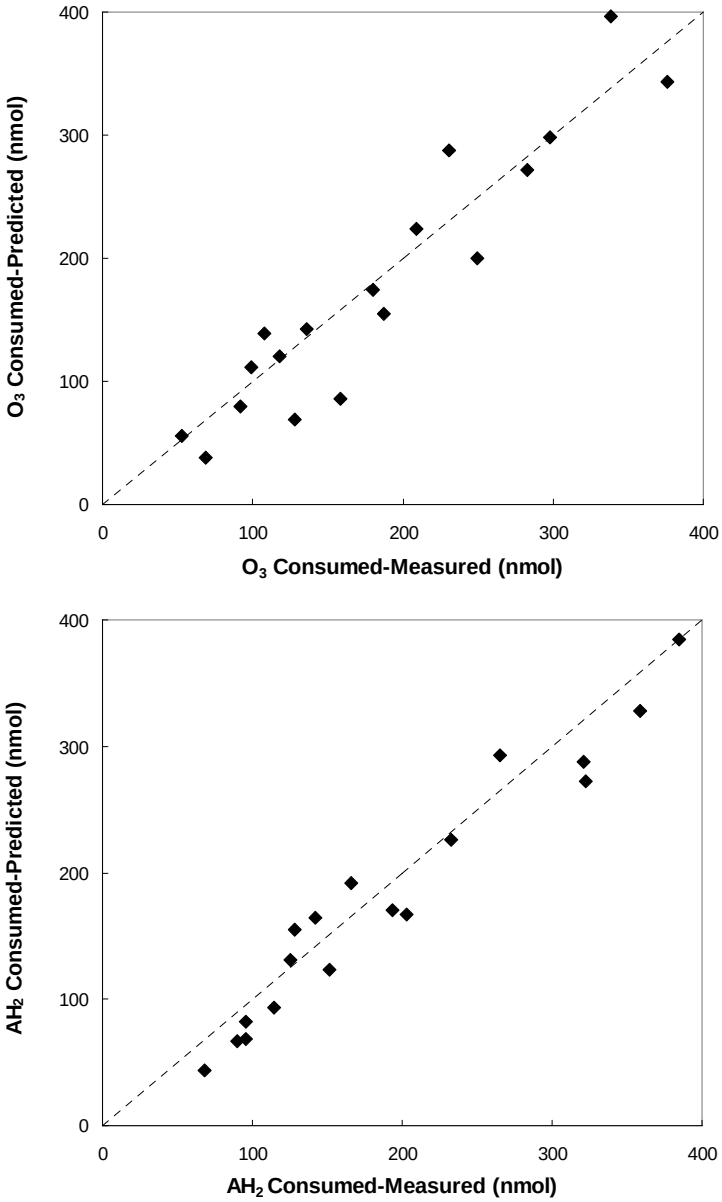

Figure **5-18**: Comparison Between Experimental Data and Corresponding Model Simulations of the Total Amounts of O_3 Absorbed and AH_2 Consumed after 5, 10 , and 15 Minutes.

Top graph illustrates the representative data of total amount of O_3 absorbed after 5,10, and 15 minutes, whereas bottom graph illustrates the total amount of AH_2 consumed after 5, 10, and 15 minutes. Dashed lines represent the line of identity. Performing a least-squared linear regression results in:
Top graph: $Y = (1.043 \pm 0.198)\ X + (-14.843 \pm 40.742)$; Bottom graph: $Y = (0.962 \pm 0.127)\ X + (-4.187 \pm 27.32)$ where ±95% confidence limits have been indicated for each of the coefficients.

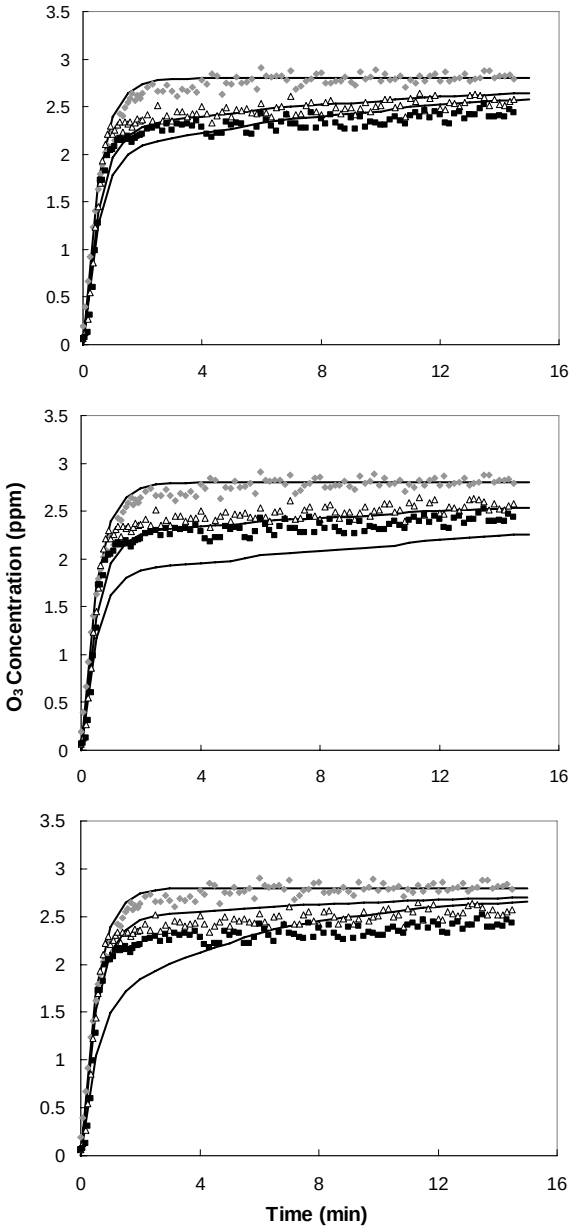

Figure **5-19**: Model Simulations (solid lined) and Experimental Data for O_3 Outlet Concentration in the GSH Experiments.

Graphs show the time course of O_3 output concentration in saline control experiments (♦) and in experiments with initial GSH concentrations of 200 μM (■), 100 μM (Δ). For clarity, only two concentrations (100 and 200 μM) of GSH are shown. A fixed flow of 500 ml/min and a fixed O_3 concentration of 3.0 ppm were employed. In simulations of GSH experiments, alternative kinetic parameters of $m = 0.5; n = 1.25;\ \eta^{O3,S} = 0.4$ (top graph), $m = n = \eta^{O3,S} = 1.0$ (middle graph), and $m = 1.0; n = 2.5;\ \eta^{O3,S} = 0.4$ (bottom graph) were investigated.

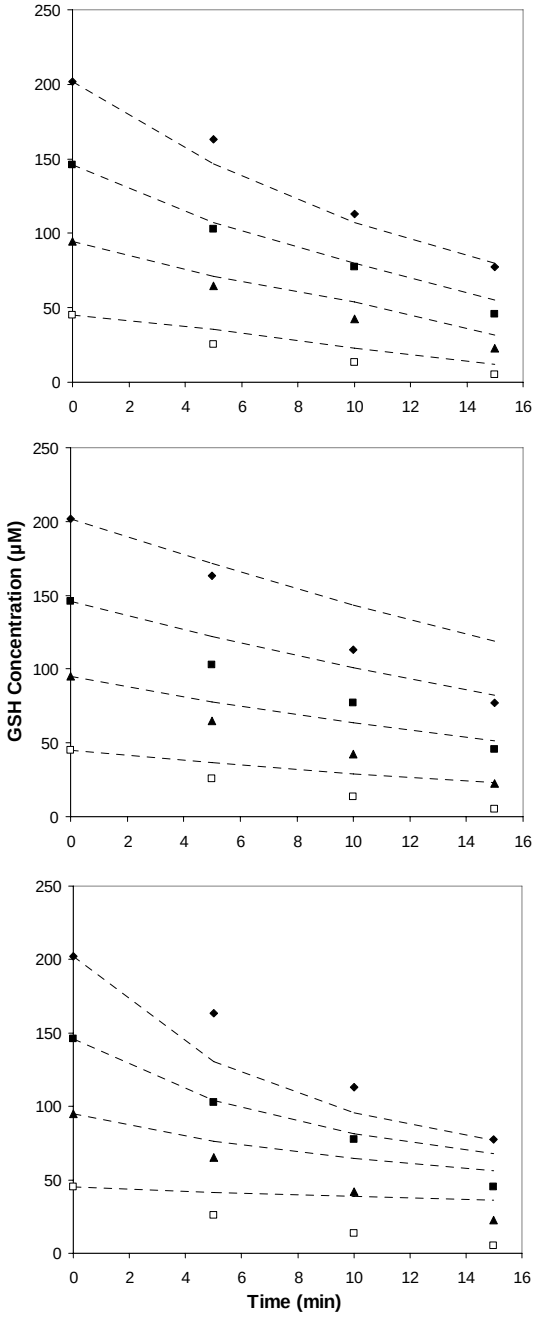

Figure **5-20**: Model Simulations (dashed lined) and Experimental Data for GSH Concentration. Graphs show the time course of GSH concentration in experiments with initial GSH concentrations of 200 µM (♦), 150µM (■), 100 µM (▲), and 50 µM (□). In simulations of GSH experiments, alternative kinetic parameters of $m = 0.5; n = 1.25;\ \eta^{O3,S} = 0.4$ (top graph), $m = n = \eta^{O3,S} = 1.0$ (middle graph), and $m = 1.0; n = 2.5;\ \eta^{O3,S} = 0.4$ (bottom graph) were investigated.

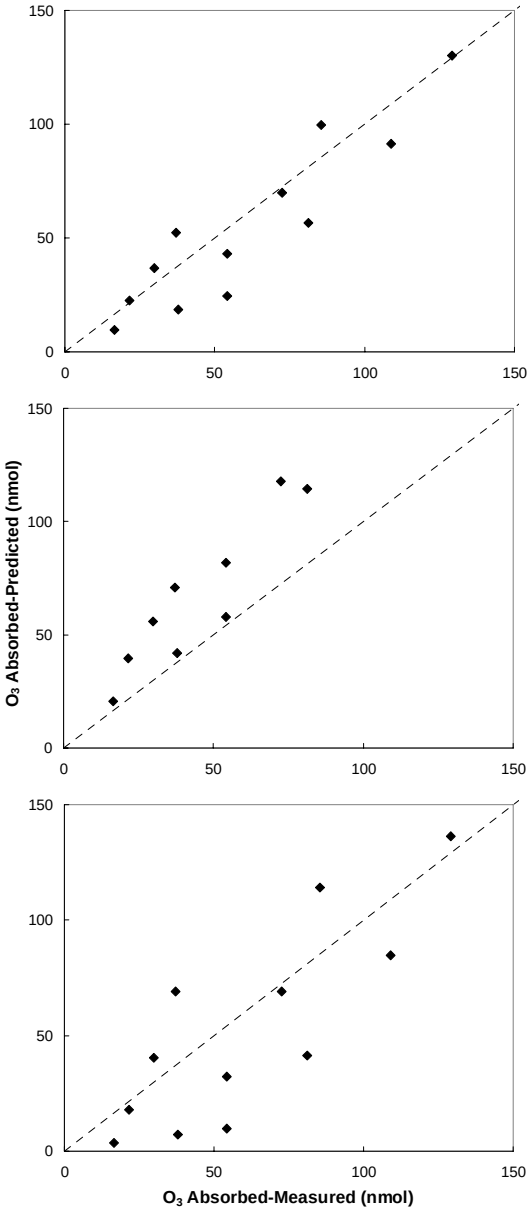

Figure **5-21**: Model Simulations and Experimental Data for O_3 Absorbed after 5, 10, and 15 Minutes in the GSH Experiments.

In simulations of GSH experiments, alternative kinetic parameters of $m = 0.5; n = 1.25;\ \eta^{O3,S} = 0.4$ (top graph), $m = n = \eta^{O3,S} = 1.0$ (middle graph), and $m = 1.0; n = 2.5;\ \eta^{O3,S} = 0.4$ (bottom graph) were investigated. Dashed lines represent the line of identity. Performing a least-squared regression analysis results in:
Top graph: Y = (0.948 ± 0.245) X + (-2.714 ± 16.424); Middle graph: Y = (1.636 ± 0.266) X + (-4.785 ± 18.510); Bottom graph: Y = (0.994 ± 0.497) X + (-8.187 ± 34.577) where ±95% confidence limits have been indicated for each of the coefficients.

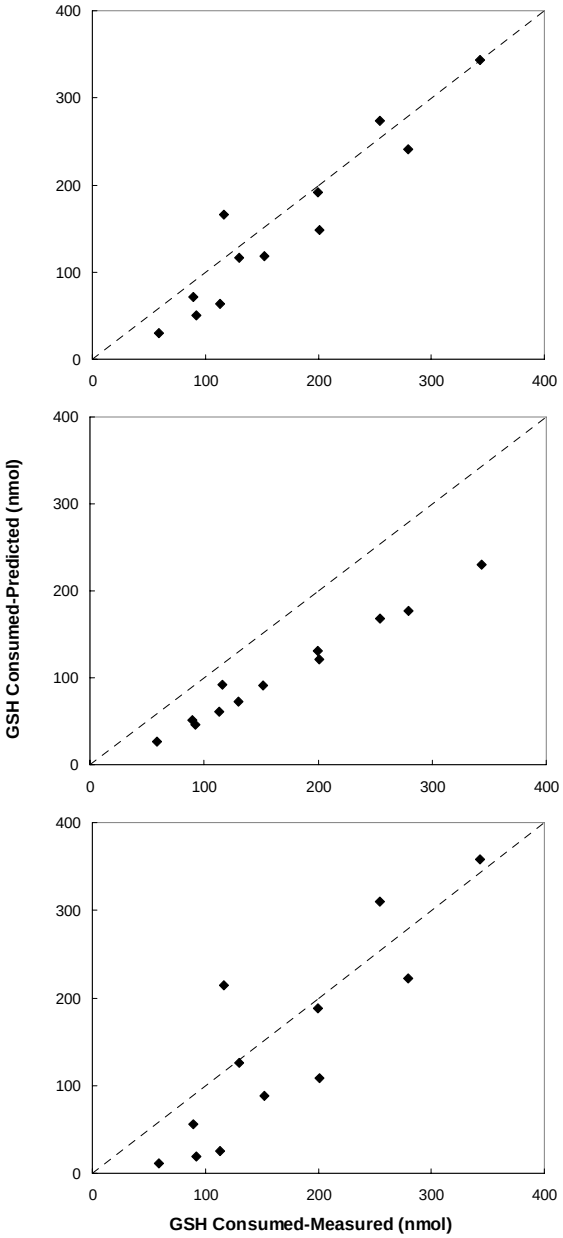

Figure **5-22**: Model Simulations and Experimental Data for the Amount of GSH consumed after 5, 10, and 15 Minutes.

In simulations of GSH experiments, alternative kinetic parameters of $m = 0.5; n = 1.25;\ \eta^{O3,S} = 0.4$ (top graph), $m = n = \eta^{O3,S} = 1.0$ (middle graph), and $m = 1.0; n = 2.5;\ \eta^{O3,S} = 0.4$ (bottom graph) were investigated. Dashed lines represent the line of identity. Performing a least-squared linear regression analysis results in:
Top graph: Y = (1.016 ± 0.202) X + (-19.203 ± 36.751); Middle graph: Y = (0.698 ± 0.067) X + (-12.506 ± 12.695); Bottom graph: Y = (1.145 ± 0.460) X + (-49.793 ± 86.923) where ±95% confidence limits have been indicated for each of the coefficients.

Table **5-1**: Comparison of Reaction Rate Constants to Previous Studies

k_r	UA	$5.8\times10^4\ M^{-1}s^{-1}$	$1.18\times10^4\ M^{-1}s^{-1}$	---	$1.4\times10^6\ M^{-1}s^{-1}$	---
	AH_2	$5.5\times10^4\ M^{-1}s^{-1}$	$1.36\times10^4\ M^{-1}s^{-1}$	$4.8\times10^7\ M^{-1}s^{-1}$	$6.0\times10^7\ M^{-1}s^{-1}$	---
	GSH	[a] $2.3\times10^4\ M^{-1}s^{-1}$ [b] $57.5\ M^{-0.75}s^{-1}$	[a] $4.6\times10^3\ M^{-1}s^{-1}$ [b] $4.94\ M^{-0.75}s^{-1}$	$2.5\times10^6\ M^{-1}s^{-1}$	---	$7.0\times10^8\ M^{-1}s^{-1}$
Reference		Current Study	Mudway & Kelly , 1998[c]	Kanofsky& Sima, 1995	Giamalva, *et al.,* 1985	Pryor, *et al., 1984*
O_3 (ppm)		3	0.1-1.5	20-40	Extremely High	Extremely High
Antioxidant (μM)		50-200	200-400	5,000-100,000	Not Given	Not Given
Reactor Type		Stirred liquid contacted with ozonated air distributed with sintered glass diffuser.	1 ml multiwell plates in a 5.6L chamber on an orbital shaker with 3 Lpm flow of ozonated air	Stagnant liquid contacted with ozonated air through an impinging jet.	Liquid-liquid reaction in stopped flow apparatus	Liquid-liquid reaction in stopped flow apparatus

[a] corresponds to kinetic parameters: $\eta^{O3,S} = m = n = 1.0$; whereas [b] corresponds to $\eta^{O3,S} = 0.4; m = 0.5; n = 1.25$. Note that our findings indicated that the latter results in the closest simulation of the data. Rate constant corresponding to 1:1 stoichiometry is shown for the purpose of comparison to rate constants reported by other research groups.

[c] k_r values have been estimated from the data of Mudway and Kelly (1998) (see Appendix E for details).

Chapter 6

INTERACTION OF ANTIOXIDANTS IN MULTICOMPONENT MIXTURES

This chapter contains the experimental data and mathematical simulations performed to study antioxidant mixtures. The chapter describes experiment conditions such as O_3 concentrations, O_3 flow rate, and antioxidant concentrations used in binary and ternary solutions of UA, AH_2, and GSH. A mathematical model applied to determine the interaction effect of antioxidants in binary mixtures is also described.

6.1 Experimental Design

To study the interaction effect of antioxidants, binary and ternary mixtures containing UA, AH_2, and GSH were exposed to O_3 using the same procedure employed for individual antioxidants. Gas flow rate and inlet O_3 concentration were 500 ml/min and 3 ppm, respectively. The concentration of each antioxidant in the mixtures ranged from 0 to 200μM. Table **6-1** shows the 24 different combinations of UA and AH_2, UA and GSH, and AH_2 and GSH in the binary solutions that were studied.

Table **6-2** shows experimental design for ternary solutions of UA, AH_2, and GSH. 20 different combinations of these three antioxidants were tested. Four different initial GSH concentrations were considered and for each concentration of GSH, four different equimolar combinations of UA+AH_2 were used.

Table **6-1**: Experimental Design for Binary Solutions of UA, AH_2, and GSH.

a(μM) / b(μM)	0	50	100	150	200
0	-	X	X	X	X
50	X	X	X	X	X
100	X	X	X	X	X
150	X	X	X	X	X
200	X	X	X	X	X

*a and b can be UA, AH_2, or GSH. Solutions were prepared using single-component solutions containing 400 μM of UA, AH_2, and GSH.

Table **6-2**: Experimental Design for Ternary Solutions of UA, AH_2, and GSH.

GSH(μM) / AH_2+UA(μM)	50	100	150	200
0	X	X	X	X
100	X	X	X	X
200	X	X	X	X
300	X	X	X	X
400	X	X	X	X

*Equimolar amount of UA and AH_2 were used in UA+AH_2 solutions. Solutions were prepared using pure solutions containing 600 μM of UA, AH_2, and GSH.

6.2 Results

6.2.1 Binary Mixtures

To understand the behavior of one antioxidant in the presence of another, the total amount of each antioxidant consumed in a composite solution after 15 minute O_3 exposure was compared to the amount of antioxidant consumed when it was individually exposed to the same concentration of O_3. All data collected for the binary mixtures in Table **6-1** are presented in Figures **6-1** to **6-3**. Figure **6-1** illustrates the effect of AH_2 on UA (top graph) as well as the effect of UA on AH_2 (bottom graph). The top graph illustrates that when initial UA concentration is held constant, increasing AH_2 concentration causes a decrease in the total amounts of UA consumed. It can be observed that highest amounts of UA consumed are reached when no AH_2 was present in the solution. Similarly, the bottom graph indicates that increasing UA concentration when initial AH_2 concentration is constant decreases depletion of AH_2. Taken together, these two graphs demonstrate that both UA and AH_2 are capable of protecting each other from oxidation when they are exposed to O_3.

Figures **6-2** and **6-3** illustrate the effects of UA and AH_2 on GSH (top graphs) and the effects of GSH on UA and AH_2 (bottom graphs). The top graphs demonstrate that increasing UA and AH_2 concentrations causes a reduction in GSH consumption. The highest amount of GSH consumed is reached when no AH_2 or UA were present in the solution. However, when the initial GSH concentration is small, the amount of GSH consumed level off at UA and AH_2 concentrations of approximately 100 μM. The bottom graphs show that increasing GSH concentration does not have an effect on UA

and AH_2 consumptions. Therefore, it can be concluded that both UA and AH_2 can protect GSH from oxidation when exposed to O_3 whereas GSH does not have as much protective effect on UA and AH_2.

Figure **6-4** shows the total amount of O_3 absorbed in the binary solutions of UA and AH_2 (top), UA and GSH (middle), and AH_2 and GSH (bottom) and compares those to the amount of O_3 absorbed when corresponding antioxidants were individually exposed to O_3. The top graph shows that the total amount of O_3 absorbed in the solution increases as the total concentration of UA and AH_2 increases. The graph also indicates that as long as the total concentration of UA and AH_2 is the same, there is no difference in total O_3 absorption between single-component and binary solutions. For example, the amounts of O_3 absorbed are the same for single-component solutions containing 200 μM of either UA or AH_2. These amounts are also the same as the amounts of O_3 absorbed in binary mixtures containing 150 μM UA and 50 μM AH_2, 50 μM UA and 150 μM AH_2, and 100 μM UA and 100 μM AH_2. This demonstrates that when it comes to O_3, the behaviors of UA and AH_2 are almost identical. This can be explained by the fact that both of these antioxidants have 1:1 stoichiometry and their reaction rate constants are similar.

The middle and bottom graphs of Figure **6-4** show that as total concentrations of UA and GSH, and AH_2 and GSH increase, the total amounts of O_3 absorbed also increases. Contrary to what was observed in the top graph, however, the total amounts of O_3 absorbed in these mixtures were dependent on the composition of the mixture. Different stoichiometries and reaction rate constants for reaction of O_3 with GSH and UA/AH_2 explains these findings.

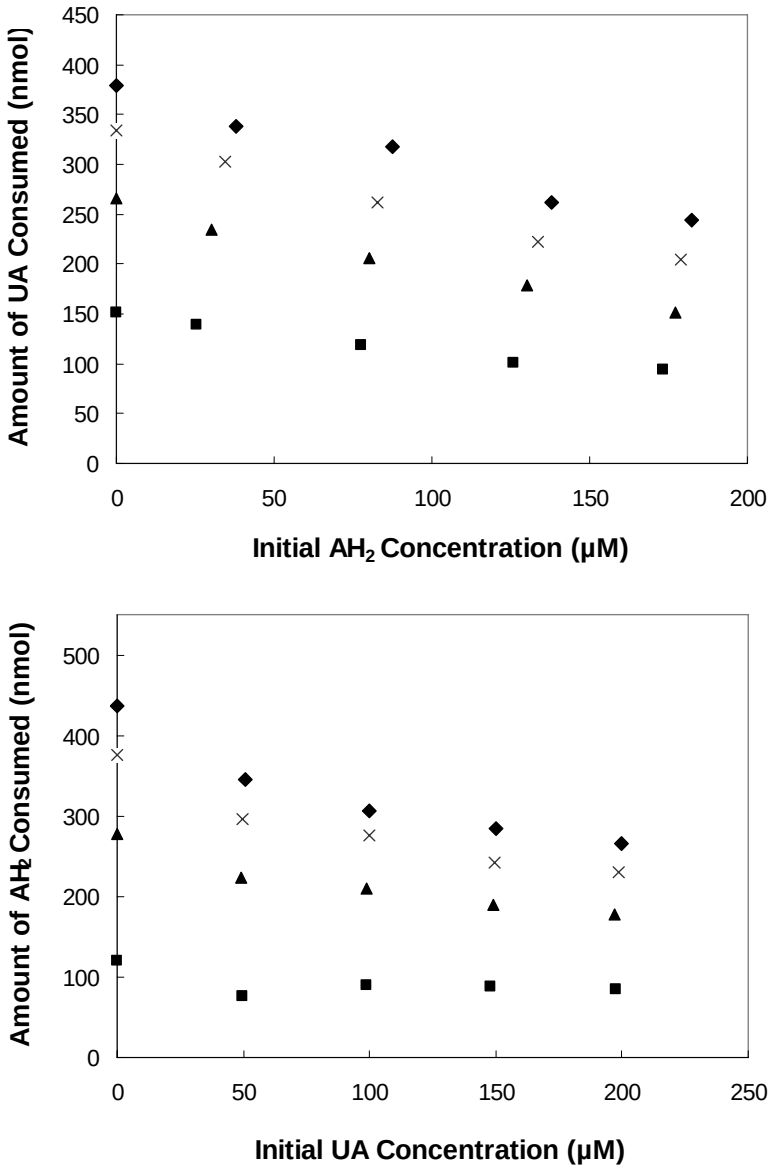

Figure **6-1**: Amounts of UA and AH_2 Consumed in Binary Solution After 15 Minutes of Exposure to 3.30 ppm O_3.

Top graph shows the effect of AH_2 concentration on the total amount of UA consumed in the experiments with initial UA concentrations of 200 µM (♦), 150 µM (×), 100 µM (▲), and 50 µM (■). Bottom graph shows the effect of UA concentration on the total amount of AH_2 consumed in the experiments with initial AH_2 concentrations of 200 µM (♦), 150 µM (×), 100 µM (▲), and 50 µM (■).

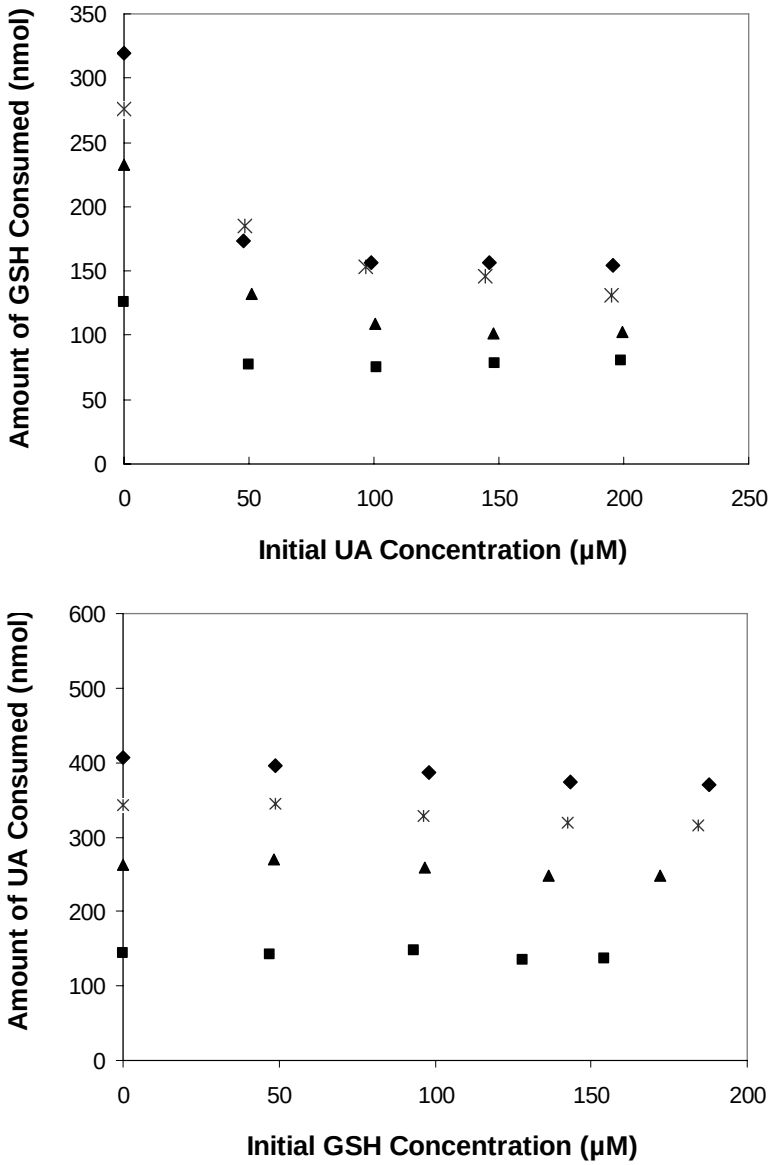

Figure **6-2**: Amounts of GSH and UA Consumed in Binary Solutions After 15 Minutes of Exposure to 3.30 ppm O_3.

Top graph shows the effect of UA concentration on the total amount of GSH consumed in the experiments with initial GSH concentrations of 200 µM (♦), 150 µM (×), 100 µM (▲), and 50 µM (■). Bottom graph shows the effect of GSH concentration on the total amount of UA consumed in the experiments with initial UA concentrations of 200 µM (♦), 150 µM (×), 100 µM (▲), and 50 µM (■).

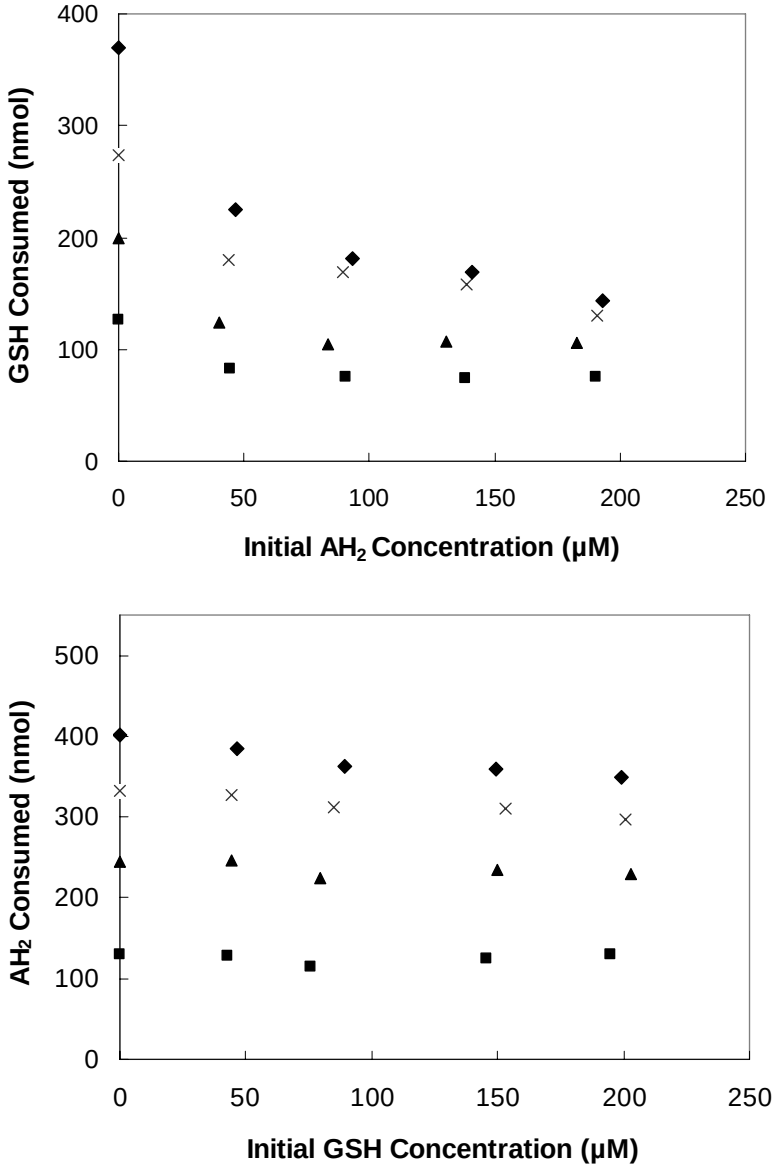

Figure **6-3**: Amounts of GSH and AH_2 Consumed in Binary Solution After 15 Minutes of Exposure to 3.30 ppm O_3.

Top graph shows the effect of AH_2 concentration on the total amount of GSH consumed in the experiments with initial GSH concentrations of 200 μM (♦), 150 μM (×), 100 μM (▲), and 50 μM (■). Bottom graph shows the effect of GSH concentration on the total amount of AH_2 consumed in the experiments with initial AH_2 concentrations of 200 μM (♦), 150 μM (×), 100 μM (▲), and 50 μM (■).

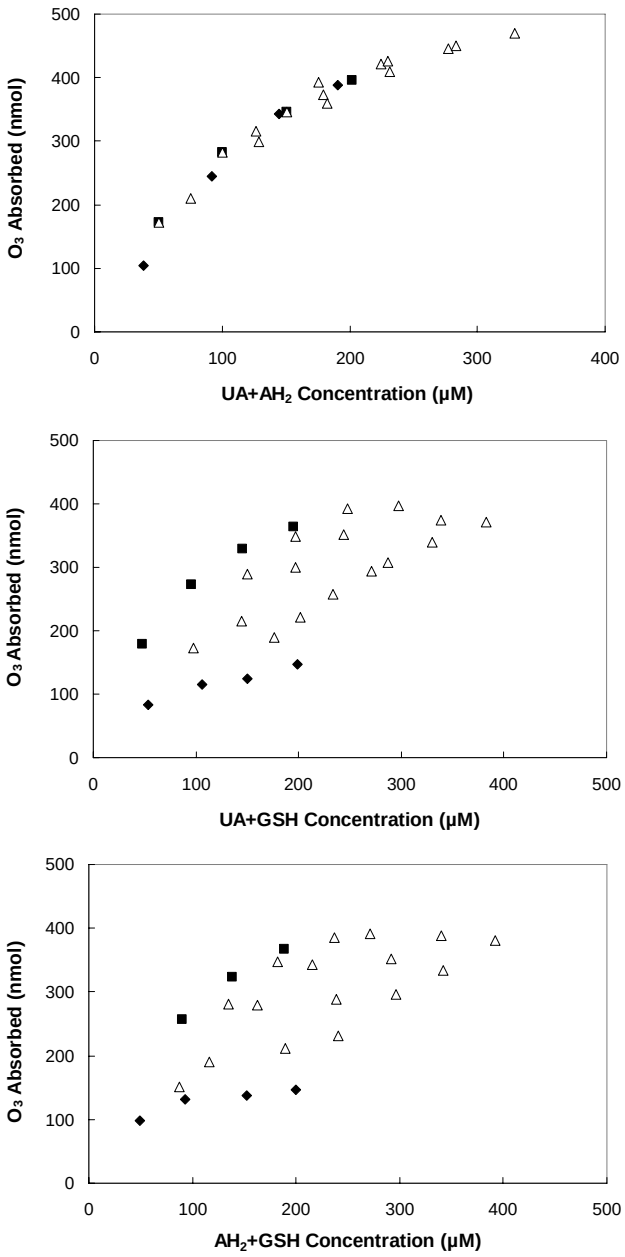

Figure **6-4**: Amounts of O_3 Absorbed in Binary Mixtures of UA+AH_2, UA+GSH, and AH_2+GSH and their Corresponding Single-Component Solutions After 15 Minutes of Exposure to O_3.

Top graph shows the amount of O_3 absorbed in the solution containing UA (■), AH_2 (♦), or the mixture of these two antioxidants (Δ). Middle graph shows the amount of O_3 absorbed in the solution containing UA (■), GSH (♦), or the mixture of these two antioxidants (Δ).Bottom graph shows the amount of O_3 absorbed in the solution containing AH_2 (■), GSH (♦), or the mixture of these two antioxidants (Δ).

6.2.2 Ternary Mixtures

In the study of binary mixtures, it was observed that UA and AH_2 influence GSH consumption in a similar manner, but GSH does not have much of an effect on the ozonation of UA and AH_2. In the ternary experiments, equimolar mixtures of UA and AH_2 were added to the GSH solution to determine if the mixtures of UA and AH_2 have the same effect on GSH consumption as UA and AH_2 alone. All data collected for the ternary mixtures identified in Table **6-2** are presented in Figure **6-5**. Figure **6-5** shows that when initial GSH concentrations are constant, the amount of GSH consumed initially decreases as the concentrations of UA+AH_2 increase. However, the amount of GSH consumed begins to increase after the concentration of UA+AH_2 reach approximately 200 μM. The possibility of reaction of GSH with oxidation products derived from O_3 oxidation of UA or AH_2, especially when higher concentrations of these two antioxidants were employed, may explain this finding. Comparing Figure **6-5** with top graphs in Figures **6-2** and **6-3** indicates that there is not much of a difference between binary and ternary mixtures up to a UA+AH_2 concentration of 200 μM. This can be explained by the fact that UA and AH_2 do not interact with each other and they both have the same effect on GSH when they individually introduced to GSH solution.

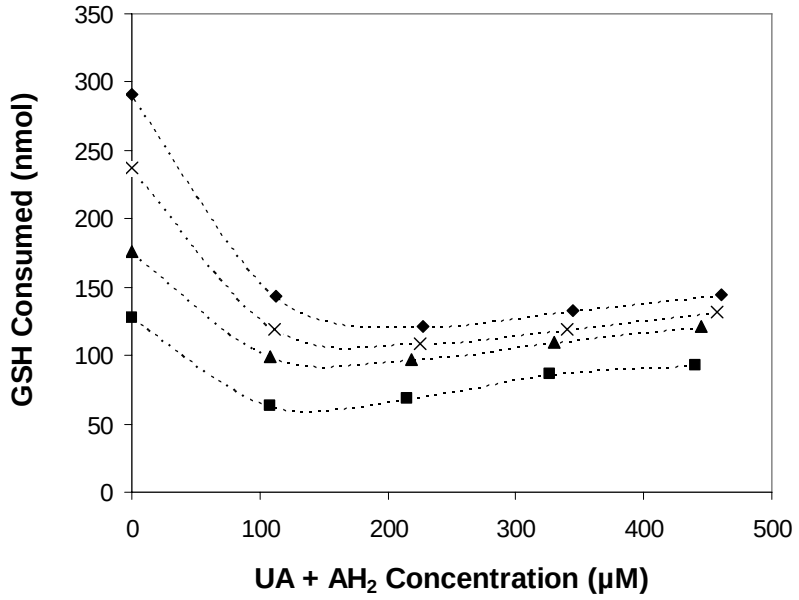

Figure **6-5**: Effect of UA and AH_2 on the Amount of GSH Consumed after 15 Minutes Exposure to 3.30 ppm O_3.

The graph shows the effect of UA+AH_2 concentration on the total amount of GSH consumed in the experiments with initial GSH concentrations of 200 µM (♦), 150 µM (×), 100 µM (▲), and 50 µM (■).

6.3 Discussion

In the previous chapter, only individual single-component antioxidant solutions were studied. Because respiratory mucus contains a multicomponent mixture of such compounds, we wished to investigate the possible interaction effect when multiple antioxidants are exposed to O_3. In particular, we wanted to determine whether the reaction rate of each antioxidant in the mixture can be predicted from their individual reaction rates determined in chapter 5.

The results indicated that both UA and AH_2 are preferred substrates compared to GSH. Therefore, when exposed to O_3, UA and AH_2 are both capable of reducing GSH consumption. On the other hand, the presence of GSH did not attenuate the total consumption of UA and AH_2. Our results also indicated that consumption of UA and AH_2 are affected by the presence of one another so they are both capable of protecting each other against O_3.

Studies investigating the interaction effect of antioxidants in multicomponent mixtures are not abundant in the literature. Cross and colleagues (1992) studied the reaction of O_3 with substrates present in the human blood plasma. Their results illustrated that UA and AH_2 were oxidized more quickly compared to other substrates and therefore they are the major scavenger of O_3 in the plasma. These investigators also showed that the more oxidizable material is present in plasma, the more O_3 will be absorbed to react with this material. In contrast to our finding, Cross and colleagues indicated that adding extra ascorbate did not slow down the loss of UA, nor did adding extra UA alter the loss of AH_2 when the liquids were exposed to 16 ppm O_3 for 1 hour.

Van der Vliet and coworkers (1995) also utilized blood plasma to investigate the reaction of plasma antioxidants with O_3. Their results illustrated that ascorbate, urate and GSH, to a lesser degree, are the most important plasma constituents that absorb O_3. Similar to our results, they demonstrated that addition of GSH to plasma (at concentrations up to 1 mM) prior to O_3 exposure, did not significantly attenuate depletion rates of ascorbate and urate. Thus, GSH was completely ineffective at protecting these two antioxidants. Their results also indicated that depletion of GSH by O_3 was slightly inhibited by ascorbate (Van der Vliet et al., 1995). Kanofsky and Sima (1995) also showed that addition of GSH to an AH_2 solution failed to inhibit the rate of reactive absorption of AH_2.

Mudway and Kelly (1996) used bronchoalveolar lavage (BAL) fluid which contains UA, AH_2, and GSH to determine the relative importance of antioxidants present in BAL as substrate for O_3. They illustrated that GSH did not represent a significant substrate for O_3, whereas AH_2 was the most important scavenger of O_3. They suggested a reactivity hierarchy of $AH_2 \rangle UA \gg GSH$ toward O_3 in human ELF.

Mudway and Kelly (1998) studied the antioxidant consumption rates in composite mixtures containing UA, AH_2, and GSH. They concluded that the overall relationships between antioxidant consumption rates in composite solutions are similar with those observed in single antioxidant solutions. Their results suggested an overall antioxidant reactivity hierarchy of $UA \rangle AH_2 \rangle GSH$ within the composite model. Comparing the overall antioxidant consumption rates in the composite model with the single antioxidant model, they observed a reduction in the consumption rates of all antioxidants in the

composite model. In other words, individual antioxidant consumption rates decreased as model complexity increased.

It is surprising that the impact of such multicomponent interaction effects on the structure of kinetic rate equations has not yet been investigated. As a first step in this direction, we utilized a combination of experimental analyses and numerical simulations applied to binary mixtures of UA and AH_2. As discussed earlier, UA and AH_2 can attenuate the consumption rate of one another up to an average of 35 % and are equally capable of protecting one other against O_3. Protection can be caused by competition between antioxidants for a limited supply of O_3, or by molecular interactions that modify the rates of the individual reaction steps.

First, we hypothesized that competition is the only factor causing the decrease in antioxidants consumptions. In that case, the stoichiometries and reaction rate constants for reaction of O_3 with individual antioxidants in the mixture are the same as corresponding values for single solutions of antioxidants. Considering these assumptions, Equation **4.6** for reaction rate of O_3 may be written as:

$$\dot{R}_{O3} = k_{r,UA}\, C_{O3,1}\, C_{UA} + k_{r,AH_2}\, C_{O3,1}\, C_{AH_2} \qquad (\mathbf{6.1})$$

Equation **4.1** may also be rewritten to account for both UA and AH_2.

$$\frac{dC_{UA}}{dt} = -k_{r,UA}\, C_{O3,1}\, C_{UA} \quad ; \quad \frac{dC_{AH_2}}{dt} = -k_{r,AH_2}\, C_{O3,1}\, C_{AH_2} \qquad (\mathbf{6.2})$$

where $k_{r,UA}$ and k_{r,AH_2} are individual reaction rate constants determined in Chapter 5. Equations **6.1**, **6.2**, **4.4**, **4.8**, and **4.10** were used to simulate the experimental data.

Figure **6-6** is a comparison between the experimental data obtained at the different binary compositions of UA+AH_2 solutions and the corresponding model simulations of O_3 absorbed and antioxidants consumed. Provided that there is no difference between experimental data and the corresponding model predictions, a linear regression between the two should be equivalent to a line of identity. As can be seen from the information in the figure caption, the slopes of the regression were not significantly different from 1.0 and the intercepts were not significantly different from zero. We thus conclude that the reaction rates between O_3 and binary solutions of UA and AH_2 can be adequately explained purely on the basis of competitive kinetics.

We used a similar procedure to study the protective effect of UA and AH_2 on GSH. We first assumed that there is no molecular interaction between UA and GSH, and between AH_2 and GSH, and that stoichiometries and reaction rate constants for UA, AH_2, and GSH in the mixture are the same as corresponding values found for the single-component solutions. In that case, we can write Equation **4.6** for reaction rate of O_3 as follows:

$$\dot{R}_{O3} = k_{r,S}\, C_{O3,1}\, C_S + 0.4\; k_{r,GSH}\, C_{O3,1}^{0.5}\, C_{GSH}^{1.25} \qquad (\mathbf{6.3})$$

Equation **4.1** may also be rewritten for either UA or AH_2 and GSH as:

$$\frac{dC_S}{dt} = -k_{r,S}\, C_{O3,1}\, C_S \quad ; \quad \frac{dC_{GSH}}{dt} = -k_{r,GSH}\, C_{O3,1}^{0.5}\, C_{GSH}^{1.25} \qquad (\mathbf{6.4})$$

where S represents UA in a binary mixture of UA and GSH, or AH_2 in a mixture of AH_2 and GSH. Solutions of Equations **6.4**, **6.3**, **4.4**, **4.8**, and **4.10** failed to provide a good simulation of experimental data. This failure was especially apparent for the predicted amounts of GSH consumed. We conclude that competition among antioxidants to react with O_3 is not the only cause of decreasing the consumption of GSH.

Our data demonstrated that UA and AH_2 could attenuate the consumption of GSH up to an average of 50%, but GSH was only able to decrease UA and AH_2 consumption by less than 8 %. Considering these findings, we tried an alternative procedure in which the reaction rate of both UA and AH_2 were maintained at their single-component values, but the reaction rate constant of GSH in the mixture was expressed as follows:

$$\left(k_{r,GSH}\right)_{mixture} = (1-\alpha)k_{r,GSH} \qquad (\mathbf{6.5})$$

where α is a binary interaction parameter that depends on the concentration of the second antioxidant in the mixture, and $k_{r,GSH}$ is the rate constant of GSH in a single-component solution. Note that α=0 corresponds to when GSH is the only antioxidant in the solution and therefore, there is no interaction effect. Substituting Equation **6.5** in **6.3** and **6.4** results in the following equations:

$$\dot{R}_{O3} = k_{r,S}\, C_{O3,1}\, C_S + 0.4\,(1-\alpha)\, k_{r,GSH}\, C_{O3,1}^{0.5}\, C_{GSH}^{1.25} \qquad (\mathbf{6.6})$$

$$\frac{dC_S}{dt} = -k_{r,S}\, C_{O3,1}\, C_S \quad ; \quad \frac{dC_{GSH}}{dt} = -(1-\alpha)\, k_{r,GSH}\, C_{O3,1}^{0.5}\, C_{GSH}^{1.25} \qquad (\mathbf{6.7})$$

where S represents either UA or AH_2, depending on the binary mixture that was considered. The optimal α for each concentration of UA or AH_2 was determined with a procedure similar to the one used for determining the reaction rates of individual antioxidants, in which the squared-error between the observed amounts of O_3 absorbed

and antioxidant consumed and their simulated values was minimized. Figure **6-7** shows the interaction parameter for UA-GSH (top graph) and AH_2-GSH (bottom graph) solutions. Individual α values on the graph correspond to when several experiments at different GSH concentrations but at a fixed UA or AH_2 concentration were applied. Graphs indicate that interaction parameters are indeed a function of UA in UA and GSH mixtures, and a function of AH_2 in the mixtures AH_2 and GSH.

Comparisons of the model simulations when α is equal to its optimal value and when α is equal to zero to the experimental data for mixtures of UA and GSH, and AH_2 and GSH are shown in Figures **6-8** to **6-11**. Figures **6-8** and **6-9** focus on GSH consumption in the presence of UA or AH_2, respectively. The model simulations with the optimal value of the binary interactions included (top graphs) were noticeably better than the simulations without an interaction effect (bottom graphs). Figures **6-10** and **6-11** present the time course of outlet O_3 concentration in representative UA-GSH, and AH_2-GSH mixtures, respectively. Again, inclusion of an interaction effect (uninterrupted curves) improves the simulation relative to the case where no interaction is present (interrupted curves).

Figures **6-12** to **6-14** are cross-plots of experimental measurements and simulations. The general impression from all these graphs is that the inclusion of binary interactions in the simulations (filled points) reduce scatter and bring the points closer to a line of identity. The results of least-squared regression analyses given in the figure captions can be used to reach this conclusion in an objective manner. First, with few exceptions, the slope coefficient is closer to one and the intercept coefficient is closer to zero when interactions are taken into account. Second, the confidence intervals about

these coefficients are generally smaller when a binary interaction is employed. Taking these factors in to account, it can be concluded that the use of a binary interaction improves the ability of the model to simulate the data.

In summary, the interaction effects of antioxidants in mixtures of UA, AH_2, and GSH were studied. Our results indicated that UA and AH_2 consumption decreased in the presence of one another, suggesting that these antioxidants can protect each other against O_3. This protective effect was mostly due to the competitive reaction of UA and AH_2 toward O_3. Numerical simulations were able to predict the experimental behavior of mixtures containing both UA and AH_2. Our results also illustrated that both UA and AH_2 can attenuate the depletion of GSH, whereas GSH does not have the same effect on UA and AH_2. It was found that the competition between UA or AH_2 and GSH was not the only factor which decreases a consumption of GSH. To obtain effective reaction rate constants for GSH in mixtures of UA-GSH and AH_2-GSH, an interaction parameter was introduced in the model. This parameter was established to be a function of either UA or AH_2. By employing the interaction parameter and therefore obtaining the effective rate constants for GSH, simulation results can more successfully match the experimental data. Studying the ternary mixtures in which equimolar concentrations of UA and AH_2 were added to GSH solution demonstrated the same findings observed in binary experiments, namely that presence of UA and AH_2 simultaneously in the mixture decreased GSH consumption.

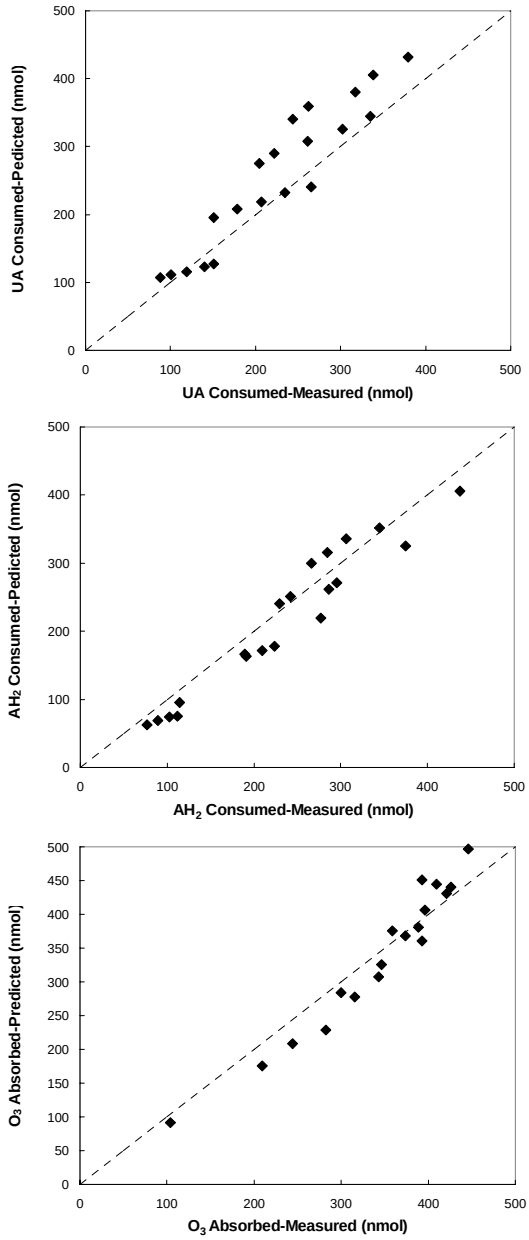

Figure **6-6**: Experimental Data and Model Simulations of O_3 Absorbed and Antioxidant Consumed After 15 Minutes of Exposure to O_3.

The total amounts of UA and AH_2 consumed, and O_3 absorbed are illustrated in top, middle and bottom graphs, respectively. Dashed lines represent the line of identity. A linear least-squared regression analysis results in:
Top graph: Y= (1.167 ± 0.169) X + (-5.227 ± 39.724); Middle graph: Y= (1.001 ± 0.117) X + (-17.424 ± 28.861)
Bottom graph: Y= (1.104 ± 0.127) X + (-38.762 ± 43.541) where ±95% confidence limits have been indicated for each of the coefficients.

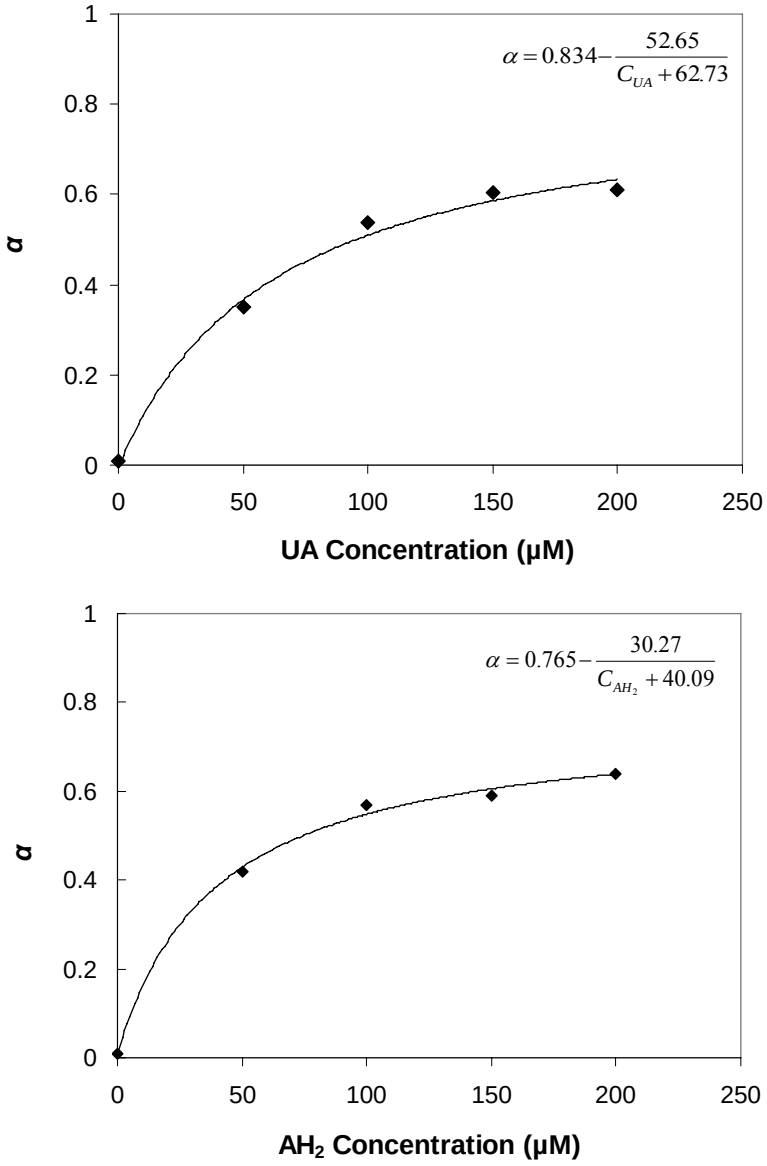

Figure **6-7**: Interaction Parameter for UA-GSH and AH_2-GSH Solutions.

Top graph represents the interaction parameter for mixture of UA and GSH, whereas bottom graph shows the interaction parameter for mixture of AH_2 and GSH. α=0 corresponds to when GSH was the only antioxidant in the solution and therefore, there was no interaction effect. Equations in each graph are empirical equations which fit the data.

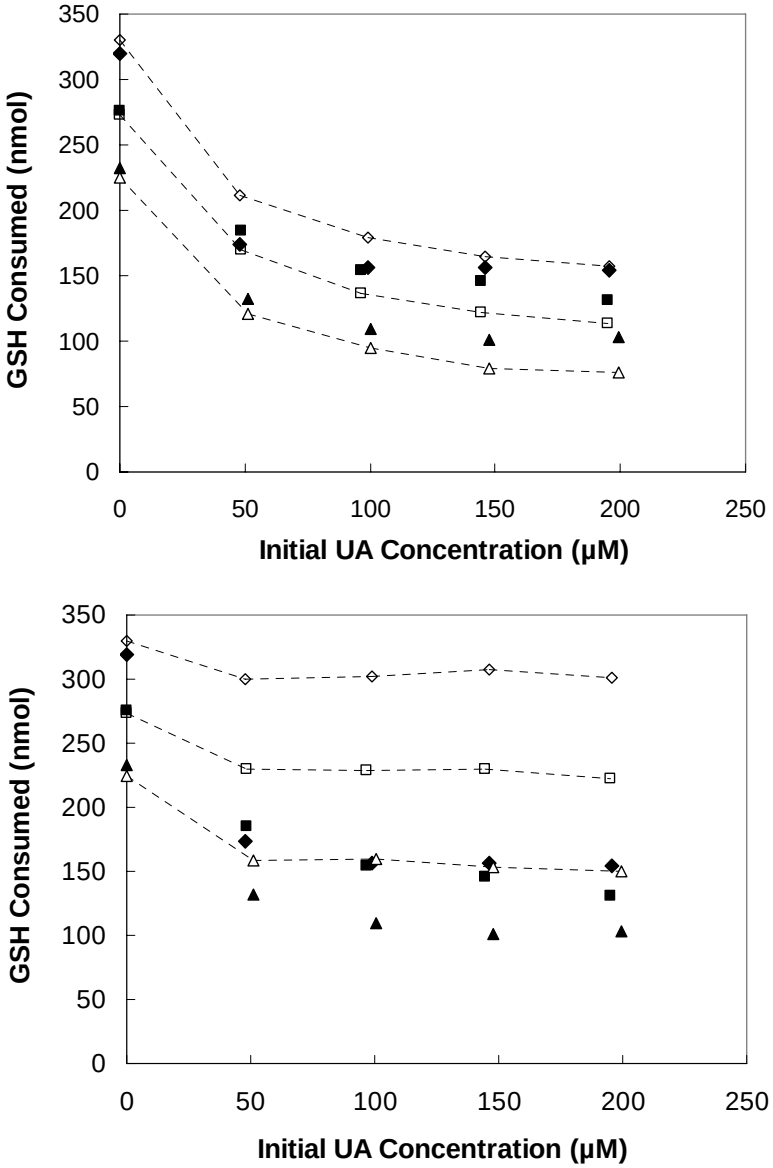

Figure **6-8** Experimental Data and Model Simulations of GSH Consumed in the Presence of UA.

Representative data illustrate the model simulations (dashed lines with open symbols) and experimental data for a fixed flow of 500 ml/min and a fixed O_3 concentration of 3.3 ppm in experiments with initial GSH Concentrations of 200 µM (♦,◊), 150 µM (■,□), and 100 µM (▲,Δ). Top graph shows the model simulations when $\alpha \neq 0$, whereas bottom graph shows simulations when $\alpha = 0$.

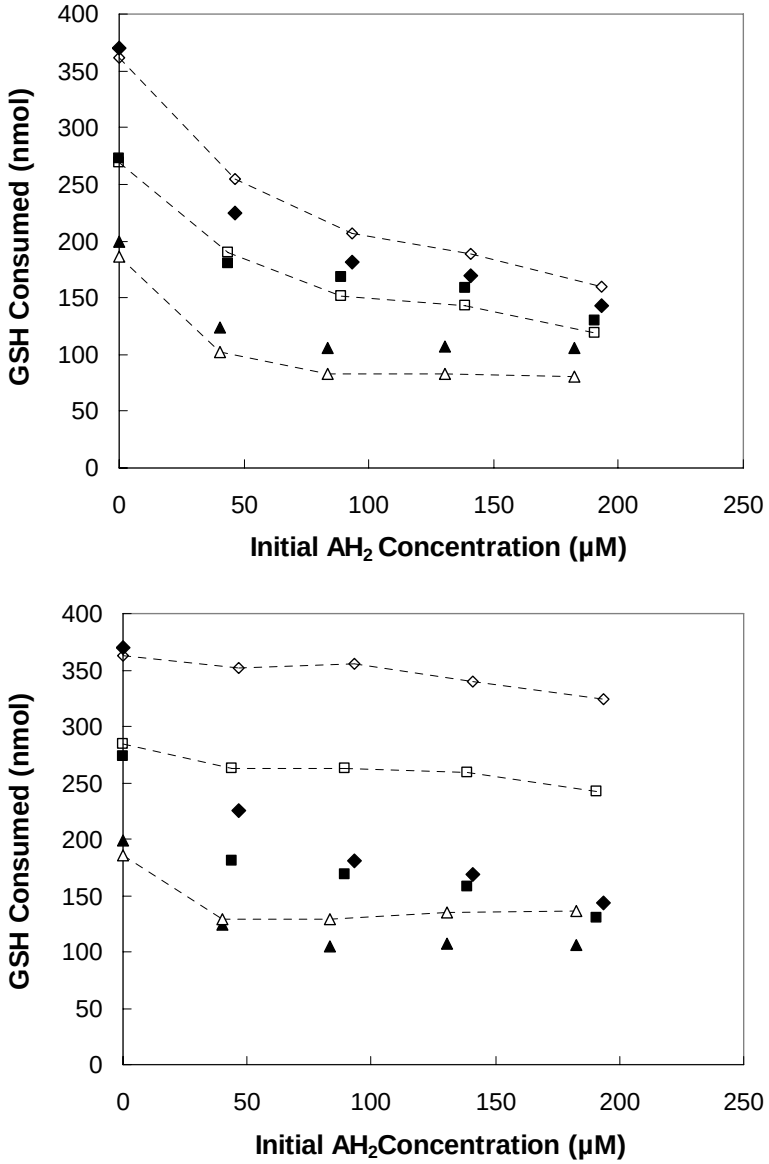

Figure **6-9**: Experimental Data and Model Simulations of GSH Consumed in the Presence of AH_2.

Representative data illustrate the model simulations (dashed lines with open symbols) and experimental data for a fixed flow of 500 ml/min and a fixed O_3 concentration of 3.3 ppm in experiments with initial GSH Concentrations of 200 µM (♦,◊), 150 µM (■,□), and 100 µM (▲,Δ). Top graph shows the model simulations when $\alpha \neq 0$, whereas bottom graph shows simulations when $\alpha = 0$.

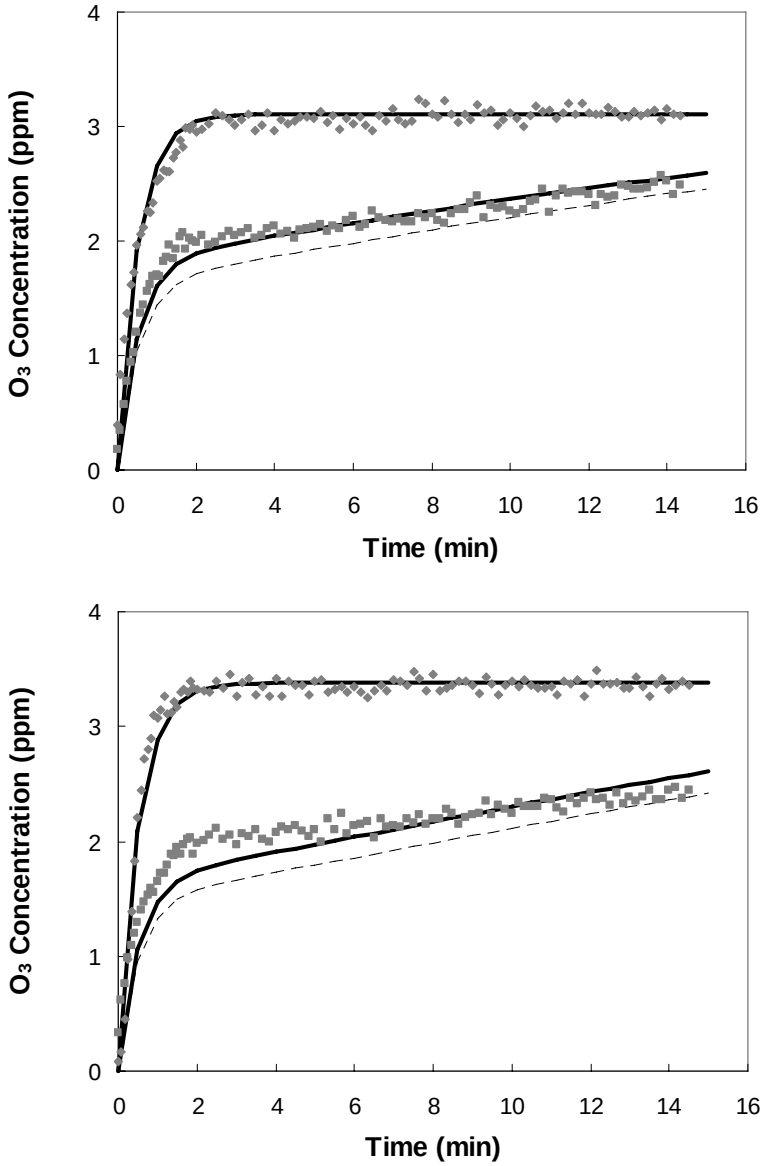

Figure **6-10**: Experimental Data and Model Simulations of the Time Course of O_3 Outlet Concentration in a Mixture of UA and GSH.

Representative data illustrate the model simulations (solid or dashed lines) and experimental data for a fixed flow of 500 ml/min and a fixed O_3 concentration of 3.3 ppm. Solid lines show simulations when $\alpha \neq 0$, whereas dashed lines shows simulations when $\alpha = 0$. (♦) corresponds to O_3 output concentration in saline control experiments and (■) corresponds to that in experiments with mixtures of UA and GSH (top graph: UA=100 μM and GSH=150 μM; bottom graph: UA=150 μM and GSH=100 μM)

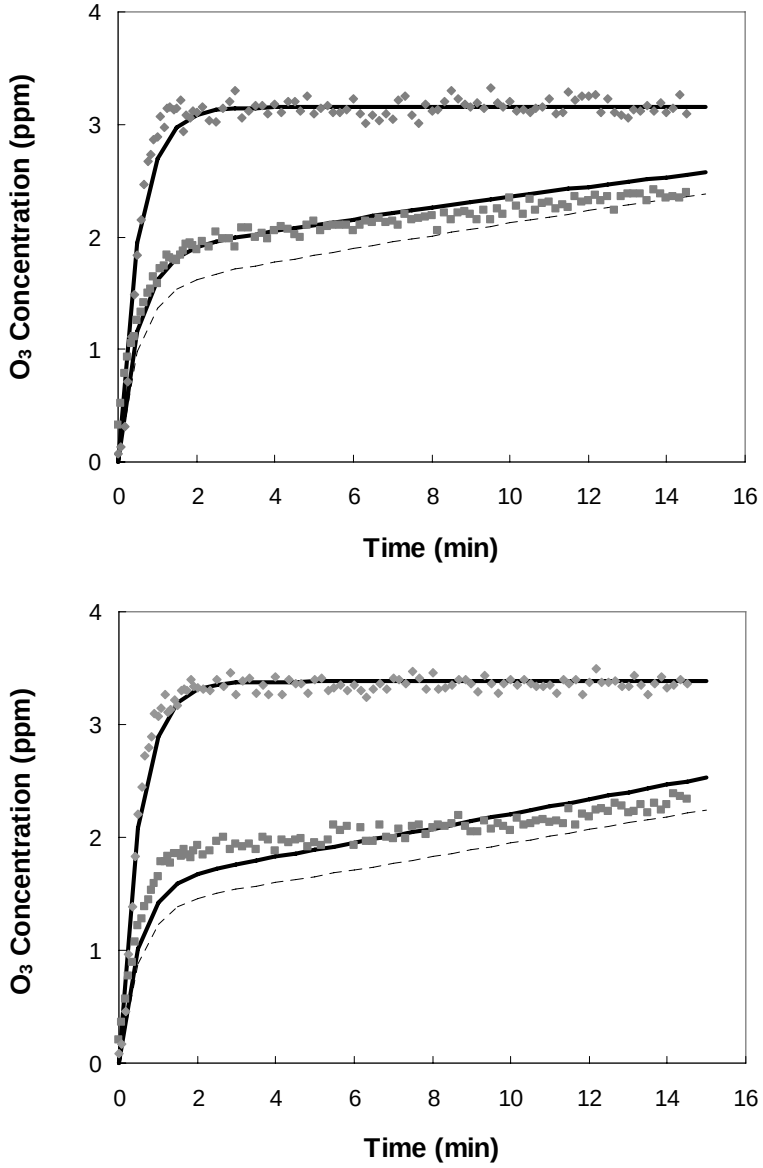

Figure **6-11**: Experimental Data and Model Simulations of the Time Course of O_3 Outlet Concentration in a Mixture of AH_2 and GSH.

Representative data illustrate the model simulations (solid or dashed lines) and experimental data for a fixed flow of 500 ml/min and a fixed O_3 concentration of 3.3 ppm. Solid lines show simulations when $\alpha \neq 0$, whereas dashed lines shows simulations when $\alpha=0$. (♦) corresponds to O_3 output concentration in saline control experiments and (■) corresponds to that in experiments with mixtures of UA and GSH (top graph: AH_2=100 μM and GSH=200 μM; bottom graph: AH_2=200 μM and GSH=100 μM)

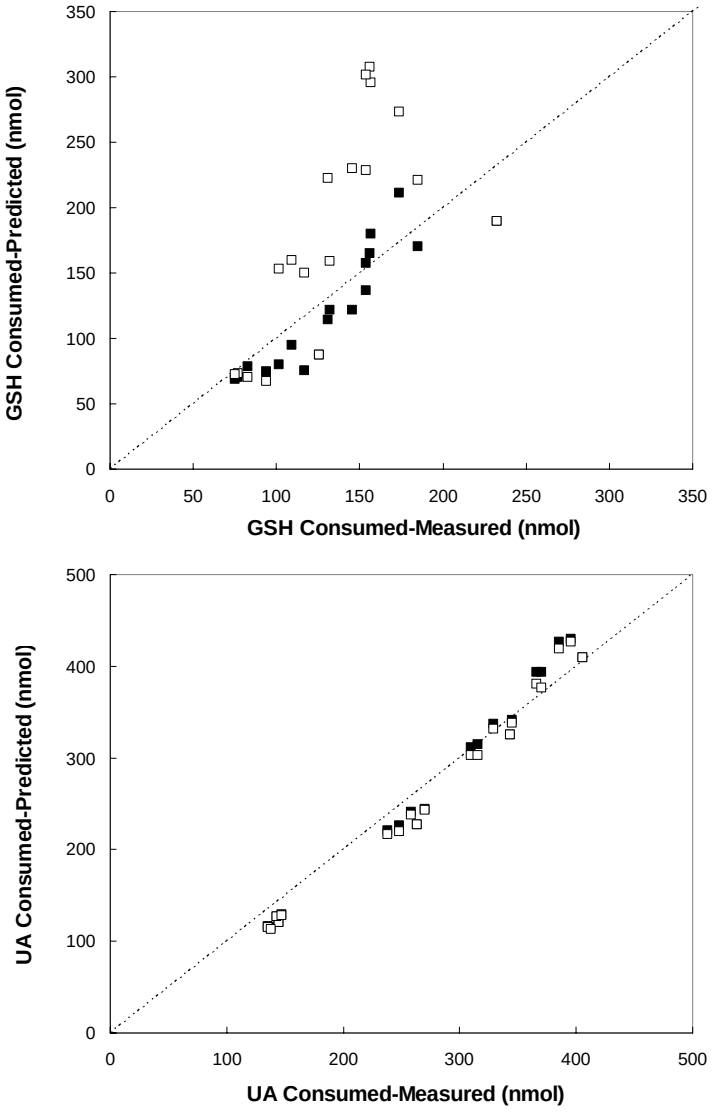

Figure **6-12**: Experimental Data and Model Simulations of Antioxidants Consumed After 15 Minutes Exposure of a UA-GSH Mixture to O_3.

The total amounts of GSH and UA consumed are illustrated in top and bottom graphs, respectively. (■) corresponds to simulations when $\alpha \neq 0$, whereas (□) corresponds to that when $\alpha = 0$. Dashed lines represent the line of identity. Linear least-squared regression analyses results in:

Top graph:

$\alpha \neq 0$: $Y = (0.979 \pm 0.206)\ X + (-8.203 \pm 28.005)$

$\alpha = 0$: $Y = (1.433 \pm 0.771)\ X + (-10.112 \pm 107.456)$

Bottom graph:

$\alpha \neq 0$: $Y = (1.010 \pm 0.076)\ X + (-34.711 \pm 21.734)$

$\alpha = 0$: $Y = (1.145 \pm 0.071)\ X + (-49.904 \pm 20.827)$

where ±95% confidence limits have been indicated for each of the coefficients.

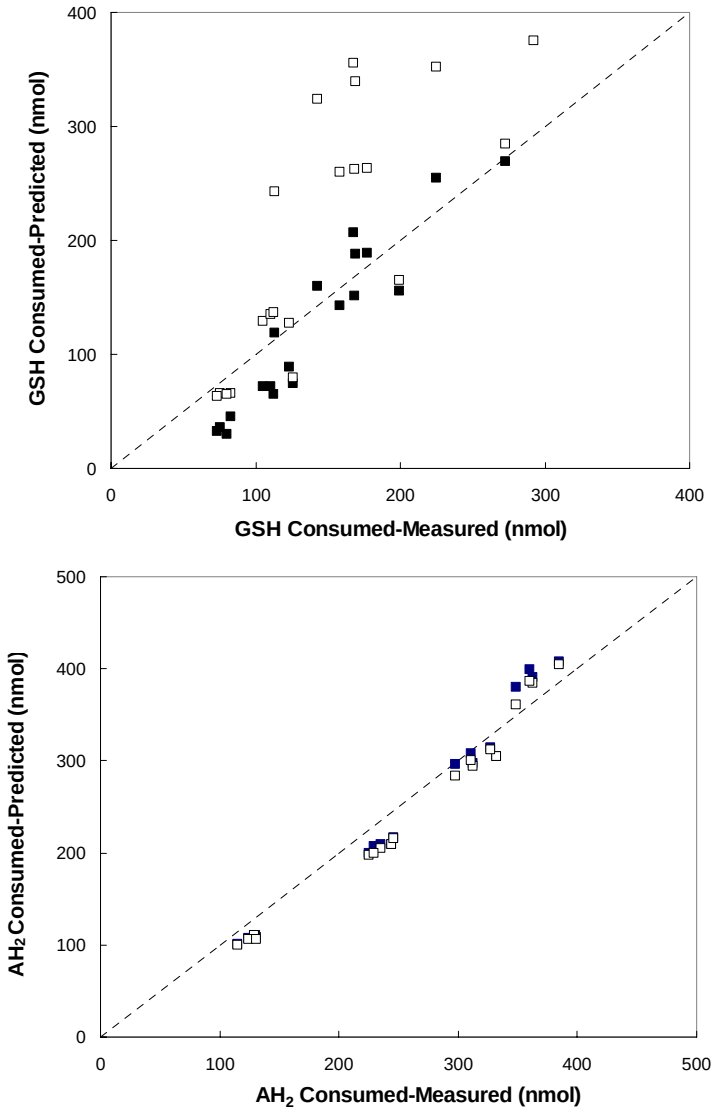

Figure **6-13**: Experimental Data and Model Simulations of Antioxidants Consumed After 15 Minutes Exposure of AH_2-GSH Mixtures to O_3.

The total amounts of GSH and AH_2 consumed are illustrated in top and bottom graphs, respectively. (■) corresponds to simulations when $\alpha \neq 0$, whereas (□) corresponds to that when $\alpha = 0$. Dashed lines represent the line of identity. Linear least-squared regression analyses results in:

Top graph:

$\alpha \neq 0$: $Y = (1.198 \pm 0.214)\ X + (-43.176 \pm 31.511)$

$\alpha = 0$: $Y = (1.488 \pm 0.686)\ X + (-14.691 \pm 103.426)$

Bottom graph:

$\alpha \neq 0$: $Y = (1.097 \pm 0.089)\ X + (-23.693 \pm 26.403)$

$\alpha = 0$: $Y = (1.039 \pm 0.284)\ X + (25.827 \pm 76.727)$

where ±95% confidence limits have been indicated for each of the coefficients.

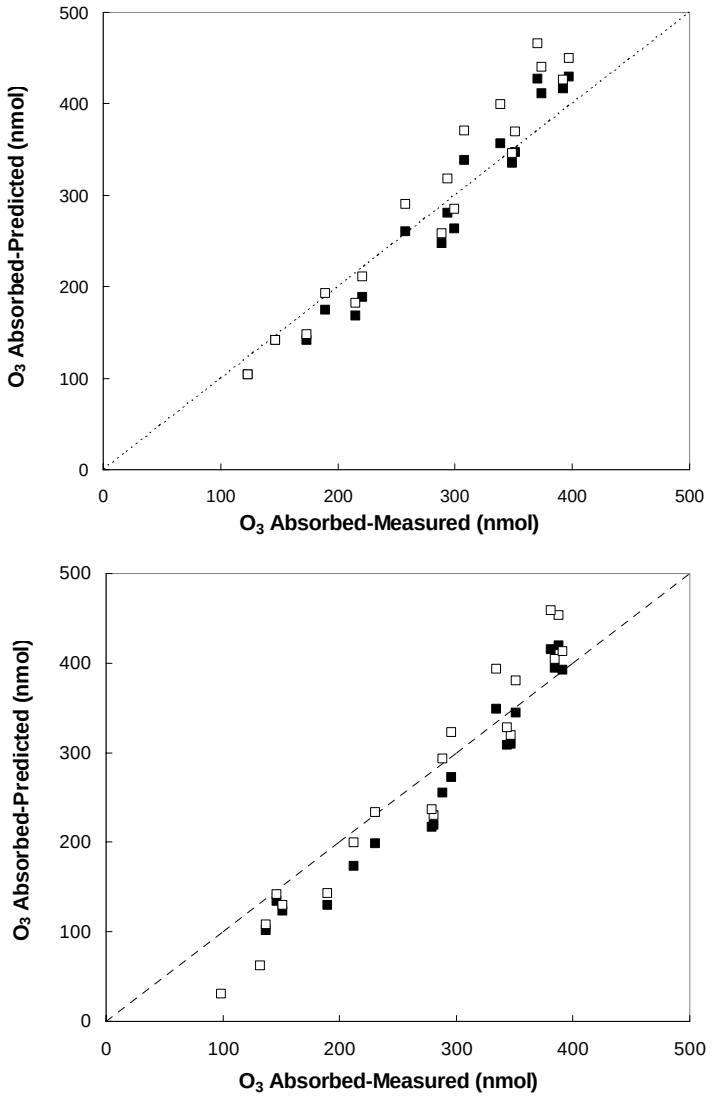

Figure **6-14**: Experimental Data and Model Simulations of O_3 Absorbed After 15 Minutes Exposure of UA-GSH and AH_2 -GSH mixtures to O_3.

The total amounts of O_3 absorbed in UA and GSH mixtures are illustrated in top graph, whereas bottom graph shows the amount of O_3 absorbed in AH_2 and GSH mixtures. (■) corresponds to simulations when $\alpha \neq 0$, whereas (□) corresponds to that when $\alpha = 0$. Dashed lines represent the line of identity. Linear least-squared regression analyses results in:

Top graph:

$\alpha \neq 0$: $Y = (1.134 \pm 0.124)\ X + (-39.485 \pm 35.713)$

$\alpha = 0$: $Y = (1.302 \pm 0.173)\ X + (-68.594 \pm 51.094)$

Bottom graph:

$\alpha \neq 0$: $Y = (1.091 \pm 0.131)\ X + (-44.633 \pm 37.911)$

$\alpha = 0$: $Y = (1.261 \pm 0.186)\ X + (-71.522 \pm 55.466)$

where ±95% confidence limits have been indicated for each of the coefficients.

Chapter 7

ANTIOXIDANT PROTECTION OF ALBUMIN

This chapter contains the experimental data and mathematical simulations performed to determine the kinetic parameters of reaction of O_3 with the tryptophan groups on albumin. Experimental conditions such as equivalent tryptophan concentrations, O_3 concentration, and gas flow rates are explained. The mathematical model applied to determine the reaction rate constant of O_3 reaction with tryptophan groups on albumin is described. In addition, the chapter discusses the experimental data obtained from studying the effectiveness of antioxidant glutathione in protecting the tryptophan residues in albumin.

7.1 Experimental Design

To study the kinetic parameters of reaction of O_3 with tryptophan groups on albumin (TRP), experiments were performed using the same procedure that was employed for individual antioxidants. The outlet ozone concentration and equivalent tryptophan concentration were measured over a reaction time of 15 minutes for several inlet ozone concentrations and albumin concentrations. Ozonated gas entered the reactor at flow rate of 500 ml/min while O_3 concentration in inlet stream varied from 1 to 5 ppm. Initial equivalent tryptophan concentrations of 20, 14, 10, and 6 μ M were employed.

To observe the effectiveness of glutathione in protecting tryptophan groups, binary mixtures containing glutathione and albumin were exposed to O_3. Gas flow rate and inlet O_3 concentration were 500 ml/min and 3 ppm, respectively. Concentration of GSH in the mixture solutions ranged from 0 to 200 μM, whereas equivalent tryptophan concentrations varied from 0 to 20 μM. Table **7-1** shows 24 different combinations of GSH and tryptophan groups employed in the experiments.

Table **7-1**: Experimental Design for Binary Solutions of GSH and Tryptophan Groups on Albumin.

TRP(μM) / GSH(μM)	0	6	10	14	20
0	-	X	X	X	X
50	X	X	X	X	X
100	X	X	X	X	X
150	X	X	X	X	X
200	X	X	X	X	X

* Since there are two TRP residues in each albumin molecule, the actual albumin concentration is half the TRP residues concentration.

7.2 Results

7.2.1 Individual Solution of Albumin

7.2.1.1 Raw Data

Representative data of outlet O_3 concentration for albumin in single-component solutions is compared to the saline control data in Figure **7-1** for a fixed gas flow of 500 ml/min and a fixed inlet O_3 concentration of 3 ppm. Observations for this figure are similar to those obtained for UA, AH_2 and GSH (Figures **5-4** to **5-6**). Recall that the rapid rise in concentration during the first 2 minutes of exposure is due to the wash-out of gas phase II (Figure **4-1)** located above the diffuser (Figure **3-8**). As time proceeds, the outlet O_3 concentration increases. This is explained by the decreasing concentration of tryptophan groups in the solution as it reacts with O_3. Figure **7-1** also indicates that as the initial concentration of tryptophan groups increases, O_3 concentration in the outlet stream decreases. However, because the concentrations of tryptophan groups employed were relatively low, changes in equivalent tryptophan concentration had a small effect on outlet O_3 concentration, and the separation between the O_3 concentrations for the saline control and the substrate experiments were small.

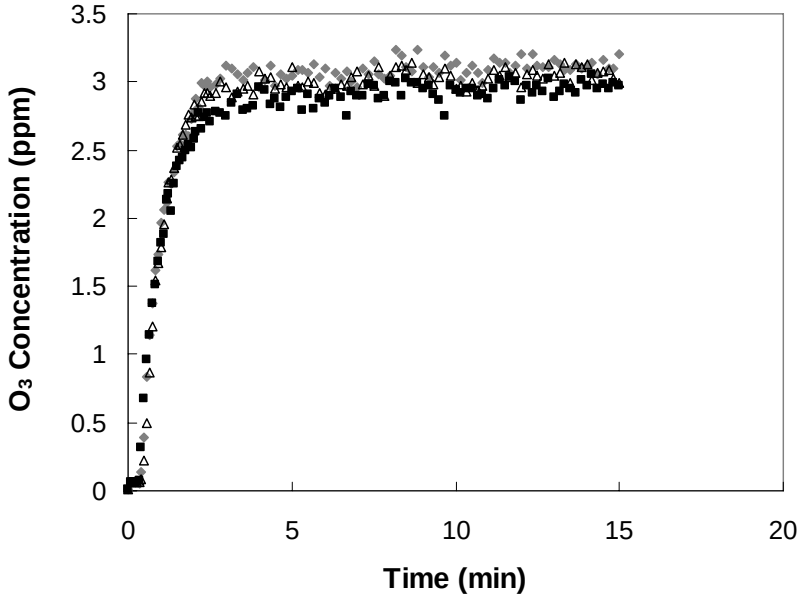

Figure **7-1**: Gas Breakthrough Curves for Tryptophan Groups.

Representative data illustrating the O_3 output concentration at a fixed flow of 500 ml/min and a fixed O_3 concentration of 3.0 ppm. Data was collected for saline solution (♦) and initial TRP groups concentrations of 6 µM (Δ), and 20 µM (■).
For clarity only two concentrations of TRP groups are shown.

7.2.1.2 Stoichiometry Analysis

The amounts of tryptophan groups on albumin consumed and O_3 absorbed are cross-plotted in Figure **7-2** for all the data collected at 5, 10, and 15 minutes of O_3 exposure in experiments with initial equivalent tryptophan concentrations of 6, 10, 14, 20 μM. The resulting correlations between O_3 absorbed and tryptophan groups consumed indicates that for 1.5 moles of O_3 absorbed, 1 mole of tryptophan residue in albumin is consumed, suggesting the reaction stoichiometry of 1.5:1.0.

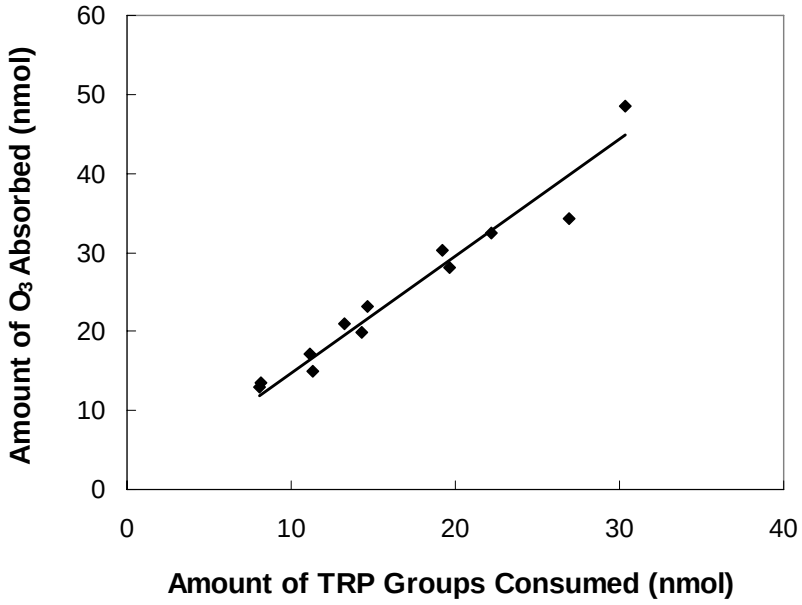

Figure **7-2**: Tryptophan Groups Consumed and O_3 Absorbed After 5, 10 and 15 Minutes of O_3 Exposure.
The linear regression shown by the solid line was used to establish the stoichiometry of the reaction between O_3 and the TRP groups. Linear least-squared regression analyses results in:
$Y = (1.479 \pm 0.082)\ X$; $R^2=0.993$
where ±95% confidence limits have been indicated for the coefficient.

7.2.2 Binary Mixture of Tryptophan Residues in Albumin and Glutathione

To study the behavior of tryptophan groups on albumin in the presence of glutathione during O_3 exposure, the total amount of tryptophan groups and glutathione consumed in binary solutions after a 15 minute exposure to O_3 was compared to the amount consumed when they were individually exposed in single-component solutions to the same concentration of O_3. All the data collected for the different compositions of binary mixtures presented in Table **7-1** are shown in Figure **7-3**. This figure compares the effect of glutathione on tryptophan groups (top graph) to that of tryptophan groups on glutathione (bottom graph). The top graph indicates that when initial equivalent tryptophan concentrations are constant, the total amount of tryptophan groups consumed decreases as glutathione concentration increases. This behavior becomes more exaggerated as the initial tryptophan groups concentration increases. Conversely, the highest amounts of tryptophan groups consumed are reached when no glutathione is present in the solutions. The bottom graph shows that increasing equivalent tryptophan concentration at a fixed initially GSH concentration decreases the glutathione consumption. However, these changes were not as drastic as the changes in tryptophan groups consumption caused by glutathione.

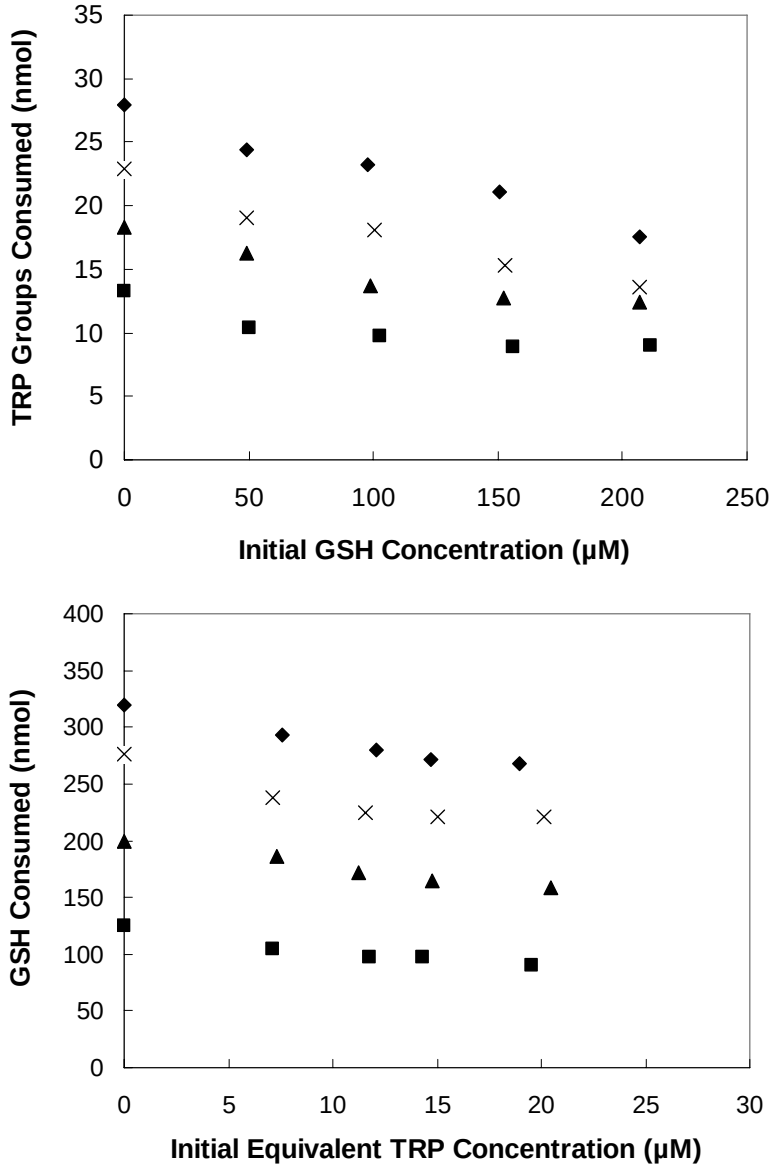

Figure **7-3**: Tryptophan Groups and Glutathione Consumed in Binary Solutions by 15 Minutes Exposure to 3.30 ppm O_3.

Top graph shows the effect of GSH concentration on the total amount of TRP groups consumed in the experiments with initial equivalent TRP concentrations of 20 μM (♦), 14 μM (×), 10 μM (▲), and 6 μM (■). Bottom graph show the effect of equivalent TRP concentration on the total amount of GSH consumed in the experiments with initial GSH concentrations of 200 μM (♦), 150 μM (×), 100 μM (▲), and 50 μM (■).

7.3 Discussion

In addition to antioxidant, proteins, mainly albumin, are important scavengers of ozone present in the epithelial lining fluid. The oxidation of proteins by O_3 can be inferred from the changes in the concentration and/or the appearance of product of a single amino acid residue (Pryor and Uppa, 1993). Because tryptophan, an amino acid present in albumin, has been shown to react readily with O_3 (Pryor et al., 1984; Ignatenko and Cherenkevich, 1985; Pryor and Uppa, 1993; Meiners et al., 1977; and Mudd et al., 1969), we wished to determine the kinetics of O_3 reaction with this amino acid residues in albumin. We were also interested in studying the effectiveness of glutathione in protecting tryptophan groups on albumin against oxidation caused by O_3.

The stoichiometry inferred from the relative consumption of O_3 and tryptophan residues in albumin was 1.5:1.0 (Figure **7-2**). This is close to the stoichiometry reported by Meiners et.al, 1977. Their result established the stoichiometry of 1.22:1 for reaction of O_3 with tryptophan with a 90% probability that the true stoichiometry lies between 1.07:1 and 1.4:1. In order to fit the mathematical model to the dynamic reaction data, we employed a procedure similar to what we used in chapter 5 for GSH. Initially, we considered reaction orders of m=n=1.0 with a stoichiometry of 1:1. We then tried alternative reaction orders of m=1.5; n=1.0 and m=3.0; n=2.0. Figure **7-4** compares the model simulations and experimental data for the time course of equivalent tryptophan concentration whereas Figures **7-5** and **7-6** are cross plots of the model predictions and experimental data for the O_3 absorbed and the tryptophan groups consumed, respectively. In each figure, the upper graph corresponds to m=1.5; n=1.0, the middle graph

corresponds to m=n=1.0 and the lower graph corresponds to m=3; n=2. Results obtained by performing the regression analysis of the cross-plots are also given in the captions of Figures **7-5** and **7-6** . The general impression of these figures in addition to the regression analyses is that a stoichiometry of m=1.5; n=1.0 results in the closest simulation of the data. For this case, the value of the reaction rate constant was $1.22 \times 10^{8}\ \mathrm{M}^{-1.5}\,\mathrm{sec}^{-1}$.

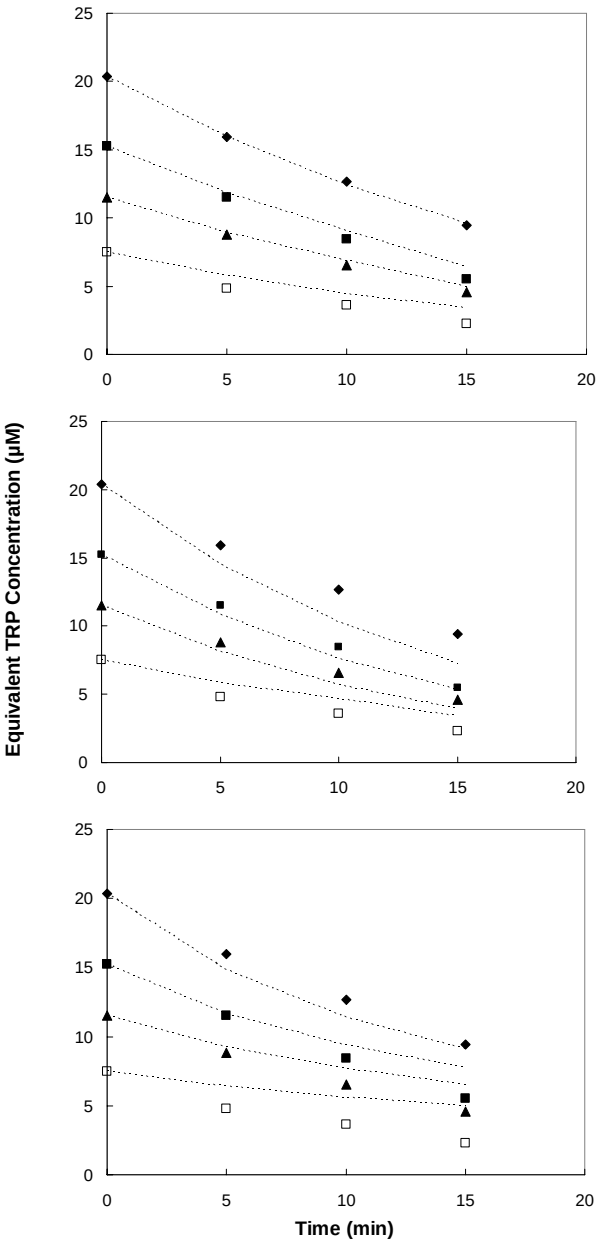

Figure **7-4**: Comparison of Model Simulations (dashed lined) to the Experimental Data of the Time Course of Equivalent Tryptophan Concentration.

Graphs show the time course of equivalent TRP concentration in experiments with initial TRP concentrations of 20 μM (♦), 14 μM (■), 10 μM (▲), and 6 μM (□). In simulations of TRP experiments, alternative kinetic parameters of $m = 1.5; n = 1.0; \eta^{O3,TRP} = 1.5$ (top graph), $m = n = \eta^{O3,TRP} = 1.0$ (middle graph), and $m = 3.0; n = 2.0; \eta^{O3,TRP} = 1.5$ (bottom graph) were investigated.

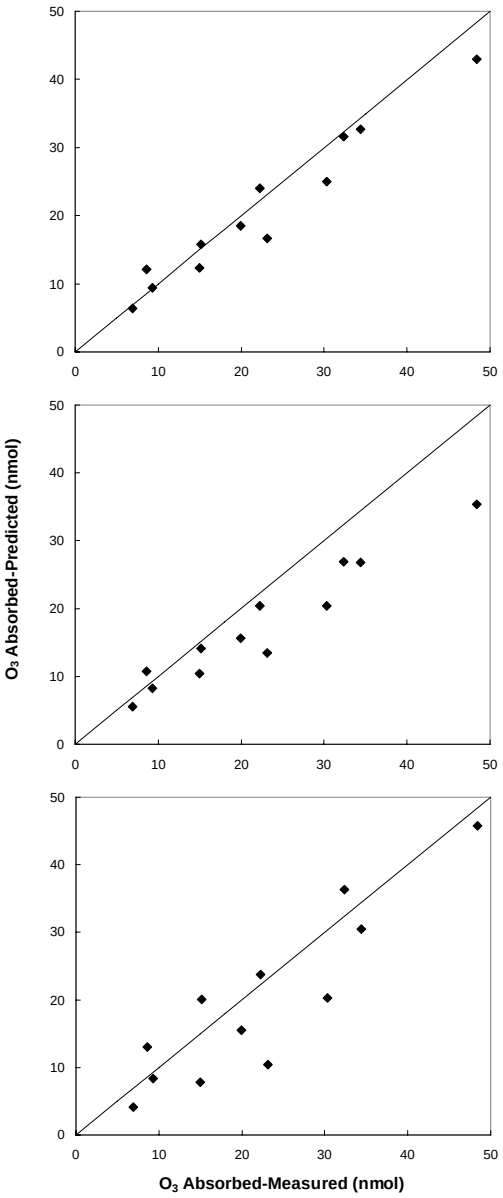

Figure **7-5**: Comparison of Model Simulations to the Experimental Data of the Total Amounts of O_3 Absorbed after 5, 10, and 15 Minutes for Tryptophan Groups Experiments.

In simulations of TRP groups experiments, alternative kinetic parameters of $m = 1.5; n = 1.0;\ \eta^{O3,TRP} = 1.5$ (top graph), $m = n = \eta^{O3,TRP} = 1.0$ (middle graph), and $m = 3.0; n = 2.0;\ \eta^{O3,TRP} = 1.5$ (bottom graph) were investigated. Dashed lines represent the line of identity. Linear least-squared regression analyses results in:
Top graph: Y = (0.871 ± 0.117) X + (1.234 ± 2.834); Middle graph: Y = (0.689 ± 0.132) X + (2.066 ± 3.326);
Bottom graph: Y = 0.911 ± 0.314) X + (-0.550± 7.912) where ±95% confidence limits have been indicated for each of the coefficients.

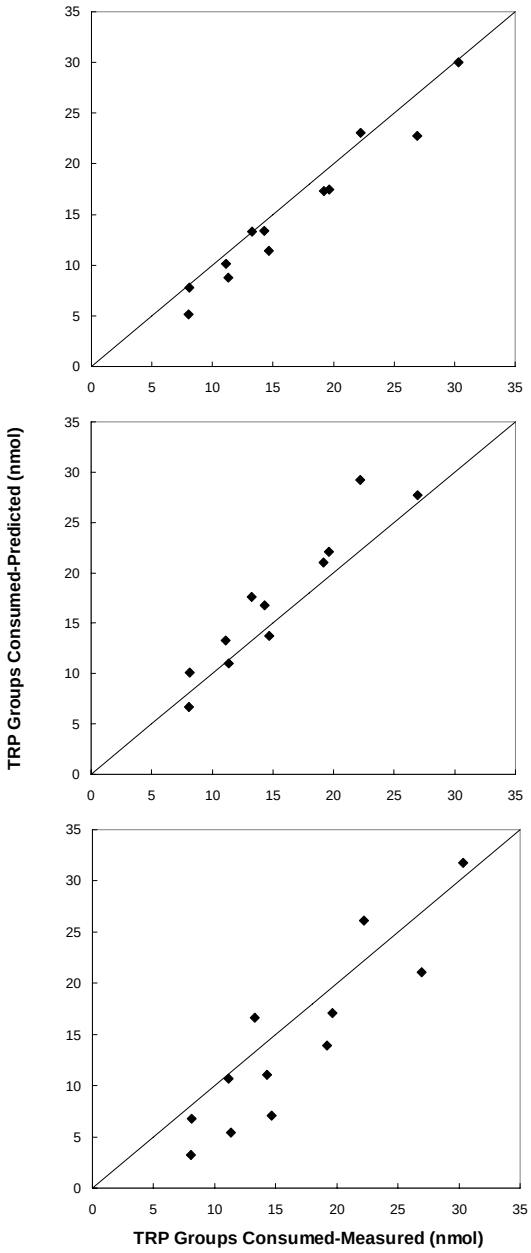

Figure **7-6**: Comparison of Model Simulations to the Experimental Data of the Total Amounts of Tryptophan Groups consumed after 5, 10, and 15 Minutes.

In simulations of TRP groups experiments, alternative kinetic parameters of $m = 1.5; n = 1.0;\ \eta^{O3,TRP} = 1.5$ (top graph), $m = n = \eta^{O3,TRP} = 1.0$ (middle graph), and $m = 3.0; n = 2.0;\ \eta^{O3,TRP} = 1.5$ (bottom graph) were investigated. Dashed lines represent the line of identity. Linear least-squared regression analyses results in:
Top graph: Y = (1.001 ± 0.148) X + (-1.585 ± 2.664); Middle graph: Y = (1.204 ± 0.218) X + (-1.154 ± 3.928);
Bottom graph: Y = (1.099 ±0.367) X + (-4.007 ± 6.604) where ±95% confidence limits have been indicated for each of the coefficients.

Several investigators have studied the reaction of O_3 with amino acids and model compounds to understand the chemical nature of the damage to proteins (Mudway and Kelly, 2000). We were able to find two studies in the literature reporting rate constants for the reaction of O_3 with tryptophan. Both of these studies used free tryptophan and assumed one to one stoichiometry for this reaction. Table **7-2** summarizes the values of the rate constant for O_3 reaction with TRP found by previous studies and also indicates the experimental conditions that were employed.

Table **7-2**: Comparison of Rate Constants of O_3 Reaction with Tryptophan to Previous Studies

k_r	[a] 3.16×10^4 $M^{-1}s^{-1}$ [b] 1.22×10^8 $M^{-1.5}s^{-1}$	7.0×10^6 $M^{-1}s^{-1}$	$5.6 \pm 0.2\times10^4$ $M^{-1}s^{-1}$
Reference	Current Study	Pryor, *et al.*,1984	Ignatenko & Cherenkevich, 1985
O_3 (ppm)	3	Extremely High	7-200
Tryptophan (μM)	6-20	Not Given	0.1-1000
Reactor Type	Stirred liquid contacted with ozonated air distributed with sintered glass diffuser.	Liquid-liquid reaction in stopped flow apparatus	ozonated air bubbles through a biomolecule solution

[a] corresponds to kinetic parameters: $m = n = \eta^{O3,TRP} = 1.0$, whereas [b] corresponds to $m = 1.5; n = 1.0;\ \eta^{O3,TRP} = 1.5$. Note that our findings indicated that the latter results in the closest simulation of the data. Rate constant corresponding to 1:1 stoichiometry is shown for the purpose of comparison to rate constants reported by other research groups.

The agreement between the study of Pryor and coworkers (1984) and the study of Ignatenko and Cherenkevich is very poor. The fact that experimental conditions under which O_3 and amino acid solution was contacted were not similar for these two studies may explain this discrepancy. Pryor and colleagues used a stopped flow reactor in which they initiated the reaction by mixing solutions containing ozone and solutions containing tryptophan. The reaction occurred in a homogenous bulk liquid phase, where the concentrations of O_3 and tryptophan were close (Pryor et al., 1984). Ignatenko and Cherenkevich (1985) measured the rate constant using a system in which ozone, in a carrier gas, was bubbled through amino acid solutions.

We believe that the rate constant obtained from assuming 1:1 stoichiometry for O_3 reaction with tryptophan is not the optimum value. However, to be able to compare our rate constant value to those reported by Pryor et al. (1984) and Ignatenko and Cherenkevich (1985), 1:1 stoichiometry was used in our simulations and corresponding rate constant was determined to be 3.16×10^4 $M^{-1} sec^{-1}$. It is observed that rate constant reported by Pryor et al. (1984) is two orders of magnitude larger than our value. Also, our rate constant value is smaller than (but of the same order of magnitude) the value reported by Ignatenko and Cherenkevich (1985). It has been suggested that the reaction rate constant of O_3 with free amino acid is the same as that with amino acid residues in proteins (Pryor and Uppa, 1993). On the contrary, Mudd et al. (1997) showed that the reactivity of tryptophan with O_3 depends on the tertiary structure of protein and chemical interaction within the protein. Therefore, the difference between our value and values reported by Pryor et al. (1984) and Ignatenko and Cherenkevich (1985) can be explained by the fact that we measured rate constants of O_3 reaction with tryptophan residues in

albumin, whereas they measure the rate constant of reaction between O_3 and free tryptophan.

In this chapter, we also wanted to determine whether or not glutathione can protect the tryptophan residues in albumin against oxidation caused by O_3. There have been few other studies that examined the effectiveness of antioxidants in protecting the protein albumin or tryptophan. Van der Vliet and colleagues (1995) investigated whether GSH could prevent oxidative damage to plasma proteins when exposed to ozone. Because RTLF contains higher amounts of GSH than plasma, these investigators added up to 1 mM of GSH to plasma before exposure to O_3. Their results indicated that GSH did not significantly inhibit the formation of protein carbonyls, an index of oxidative damage to proteins. This was explained by the fact that the majority of protein carbonyls are formed after prolonged exposure to O_3, by which time the added thiols are largely oxidized (Van der Vliet et al., 1995).

Ben-Jebria and colleagues (1998) examined whether glutathione is capable of protecting the albumin against oxidation caused by NO_2. Their results demonstrated that addition of GSH had no effect on decreasing the albumin depletion and therefore it did not provide any protection to the albumin. Kanofsky and Sima (1995) measured the ability of glutathione to inhibit the oxidation of tryptophan in an aqueous solution. Concentrations of GSH, tryptophan, and O_3 were 400 μM to 3.2 mM, 400 μM, and 79 ppm, respectively. Their findings indicated a decrease in tryptophan consumption rate (Kanofsky and Sima, 1995).

In the current study, we performed experiments using mixtures containing GSH and tryptophan residues in albumin, and compared them to experiments on single-

component solutions of these substrates. The results indicated that both GSH and tryptophan groups can attenuate consumption of each other. However, the effect of GSH on tryptophan groups is larger than that of tryptophan groups on GSH. This demonstrates that glutathione is indeed capable of protecting tryptophan residues in albumin against O_3. Our observations were similar to that reported by Kanofsky and Sima (1995).

To further understand the protective effect of GSH on tryptophan groups, we employed a procedure similar to the one used to explain the behavior of UA-AH_2 mixtures. As explained in chapter 6, protection can be caused by either the competition between substrates for a limited supply of O_3 or by molecular interaction between the substrates. First, we assumed that the decrease in consumption is just due to competition so that the stoichiometries and reaction rate constants in the tryptophan groups-GSH mixture are the same as the corresponding values for the single-component solutions. Equations **6.1** and **6.2** can then be rewritten for GSH and tryptophan residues in albumin as follows:

$$\dot{R}_{O3} = 0.4\, k_{r,GSH}\, C_{O3,1}^{0.5}\, C_{GSH}^{1.25} + 1.5\, k_{r,TRP}\, C_{O3,1}^{1.5}\, C_{TRP} \qquad (\mathbf{7.1})$$

$$\frac{dC_{GSH}}{dt} = -k_{r,GSH}\, C_{O3,1}^{0.5}\, C_{GSH}^{1.25} \quad ; \quad \frac{dC_{TRP}}{dt} = -k_{r,TRP}\, C_{O3,1}^{1.5}\, C_{TRP} \qquad (\mathbf{7.2})$$

Using Equations **7.1**, **7.2**, **4.4**, **4.8**, and **4.10**, we were unable to provide a reasonable simulation of the experimental data.

The next option was to account for possible interactions between tryptophan groups and GSH ozonation. Unlike UA-GSH and AH_2-GSH mixtures for which the effects of GSH on UA and GSH on AH_2 were negligible compared to the effects of UA on GSH and AH_2 on GSH, tryptophan groups on albumin and GSH both have a significant effect on each other. In particular, our results indicated that GSH attenuated the consumption of tryptophan residues up to an average of 36%, whereas tryptophan groups decreased the consumption of GSH up to an average of 20%. Therefore, interaction coefficients had to be determined for both GSH and tryptophan residues. This led to a mathematical model in which two parameters had to be optimized, and it was not possible to obtain simulations that were in a good agreement with the experimental data.

In summary, we determined the kinetic parameters of O_3 reaction with tryptophan residues in albumin using a procedure similar to the one used for UA, AH_2, and GSH. The reaction of O_3 with tryptophan groups on albumin was found to have a 1.5:1.0 stoichiometry. By simulating the O_3 absorbed and tryptophan groups consumed with a mathematical model, the reaction rate constant of O_3 with tryptophan residues in albumin was determined to be 1.22×10^8 $M^{-1.5}\,sec^{-1}$. In addition, the effectiveness of GSH on protecting tryptophan groups was examined. We showed that both GSH and tryptophan groups can attenuate the consumptions of the other, indicating that both are capable of protecting each other from oxidations caused by O_3.

Chapter 8

KINETICS OF OZONE REACTION WITH SAMPLES OF NASAL WASHINGS

This chapter describes the experiments performed using samples of nasal washings. The procedure used to obtain nasal lavage samples, and experiments conditions such as O_3 concentrations and gas flow rate are explained. In this study, we were interested in kinetic information that can be obtained for a biological sample of nasal lavage.

8.1 Experimental Designs

Samples of nasal washings were collected from seven healthy, non smoker volunteers. Subjects were 4 females and 3 males, with average age of 28.4 ± 3.9; average height of 169.4 ± 10.6 cm; and average weight of 69.4 ± 15.4 kg. Experiments were carried out with the interfacial reactor using a procedure similar to that used for the single-component antioxidant solutions. To begin an experiment, three milliliters solution of nasal washings were charged to the reactor and an ozonated air flow of 500 ml/min was initiated. The outlet O_3 concentration was then monitored for a 10-minute interval; this shorter exposure time was used because substrate concentrations in lavage samples were below the range of antioxidant concentrations used in the single-component experiments. Experiments were conducted at room temperature ($T = 25 \pm 1\ ^{\circ}C$) with alternate inlet O_3 concentrations of 0.4 and 0.85 ppm. Solution samples obtained

immediately before the exposure (t=0 min) and after the exposure (t=10 min) were injected into the HPLC and analyzed for UA concentration.

8.1.1 Procedure for Obtaining Nasal Washings

The technique used to collect nasal washing was adapted from Koren et al. (1990). Five milliliters of sterile isotonic saline, warmed to 37 ^{o}C, was instilled into one of the subject's nostrils using a 5 ml needleless syringe while the subject kept his or her head tilted back and breathed orally to maintain the velum closed. After 10 seconds, the subject tilted his or her head forward and the solution was expelled into a sterile plastic specimen cup placed in front of the nose. Immediately thereafter, another five milliliters of saline were introduced into the other nostril, and 10 seconds later, the subject drained the solution into the same cup. This washing procedure took approximately one minute.

After collection was complete, the percent recovery of fluid was determined from the volume of fluid in the specimen cup relative to the 10 ml instilled into the nostrils. The nasal washings were then passed through a 0.45 μm filter (Gelman Science, Ann Arbor, MI) to remove cell debris and other particulates before analysis. Experiments were repeated when the nasal washing recovery was less than 65%.

8.2 Results and Discussion

As the nose is the primary portal of entry for air in humans, it is the first region of the respiratory system that comes in contact with inspired pollutant such as O_3 (Mudway

and Kelly, 2000; Calderon-Garciduenas et al., 1998). Consequently, the upper respiratory region experiences the highest concentration of any inhaled toxic agent. Therefore, if these oxidants are going to have an influence on the respiratory tract, these effects should be detected first in the nasal passages (Mudway and Kelly, 2000). A study by Koren and coworkers (1990) demonstrated that short exposures to pollutants, such as O_3, elicit an acute inflammatory response in the upper respiratory tract of humans. Also, a study conducted in Mexico City demonstrated that daily episodes of high levels of O_3 (up to 300 ppb) are responsible for nasal tissue damage (Valverde et al., 1997). Such responses in the nasal cavities are probably related to high efficiency of O_3 uptake. Gerrity and colleagues (1988) reported that approximately 40% of inhaled O_3 is absorbed in the nose and nasopharynx during quiet breathing, whereas Kabel et al. (1994) and Nodelman and Ultman (1999) measured approximately 80% and 85% O_3 absorption during a quiet breathing cycle. These findings indicate the importance of the nasal region in preventing the lower airways from exposure to high doses of O_3.

Because of the relatively limited solubility of ozone in aqueous solutions, the primary removal of ozone from inhaled air into the nasal mucus layer is due to the reactive absorption (Pryor et al., 1992). Nasal lining fluid contains a variety of substrates such as UA, AH_2, GSH, albumin and mucins that can react with O_3. UA has been identified as a major antioxidant in nasal mucous (Van der Vliet et al., 1999; Peden et al., 1990, 1993). Nasal washing has been used for years to identify components of the fluid lining the nasal cavity. It is a simple and relatively non-invasive technique that allows multiple sequential sampling from the same person (Mudway and Kelly, 2000).

One of the limitations of the lavage method is the dilution of RTLF by the washing medium. Substrate levels in the nasal lavage samples can be corrected for this by using a dilution factor obtained from the distribution of urea between blood and nasal lavage (Kaulbach et al., 1993). Assuming that urea diffuses so rapidly that its concentration in blood and RTLF is identical but the entry of urea into RTLF is negligible during the lavage process, a dilution factor can be computed as the ratio of the urea concentrations in blood and in lavage. Because of the latter assumption, the washing procedure was carried out as rapidly as possible. To correct our values for UA concentration, we used a dilution factor reported by Santiago (2001). Table **8-1** compares the corrected UA concentrations obtained in this study values reported by different research groups. Considering the large intersubject variation of the data implied by the standard deviations, we conclude that our data is consistent with those of other researchers.

Table **8-1**: Comparison of UA Levels Obtained with Values Reported in Literature

	Cross et al., 1994	*Van der Vliet et al., 1999*	*Santiago, 2001*	*Current Study*
Uric Acid (μM)	160	225 ± 105	160.5 ± 59.0	281.6 ± 179.33
Dilution Factor (fold)	40*	10-20	11.3 ± 5.1 (5-25)	11.3**

* Dilution factor assumed, not measured; ** Average dilution factor found by Santiago 2001 was employed in the current study. Values represent average ± SD.

Because UA is a major antioxidant in the nose, we focused on the reaction of this particular antioxidant with O_3. In other words, we wished to determine whether UA is a good marker for evaluating the kinetics of O_3 reaction with nasal lavage solutions. Each sample of nasal lavage obtained from an individual subject was exposed to two inlet O_3 concentrations of 0.4 and 0.85 ppm for 10 minutes. The total amounts of UA consumed and O_3 absorbed after 10 minutes were determined. To understand whether ozonation of UA in the lavage sample is similar to that in pure UA solution, the total amount of O_3 absorbed in a sample of lavage was compared to amount of O_3 absorbed when the same concentration of UA in a single-component solution was exposed to O_3. This comparison is shown in Figure **8-1**. Different initial UA concentrations in lavage samples correspond to different subjects. Figure **8-1** shows that as long as the initial UA concentration in the solution is the same, there is no difference between the amount of O_3 absorbed in nasal lavage sample and that in pure UA solution.

To further examine this finding, we compared the total amount of UA consumed in lavage samples with corresponding amount of O_3 absorbed. Knowing that the reaction of O_3 with UA has 1:1 stoichiometry, the amount of UA consumed in nasal lavage should be the same as that of O_3 absorbed if UA was indeed the only O_3 scavenger in lavage samples. Figure **8-2** compares the amount of O_3 absorbed and amount of UA consumed in samples of nasal washings when the inlet O_3 concentration was 0.85 (upper graph) or 0.4 ppm (middle graph).. The corresponding data for single-component UA solutions are also shown (bottom graph). As expected, the total amount of O_3 absorbed and UA consumed in single-component UA solutions are the same. However, the total amounts of O_3 absorbed in nasal lavage samples are consistently higher than the amount of UA

consumed. Considering that O_3 reaction with UA has 1:1 stoichiometry, comparing the O_3 absorption with UA consumption demonstrates that only 50% of O_3 absorption in the lavage samples is actually due to UA (Figure **8-3**). This indicates that in addition to UA, other materials are also present in lavage samples that successfully compete for half of the O_3.

A comparison between the total amount of UA consumed in nasal lavage samples and UA consumed in pure UA solution is illustrated in Figure **8-4**. This figure indicates that total amount of UA consumed in pure UA solutions are consistently higher than those in nasal lavage samples. The lower UA consumption in nasal lavage samples demonstrates that other materials present in the lavage samples inhibit the O_3 reaction with UA and hence, do not allow UA to react with O_3 to its full extent.

As was explained before, in addition to UA, other components such as AH_2, GSH, mucins, and albumin are also present in the nasal lining fluid. Because concentrations of AH_2 and GSH in the nasal lining fluid are smaller than UA concentration (Cross et al., 1994; Van der Vliet et al., 1999; and Santiago, 2001), and UA has been shown to have more reactivity toward O_3 than AH_2 and GSH, the remainder of O_3 absorbed cannot be due to the reactive absorption of these two antioxidants. A study by Mudway et al. (1999) which indicated that exposure of healthy human subjects to O_3 resulted in a marked depletion in UA, a very small depletion in GSH, and no significant loss in AH_2, supports this argument. Therefore, more complex compounds such as proteins and mucins, whose molecules can each react with several molecules of O_3, may be important contributors to the total absorption of O_3 in the lavage samples.

In summary, we studied the reaction of nasal lavage samples with O_3, focusing on the contribution of UA because it is a major antioxidant in nasal lining fluid. Our results demonstrated that approximately 50% of the total O_3 absorption in nasal lavage is due to UA. Other compounds such as albumin and mucin whose reaction with O_3 has a non-unity stoichiometry may also be important contributors to the total absorption of O_3 in the lavage samples.

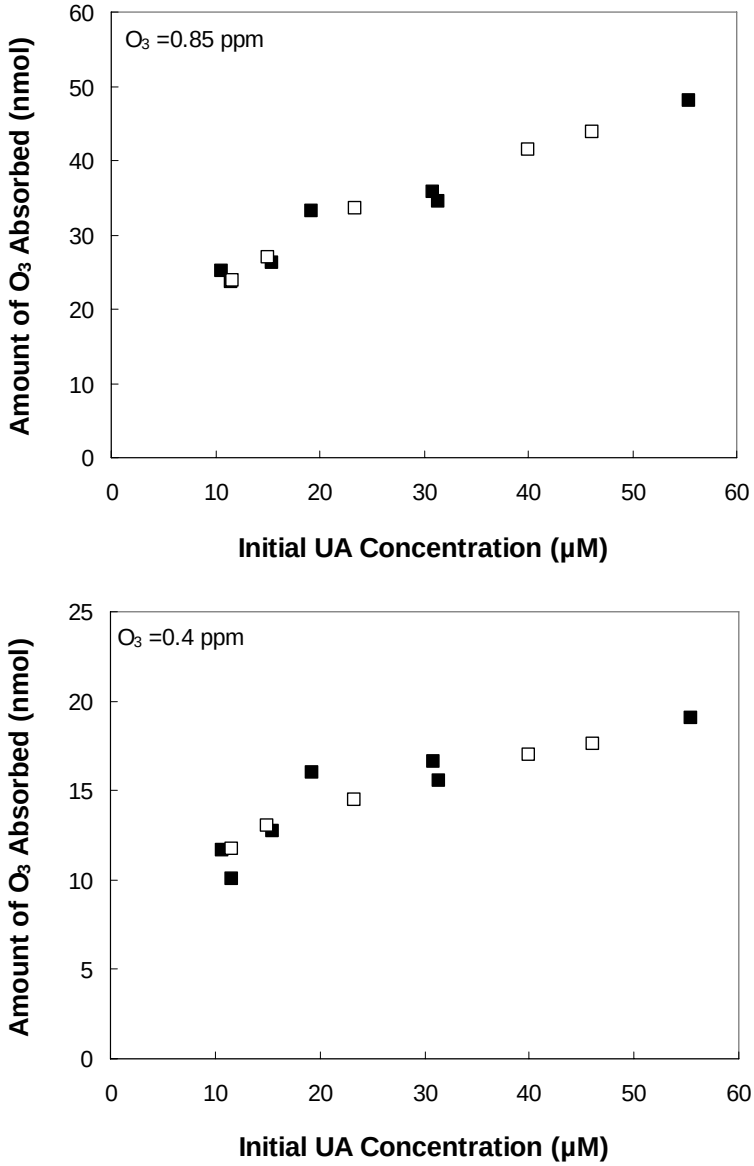

Figure **8-1**: O_3 Absorbed in Samples of Nasal Lavage and in Single-Component UA Solutions.

Top and bottom graphs correspond to experiments with inlet O_3 concentration 0.85 and 0.4 ppm, respectively. ■ illustrates the total amount of O_3 absorbed in samples of nasal lavage, whereas □ shows the amount of O_3 absorbed in pure UA solutions.

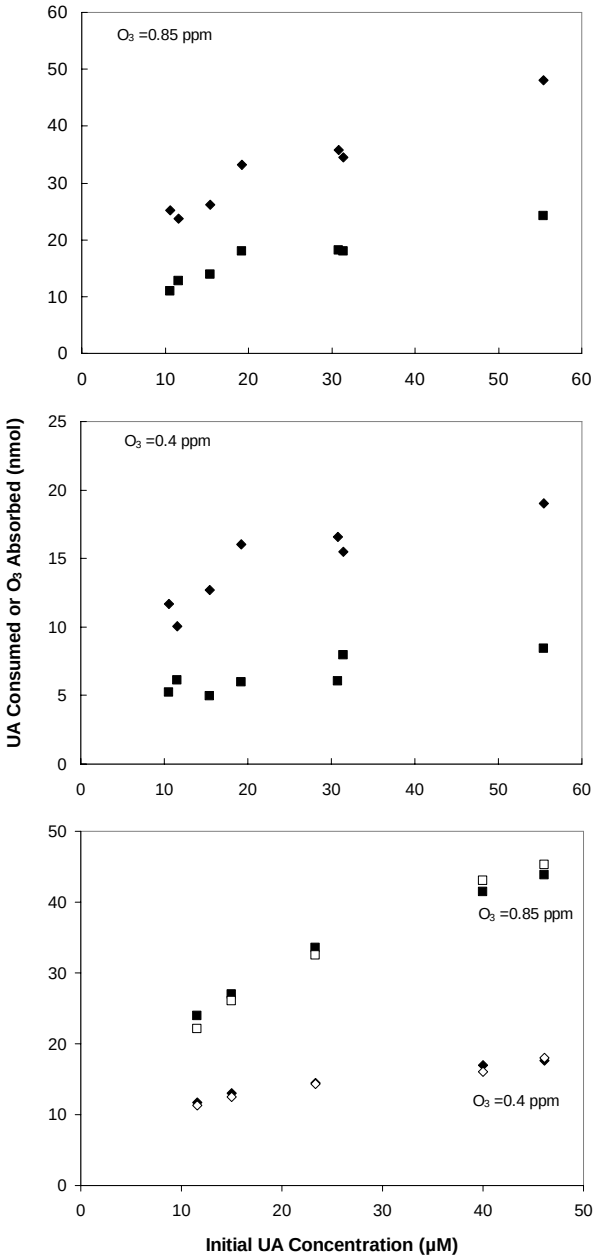

Figure **8-2**: O_3 Absorbed and UA Consumed in Nasal Lavage and in Single-Component UA Solutions.

Top and middle graph illustrate data obtained when nasal lavage samples obtained from individual subject were exposed to inlet O_3 concentrations of 0.85 and 0.4 ppm, respectively. ♦ corresponds to the total amount of O_3 absorbed, whereas ■ corresponds to the total amount of UA consumed.

Bottom graph illustrates a comparison between total amount of O_3 absorbed and UA consumed for single-component UA solutions. ■ and □ show O_3 absorption and UA consumption data, respectively for inlet O_3 concentration of 0.85 ppm, whereas ♦ and ◊ illustrate total amount of O_3 absorbed and UA consumed for inlet O_3 concentration 0.4 ppm.

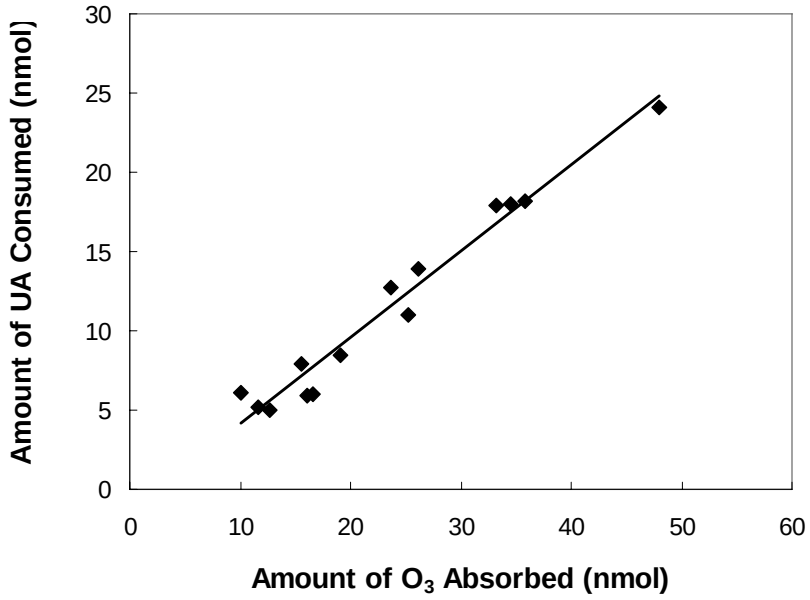

Figure **8-3**: UA Contribution to the O_3 Absorption in Nasal Lavage Samples.

Data illustrate the total amount of O_3 absorbed and corresponding amount of UA consumed. The linear regression shown by the solid line was used to establish the contribution of UA to the O_3 absorption in nasal lavage samples.

Performing a least-squared linear regression analysis results in:
$Y = (0.543 \pm 0.064)\ X + (-1.267 \pm -1.661)$; $R^2 = 0.9656$ where ±95% confidence limits have been indicated for each of the coefficients.

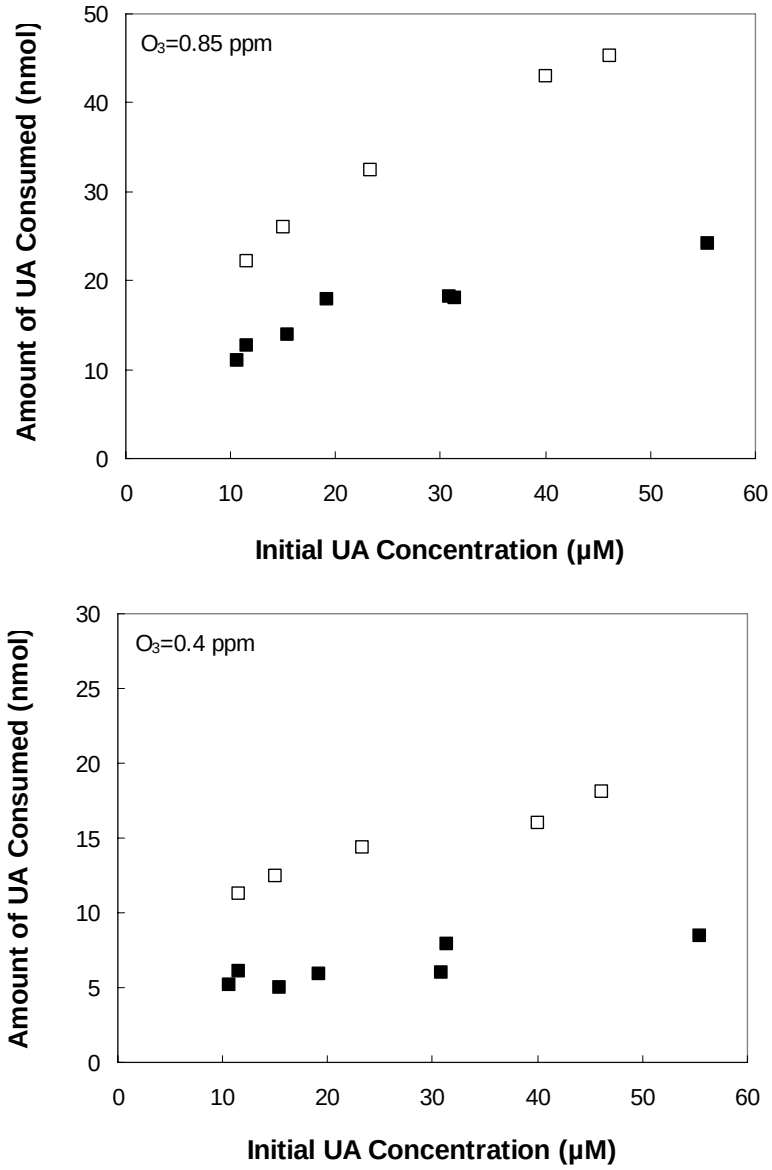

Figure **8-4**: Comparison of the Total Amount of UA Consumed in Samples of Nasal Lavage to that in Pure UA Solution.

Top and bottom graphs correspond to experiments with inlet O_3 concentration 0.85 and 0.4 ppm, respectively. ■ illustrates the total amount of UA consumed in samples of nasal lavage, whereas □ shows the amount of UA consumed in pure UA solutions.

Chapter 9

SUMMARY AND FUTURE WORK

Because O_3 is an inevitable component of air pollution, there is a continuing need for better understanding and describing its toxicokinetics in the respiratory tract. The goal of this thesis was to understand and to quantify the reaction between O_3 and antioxidants under conditions that are similar to those encountered when polluted air is inhaled into the respiratory system. In particular, we were interested in determining kinetic parameters, such as rate constants and the stoichiometries of the reactions between O_3 and individual antioxidants, as well as mixtures of antioxidants. In addition, we wanted to investigate the kinetic information that can be obtained when samples of nasal lavage were exposed to O_3.

To accomplish these goals, an exposure system containing an O_3 generator, O_3 analyzer and a semi-batch interfacial reactor was first developed. Because UA is a stable compound and has also been identified as a major antioxidant in the upper respiratory tract, this substance was initially employed to determine the experimental conditions under which experiments would be reaction limited. In particular, gas flow and magnetic stirrer speed were progressively increased until O_3 absorption reached an upper limit, indicating that both gas-phase and liquid-phase diffusion resistances were negligible. The unique aspect of this investigation was the simultaneous, time-dependent measurements of O_3 absorption and antioxidant depletion.

To explain the experimental data, and specifically to predict the rate constants for reactions between O_3 and antioxidants, a mathematical model was developed. Because there was no significant mass transfer resistance in the gas and the liquid phases, interfacial equilibrium could be stipulated between these two compartments. The optimal reaction rate constant was determined using an optimization program in which the squared-error between the observed amounts of O_3 absorbed and antioxidant consumed and their simulated values was minimized.

After designing the exposure system and developing the mathematical model, we initially studied the kinetic parameters of reaction between O_3 and UA, AH_2 and GSH in single-component solutions containing initial antioxidants concentrations of 50-200 μM. To quantify reaction kinetics, we employed a process that utilized a combination of experimental analyses and numerical simulations. Simultaneous measurement of time-dependent changes in both O_3 absorption and antioxidant consumption enabled us to determine the stoichiometry of 1:1, 1:1 and 1:2.5 for the reaction between O_3 and UA, AH_2, and GSH, respectively. The reactivity between O_3 and these antioxidants was found to be in the following order: UA ≈ AH_2 > GSH. By employing the optimization program, the reaction rate constants of O_3 with UA, AH_2, and GSH were found to be $5.83\times10^4\ M^{-1}sec^{-1}$, $5.5\times10^4\ M^{-1}sec^{-1}$ and $57.5\ M^{-0.75}\ sec^{-1}$, respectively. We believe that the reaction stoichiometries and the reaction rate equations that we inferred are essential for developing mathematical methods to predict the distribution of O_3 dose to target tissues in the respiratory tract.

The interaction of antioxidants was investigated in binary and ternary mixtures containing UA, AH_2, and GSH using the same procedure employed for the single-component antioxidant solutions. The concentration of each antioxidant in the mixtures ranged form 0 to 200 μM. Measurements made on UA-AH_2 mixtures indicated that the consumption of UA and AH_2 are diminished in the presence of one another. Numerical simulations verified that this effect is mostly due to the competitive reaction of UA and AH_2 toward O_3. Measurements made on UA-GSH and AH_2-GSH mixtures indicated that both UA and AH_2 can attenuate the consumption of GSH, whereas GSH does not have the same effect on UA and AH_2. Numerical simulations demonstrated that competition between antioxidants for reacting with O_3 is not the only factor that causes a decrease in GSH depletion. Therefore, to explain the behavior of GSH in the mixtures, an interaction parameter was introduced in the model to determine the effect of UA and AH_2 on the reaction rate constant of GSH. Employing the interaction parameter in the model improved simulations of the experimental data. Ternary mixtures of antioxidants, in which equimolar concentrations of UA and AH_2 were added to GSH solution, were also investigated. Similar to the observations in the binary solution experiments, the presence of UA and AH_2 simultaneously in the mixture also diminished GSH consumption.

Kinetic parameters of reaction between O_3 and albumin were examined with a procedure similar to the one used for the antioxidants. Using simultaneous measurements of time-dependent changes in both O_3 absorption and tryptophan consumption, we found a stoichiometry of 1.5:1.0 for reaction between O_3 and a tryptophan residue in albumin. Also, by employing the optimization program, the rate constant of the O_3 reaction with a tryptophan residue was determined to be $1.22 \times 10^8\ \mathrm{M}^{-1.5}\,\mathrm{sec}^{-1}$. The effectiveness of

GSH for protecting tryptophan groups was investigated in binary solutions of GSH and albumin. Our results showed that GSH and tryptophan can attenuate the consumption of one other, indicating that both are capable of protecting each other from oxidation caused by O_3. However, the changes in GSH consumption caused by tryptophan were not as drastic as the changes in tryptophan residue consumption caused by GSH. This indicated that GSH is more effective in preventing tryptophan groups on albumin from O_3 oxidation than tryptophan residues are in inhibiting GSH reaction.

In the last study, reaction of nasal lavage samples with O_3 was investigated. The results from this in vitro study demonstrated that approximately 50% of the total O_3 absorption in nasal lavage is due to UA. This indicated that UA acts as an effective scavenger of ozone. Other compounds such as albumin and mucin with a stoichiometry in which several molecules of ozone react with each molecule of substrate may also be important contributors to the total absorption of O_3 in the lavage samples. The nasal lavage samples used in this study were obtained from seven subjects. Therefore, to verify the results obtained in this study, we recommend performing more experiments in the future using nasal lavage samples obtained from both the previous and new subjects. Furthermore, because UA was found to be responsible for only 50% of O_3 absorption in lavage samples, we recommend examining other compounds present in nasal lining fluid such as GSH, AH_2, and albumin to understand whether the remainder of O_3 absorbed in the samples of nasal lavage is due to reactive absorption of these substrates.

In this thesis, we have carefully designed the experimental conditions under which the kinetics of O_3 reaction with major respiratory substrates could be studied under physiologically-relevant conditions. It is widely accepted that the oxidation of proteins

and lipids present in cell membranes are the most important pathways of O_3-induced injury. Therefore, we recommend the future use of the exposure system and the mathematical model developed in this study to investigate the reaction of O_3 with these biological substrates.

Future work should also focus on the products of reaction resulting from O_3 exposure to the RTLF. Some of these secondary substances may themselves be toxic, and a knowledge of their kinetics would provide a more complete perspective of O_3 toxicity.

Finally, the exposure system and the mathematical model developed in this study could be employed in future studies to investigate kinetic parameters of reaction between other reactive air pollutants, such as nitrogen dioxide and chlorine with biological substrates present in the respiratory tract.

Bibliography

Ames, N. B.; Cathcart, R.; Schwiers, E.; Hochstein, P., Uric Acid Provides an Antioxidant Defense in Humans against Oxidant-and Radical-caused Aging and Cancer: A Hypothesis, *Proc. Natl. Acad. Sci.*, 1981, 78, No. 11, 6858-6862.

Ballinger, C. A.; Cueto, R.; Squadrito, G.; Coffin, J. F.; Velsor, L. W.; Pryor, W. A.; Postlethwait, E. M., Antioxidant-mediated Augmentation of Ozone-induced Membrane Oxidation, *Free Radical Biology & Medicine,* 2005, 38, 515-526.

Bader, H.; Hoigne, J., Determination of Ozone in Water by the Indigo Method, *In Water Research.,* Oxford, New York: Pergamon Press, 1981, 155, 449-456.

Bates, D. M.; Watts, D. G., Nonlinear Regression and Its Application, Wiley, New York, 1988.

Becker, B., Towards the Physiological Function of Uric Acid, *Free Radic. Biol. Med.*, 1993, 14, 615-631.

Ben-Jebria, A.; Satchithanandam, L.; Gusic, R. J.; Gervais, T. R.; Ultman, J. S., Kinetics of Protein Depletion in Rat Bronchoalveolar Lavage Fluid Following in vitro Exposure to Nitrogen Dioxide, *Environmental Toxicology and Pharmacology*, 1998, 6, 177-185.

Berlett, B. S.; Levine, R. L.; Stadtman, E. R., Comparison of the Effects of Ozone on the Modification of Amino Acid Residues in Glutamine Synthetase and Bovine Serum Albumin, *The Journal of Biological Chemistry*, 1996, 271, No. 8, 4177-4182.

Brown, L. A.; Jones, D. P., Chemistry and Biochemistry of Ascorbic Acid. In *Handbook of Antioxidants*; Cadenas, E.; Packer, L., Eds; Marcel Dekker: New York, NY, 1996, 243-256.

Buettner, G. R.; Jurkiewicz, B. A., Chemistry and Biochemistry of Ascorbic Acid. In *Handbook of Antioxidants*; Cadenas, E.; Packer, L., Eds; Marcel Dekker: New York, NY, 1996, 91-154.

Byvoet, P.; Balis, J. U.; Shelley, S. A.; Montgomery, M. R.; Barber, M. J., Detection of Hydroxyl Radicals upon Interaction of Ozone with Aqueous Media or Extracellular surface: The Role of Trace Iron, *Archives of Biochemistry and Physics*, 1995, 319, No. 2, 464-469.

Calderon-Garciduenas, L.; Rodriguez-Alcaraz, A.; Villarreal-Calderon, A.; Lyght, O.; Janszen, D.; Morgan, K. T., Nasal Epithelium as a Sentinel for Airborne Environmental Pollution, *Toxicological Sciences*, 1998, 46, 352-364.

Committee of the Environmental and Occupational Health Assembly of the American Thoracic Society, Health Effects of Outdoor Air Pollution, *Am. J. Respir. Cirt. Care Med.*, 1996, 153, 3-50.

Cross, C. E.; Van der Vliet, A.; O'Neill, C. A.; Louie, S.; Halliwell, B., Oxidants, Antioxidants, and Respiratory Tract Lining Fluids, *Environmental Health Perspectives*, 1994, 102, 185-191.

Cross, C. E.; Motchnik, P. A.; Bruener, B. A.; Jones, D. A.; Kaur, H.; Ames, B. N.; Halliwell, B., Oxidative Damage to Plasma Constituents by Ozone, *Federation of European Biochemical Societies*, 1992, 298, No. 2, 269-272.

Davis, W. B.; Pacht, E. R., Extracelllular Antioxidant Defenses, *In The Lung: Scientific Foundations* Edited by R. G. Crystal and J. B. West, Raven Press, New York, 1991, 1821-1827.

Devlin, R. B.; Folinsbee, L. J.; Biscardi, F.; Hatch, G.; Becker, S.; Madden, M. C.; Robbins, M.; Koren, H. S., Inflammation and Cell Damage Induced by Repeated Exposure of Humans to Ozone, *Inhalation Toxicology*, 1997, 9, 211-235.

Doodey, M. M.; Mudd, J. B., Reaction of Ozone with Lysozyme under Different Exposure Conditions, *Archives of Biochemistry and Physics*, 1982, 218, No.2, 459-471.

Ford, E.; Hughes, M. N.; Wardman, P., Kinetics of the Reactions of Nitrogen Dioxide with Glutathione, Cysteine, and Uric Acid at Physiological pH, *Free Radical Biology & Medicine*, 2002, 32, No. 12, 1314-1323.

Frischer, T.; Studnicka, M.; Gartner, C.; Tauber, E.; Horak, F.; Veiter, A.; Spengler, J.; Kuhr, J.; Urbanek, R., Lung Function Growth and Ambient Ozone, *Am. J. Respir. Crit. Care Med.*, 1999, 160, 390-396.

Gerrity, T. R.; Weaver, R. A.; Berntsen, J.; House, D. E.; O'Neil, J. J., Extrathoracic and Intrathoracic Removal of Ozone in Tidal-breathing Humans, *J. Appl. Physiol.*, 1988, 65, No. 1, 393-400.

Giamalva, D.; Church, D., F.; Pryor, W. A., A Comparison of the Rates of Ozonation of Biological Antioxidants and Oleate and Linoleate Esters, *Biochemical and Biophysical Research Communications*, 1985, 133, 2, 773-779.

Galiza, A.; Kinney, P., Long-Term Residence in Areas of High Ozone: Associations with Respiratory Health in a Nationwide Sample of Nonsmoking Young Adults, *Environmental Health Prospective*, 1999, 107, No. 8, 675-679.

Goldstein, B. D.; McDonagh, E. M.; Effect of Ozone on Cell Membrane Protein Florescence, In Vitro Studies Utilizing the Red Cell Membrane, *Environmental Research*, 1975, 9, 179-186.

Grootveld, M.; Halliwell, B., Measurement of Allantoin and Uric Acid in Human Body Fluids, *Biochem. J.*, 1987, 243, 803-808.

Halliwell, B., Uric Acid: An Example of Antioxidant Evaluation, In *Handbook of Antioxidants*; Cadenas, E.; Packer, L., Eds; Marcel Dekker: New York, Ny, 1996, 243-256.

Hatch, G. E., Comparative Biochemistry of Airway Lining Fluid, *Comparative Biology of the Normal Lung*, 1992, 33, 617-632.

Housley, D. G.; Mudway, I.; Kelly, F. J.; Eccles, R.; Richards, R. J., Depletion of Urate in Human Nasal Lavage Following In Vitro Ozone Exposure, *Int. J. Biochem. Cell boil.*, 27, No.11, 1153-1159.

Howell, R. R.; Wyngaarden, J. B., On the Mechanism of Peroxidation of Uric Acids by Hemoproteins, *The Journal of Biological Chemistry*, 1960, 235, No. 12, 3544-3550.

Ignatenko, A.; Cherenkevich, S. N., Reactivity of Amino Acids and Proteins in Reactions with Ozone, *Kinet. Katal.*, 1985, 26, 1332-1335.

Kabel, J. R.; BenJebria, A.; Ultman, J. S., Longitudinal Distribution of Ozone Absorption in the Lung: Comparison of Nasal and Oral Quiet Breathing, *J. Appl. Physiol.*, 1994, 77, No. 6, 2584-2592.

Kaliner, M. A., Human Nasal Respiratory Secretions and Host Defense, *Am. Rev. Respir. Dis.*, 1991, 144, S52-S56.

Kanofsky, J. R.; Sima, P. D., Reactive Absorption of Ozone by Aqueous Biomolecule Solutions: Implications for the Role of Sulfhydryl Compounds as Targets for Ozone, *Archives of biochemistry and Biophysics*, 1995, 316, 52-62.

Kanofsky, J.R.; Sima, P. D., Singlet Oxygen Chemiluminescence at Gas-Liquid Interfaces: Theoretical Analysis with a One-Dimensional Model of Singlet Oxygen Quenching and Diffusion, *Archives of biochemistry and Biophysics*, 1994, 312, No.1, 244-253.

Kanofsky, J.R.; Sima, P. D., Singlet Oxygen Production from the Reactions of Ozone with Biological Molecules, *The Journal of Biological Chemistry*, 1991, 266, No.14, 9039-9042.

Kanofsky, J.R.; Sima, P. D., Reactive Absorption of Ozone: An Assay for Reaction Rates of Ozone with Sulfhydryl Compounds with Other biological Molecules, *Methods in Enzymology*, 2000, 319, 505-512.

Kaulbach, H. C.; White, M. V.; Igarashi, Y.; Hahn, B. K.; Kaliner, M. A., Estimation of Nasal Epithelial Lining Fluid using Urea as a Marker, *J. Allergy Clin. Immunol.*, 1993, 92, 457-465.

Kaur, H.; Halliwell, B., Action of Biologically-Relevant Oxidizing Species upon Uric Acid. Identification of Uric Acid Oxidation Products, *Chem. Biol. Interactions*, 1990, 73, 235-247.

Kelly, F. J.; Dunster, C.; Mudway, I., Air Pollution and the elderly: Oxidant/Antioxidant Issues Worth Consideration, *Eur. Respire. J.*, 2003, 21Suppl. 40, 70s-75s.

Kelly, F. J.; Mudway, I.; Krishna, M. T.; Holgate, S. T., The Free Radical Basis of Air Pollution: Focus on Ozone, *Respiratory Medicine*, 1995, 89, 647-656.

Knight, K. L.; Mudd, J. B., The Reaction of Ozone with Glyceraldehyde-3-phosphate Dehydrogenase, *Archives of Biochemistry and Biophysics*, 1984, 229, No. 1, 259-269.

Koren, H. S.; Hatch, G. E.; Graham, D. E., Nasal Lavage as a Tool in Assessing acute Inflammation in Response to Inhaled Pollutants , *Toxicology*, 1990, 60, 15-25.

Kosower, E. W., Chemical Properties of Glutathione. In *Glutathione: Metabolism and Function*, Arias, I. M.; Jakoby, W. B., Eds; Raven Press: New York, NY, 1976, 1-15.

Krishna, M. T.; Springall, D. R.; Frew, A. J.; Polak, J. M.; Holgate, S. T., Mediators of Inflammation in Response to Air Pollution: a Focus on Ozone and Nitrogen Dioxide, *J. R. Coll. Physicians London*, 1996, 30, 61-66.

Larson, R. A., Ed. Naturally Occurring Antioxidants; Lewis Publishers, Boca Raton, New York, 1997.

Langford, S. D.; Bidani, A.; Postlethwait, E. M., Ozone–Reactive Absorption by Pulmonary Epithelial Lining Fluid Constituents, *Toxicology and Applied Pharmacology, 1995,* 132, 122-130.

Lippmann, M., Health Effects of Tropospheric Ozone, *Environ. Sci. Technol.*, 1991, 25, No. 12, 1954-1962.

Lykkesfeldt, J.; christen, S.; Wallock, L. M.; Chang, H. H.; Jacob, R. A.; Ames, B. N., Ascorbate is Depleted by Smoking and Repleted by Moderate Supplementation: A Study in Male Smokers and Nonsmokers with Matched Dietary Antioxidant Intakes, *Am. J. Clin. Nutr.*, 2000, 71, 530-536.

MacDougal, C. S.; Rigas, M. L.; Ben-Jebria, A.; Ultman, J.S., A Respiratory Ozone Analyzer Optimized for High Resolution and Swift Dynamic Response During Exercise Conditions , *Archives of Environmental Health,1998,* 53, 2, 161-174.

Maple, K. R.; Meson, R. P., Free Radical Metabolite of Uric Acid, *The Journal of Biological Chemistry*, 1988, 263, No. 4, 1709-1712.

Matzen, R. N., Effect of Vitamin C and Hydrocortisone on the Pulmonary Edema Produced by Ozone in Mice, *J. Appl. Physiol. Respir. Environ. Exercise Physiol.*, 1957, 11, 105-109.

Meadows, J.; Smith, R. C., Uric Acid Protection of Nucleobases from Ozone-Induced Degradation, *Archives of Biochemistry and physics*, 1986, 246, No. 2, 838-845.

Meadows, J.; Smith, R. C.; Reeves, J., Uric Acid Protects Membranes and Linolenic Acid from Ozone-Induced Oxidation, *Biochemical and biophysical research Communications*, 1986, 137, No. 1, 536-541.

Meiners, B. A.; Peters, R. E.; Mudd J. B., Effects of Ozone on Indole Compounds and Rat Lung Monoamine Oxidase, *Environmental Research*, 1977, 14, 99-112.

Mudd, J. B.; Dawson, P. J.; Tseng, S.; liu, F., Reaction of Ozone with Protein Tryptpphans: Band III, Serum Albumin, and Cytochrome C, *Archives of Biochemistry and Biophysics*, 1997, 338, No. 2, 143-149.

Mudd, J. B.; Leavitt, R.; Ongun, A.; McManus, T. T., Reaction of Ozone with Amino Acids and Proteins, *Atmospheric Environment*, 1969, 3, 669-682.

Mudway, I. S.; Blomberg A. ; Frew, A. J.; Holgate, S. T.; Sandstrom, T.; Kelly, F. J., Antioxidant Consumption and Repletion Kinetics in Nasal Lavage Fluid Following exposure of Healthy Human Volunteers to Ozone , *European Respiratory Journal*,1999, 13, 1429-1438.

Mudway, I. S.; Housley, D.; Eccles, R.; Richards R. J.; Datta, A. K.; Tetley, T. D.; Kelly, F. J., Differential Depletion of Human Respiratory Tract Antioxidants in Response to Ozone Challenge , *Free Rad. Res.* 1996, 25, 6, 499-513.

Mudway, I. S.; Kelly, F. J., Modeling the Interactions of Ozone with Pulmonary Epithelial Lining Fluid Antioxidants, *Toxicology and Applied Pharmacology*, 1997, 148, 91-100.

Mudway, I. S.; Kelly, F. J., Ozone and the Lung: A Sensitive Issue, *Molecular Aspects of Medicine*, 2000, 21, 1-48.

Mudway, I. S.; Stenfors, N.; Blomberg A. ; Helleday, R.; Dunster, C.; Marklund, S. L.; Frew, A. J.; Sandstorm, T.; Kelly, F. J., Differences in Basal Airway Antioxidant Concentrations are not Predictive of Individual Responsiveness to Ozone: A Comparison of Healthy and Mild Asthmatic Subjects, *Free Radical biology & Medicine*, 2001, 31, No. 8, 962-974.

Mustafa, M. G., Biochemical Basis of Ozone Toxicity, *Free Radical Biology & Medicine,* 1990, 9, 245-265.

Nodelman, V.; Ultman, J. S., Longitudinal Distribution of Chlorine Absorption in Human Airways: A Comparison to Ozone Absorption, *J. Appl. Physiol.*, 1999, 87, No. 6, 2073-2080.

O'Neil, C.; Van der Vliet, A.; Hu, M.; Kaur, H.; Cross, C. E.; Louie, s.; Halliway, B., Oxidation of Biologic Molecules by Ozone: The Effect of pH, *J. Lab. Clin. Med.*, 1993, 122, No. 5, 497-505.

Packer, J. E; Slater, T. F.; Wilson, R. L., Direct Observation of a Free Radical Interaction Between Vitamin E and Vitamin C, *Nature*, 1979, 278, 737-738.

Peden, D. B.; Hohman, R.; Brown, M. E.; Mason, R. T.; Berkebile, C.; Fales, H. M.; Kaliner, M. A., Uric Acid is a Major Antioxidant in Human Nasal Airway Secretions, *Proc. Natl. Acad. Sci.,* 1990, 87, 7638-7642.

Peden, D. B.; Swiersz, M.; Ohkubo, K.; Hahn, B.; Emery, B.; Kaliner, M. A., Nasal Secretion of the Ozone Scavenger Uric Acid , *Am. Rev. Respir. Dis.*, 1993,148, 455-461.

Pryor, W. A., How Far Does Ozone Penetrate into the Pulmonary Air/Tissue Boundary Before it Reacts?, *Free Radical Biology & Medicine,* 1992, 12, 83-88.

Pryor, W. A., Mechanism of Radical Formation from Reactions of Ozone with Target Molecules in the Lung, *Free Radical Biology & Medicine,* 1994, 17, No. 5, 451-465.

Pryor, W. A.; Giamalva, D.; Church, D. F., Kinetics of Ozone. 1. Electron-Deficient Alkenes, *J. Am. Chem. Soc.*, 1983, 105, 6858-6861.

Pryor, W. A.; Giamalva, D.; Church, D. F., Kinetics of Ozone. 2. Amino Acids and Model Compounds in Water and Comparisons to Rates in Nonpolar Solvents , *J. Am. Chem. Soc.* 1984, 106, 7094-7100.

Pryor, W. A.; Squadraito, G. L.; Friedman, M., A New Mechanism for the Toxicity of Ozone , *Toxicology letters*, 1995a, 82/83, 287-293.

Pryor, W. A.; Squadraito, G. L.; Friedman, M., The Cascade Mechanism to Explain Ozone Toxicity: The Role of Lipid Ozonation Products, *Free Radical Biology & Medicine*, 1995b, 19, No. 6, 935-941.

Pryor, W. A.; Uppu, R. M., A Kinetic Model for the Competitive Reactions of Ozone with Amino Residues in Proteins in Reverse Micelles, *The Journal of Biological Chemistry*, 1993, 268, No. 5, 3120-3126.

Rutkowski, J. M.; Santiago, L. Y.; Ben-Jebria, A.; Ultman, J. S., Development of an Assay for Ozone-Specific Antioxidant Capacity, *Inhalation Toxicology*, 2003, 15, 1369-1385.

Romieu, I.; Meneses, F.; Ramirez, M.; Ruiz S.; Padilla, R. P.; Sienra, J. J.; Gerber, M.; Grievink, L.; Dekker, R.; Walda, I.; brunekreef, B., Antioxidant Supplementation and Respiratory Functions among Workers Exposed to High Levels of Ozone, *Am. J. Respir. Crit. Care Med*., 1998, 158, 226-232.

Santiago, L. Y., Absorption of Ozone in the Human Nose during Unidirectional Airflow. Ph.D. Thesis. The Pennsylvania State University. Department of Chemical Engineering, 2001.

Santiago, L. Y.; Hann, M. C.; Ben-Jebria, A.; Ultman, J. S., Exposure System for Measurement of Nasal Ozone Absorption, *J. Appl. Physiol.*, 2001, 97, 725-735.

Shaw, C. A., Ed. Glutathione in the Nervous System; Taylor and Francis: Washington DC, 1998, 3-9.

Simic, M. G.; Jovanovic, S. V.; Antioxidation Mechanisms of Uric Acid, *J. Am. Chem. Soc.*, 1989, 111, 5778-5782.

Tyler, W. S.; Tyler, N. K.; Geillispie, M. J.; Barstow, T. J., Comparison of Daily and Seasonal Exposures of Young Monkeys to Ozone, *Toxicology*, 1988, 50, No. 2, 131-44.

Uppu, R. M.; Cueto, R.; Squadrito, G. L.; Pryor, W. A., What does Ozone React with at the Air/Lung Interface? Model Studies Using Human Red Blood Cell Membranes, *Archives of Biochemistry and Biophysics*, 1995, 319, No. 1, 257-266.

Valverde, M.; Del Carmen Lopez, M.; Lopez, I.; Sanchez, I.; Fortoul, I.; Ostrosky-Wegman, P.; Rojas, E., DNA Damage in Leukocytes and Buccal and Nasal Epithelial Cells of Individuals Exposed to Air Pollution in Mexico City, *Environmental and Molecular Mutagenesis*, 1997, 30,147-152.

Van der Vliet, A.; O'Neill, C. A.; Eiserich, J. P.; Cross, C. E., Oxidative Damage to Extracellular Fluids by Ozone and Possible Protective Effects of Thiols, *Archives of Biochemistry and Biophysics*, 1995, 321, No. 1, 43-50.

Van der Vliet, A.; O'Neill, C. A.; Cross, C. E.; Koostra, J. M.; Volz, W. G.; Halliwell, B.; Louie, S., Determination of Low-Molecular-Mass antioxidant Concentrations in Human Respiratory Tract Lining Fluids, *Am. Physiol. Soc.*, 1999, 276, L289-L296.

Wright, E. S.; Dziedzic, D.; Wheeler, C. S., Cellular, Biochemical and Functional Effects of Ozone: New Research and Perspectives on Ozone Health Effects, *Toxicology Letters*, 1990, 51, 125-145.

Wiester, M. J.; Stevens, M. A.; Menache, M. G.; McKee, J. L. Jr.; Gerrity, T. R., Ozone Uptake in Healthy Adult Males during Quiet Breathing, *Fundamental and Applied Toxicology*, 1996, 29, 102-109.

Appendix A

OZONE GENERATOR

Ozone generator (Model 165 C, Thermo Environmental Instruments INC., Franklin, Massachusetts) was used to generate ozone. The model 165C ozone generator is a lightweight portable transfer calibrator capable of producing over 1000 ppb at 3 LPM. The model 165C is equipped with an internal ozone generator. Ozone is produced by exposing air to light at 185 nm. The instrument varies the ozone level by changing the flow of zero-air through the ozone generator. The light intensity is held constant by using a highly stable lamp power supply. Pressurized ozone free air is connected to the “Air In” fitting on rear of the ozonator. The pressure control is set so that approximates 5 to 8 psig of air is shown on a digital pressure display. Pressure of 7.5 psig was used in our experiments. Ozone level can be set for two concentration level ”A” or level “B”. There are potentiometer adjustments for ozone level “A” on the generator. They adjust the lamp intensity for ozone concentration level “A”.

Two output ports are located on the back of the generator, ozone port and vent port. Vent port regulates the output flow from the instrument by providing a pressure release. In our experiment, flow from ozone port passed through rotometer on its way to the reactor. The rotometer caused a large amount of resistance and consequently large amount of pressure drop. Therefore we were not able to get any flow toward the reactor. In order to get sufficient flow, a valve had to be used at the vent port of the O_3 generator. The vent and ozone ports are parallel and therefore any decrease in the flow through the

vent port causes an increase in the flow through the ozone port. The valve at the vent port was always completely open. We tried to calibrate the ozonator for different flow rates. It was realized that using valve at the exhaust vent caused some unexpected non linear behavior in ozone production, probably due to the increased pressure at the generator output. Figure **A-1** shows the calibration curves of O_3 generator. The top graph shows the ozonator calibration when there was no valve at the vent port, whereas the bottom graph shows the calibration when a valve was used at the vent port of the O_3 generator. It is observed from these graphs that using a valve at the exhaust vent caused an increase in ozone production by factor of three.

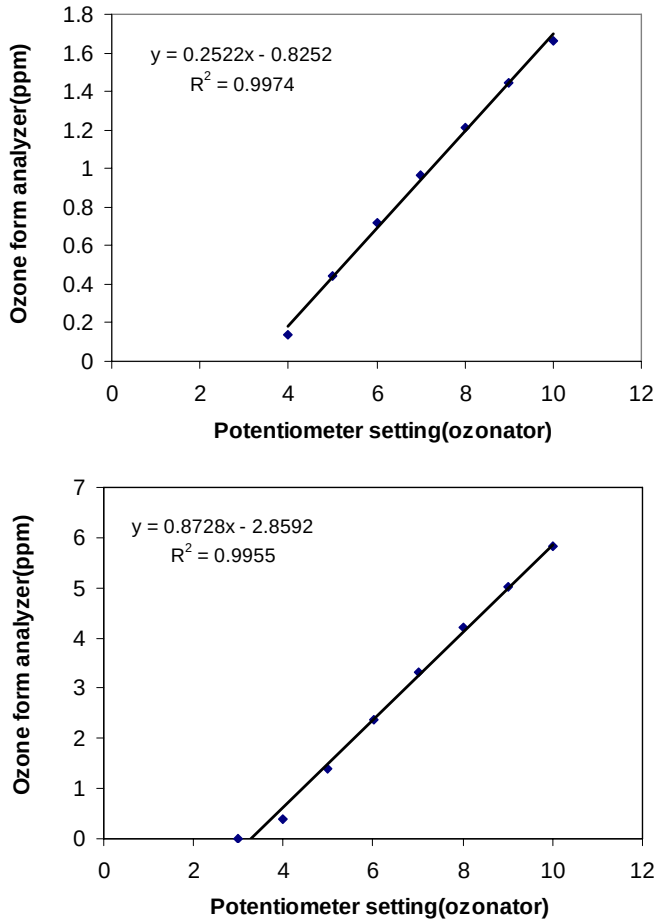

Figure **A-1**: O_3 Generator Calibration

Top graph shows the ozonator calibration when there was no valve at the vent port, whereas bottom graph shows the calibration when a valve was used at the vent port of the O_3 generator.

Appendix B

OZONE ANALYZER

A fast- responding, chemiluminescent O_3 analyzer (MacDougal et al., 1998) was used to continuously record the O_3 concentration in the air leaving the reactor. The ozone analyzer could sample ozonated air from both inlet and outlet stream. Operation of this instrument is based on homogenous chemiluminescent reaction of O_3 with ethylene as the reactant gas. Optimum conditions for operating this analyzer are as follows:

- Reaction chamber pressure = 350 torr
- Ethylene/sample flow ratio = 4:1
- Sampling flow = 600 ml/min.

In our experiments reaction chamber pressure of 355 torr, sampling flow of 200 ml/min, and ethylene flow of 800ml/min were used. O_3 concentration was determined using calibration equation of analyzer which converts voltage to parts per million (ppm) (Figure **B-1**).

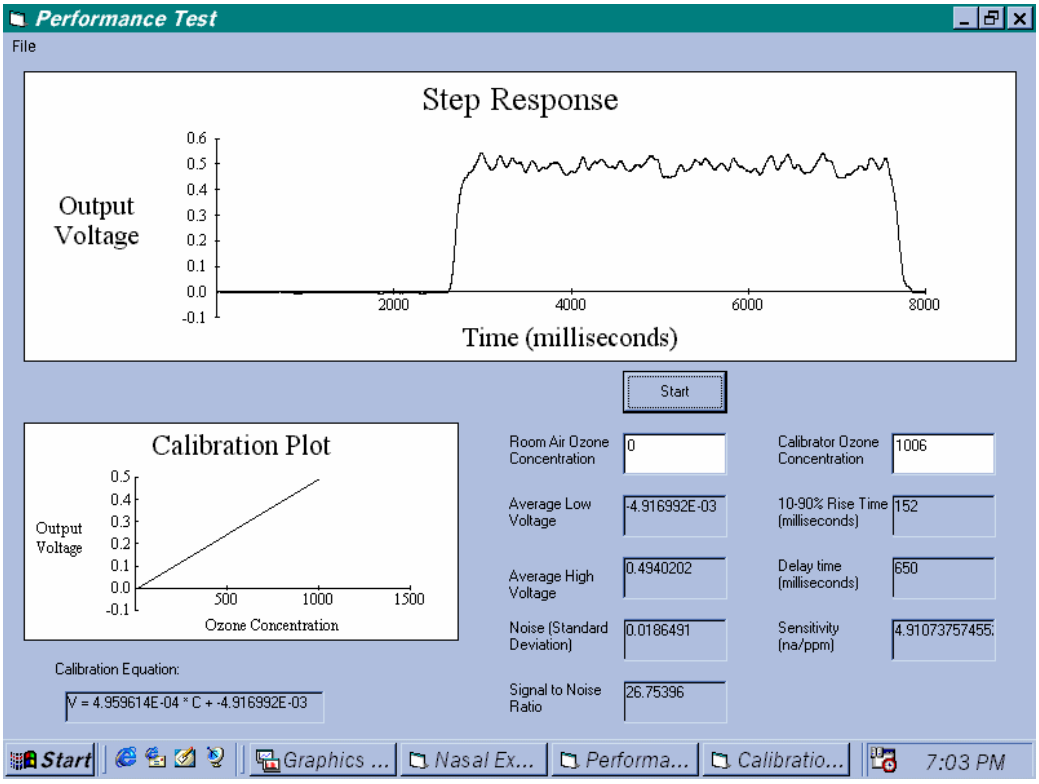

Figure **B-1**: Calibration Curve Developed for O_3 Analyzer Using the Calibrator.

By using the calibration equation which converts voltage to parts per million (ppm), O_3 concentration can be determined.

Appendix C

DATA ACQUISITION SYSTEM

A personal computer equipped with a data acquisition card (DAQ 802, Omega Engineering, INC., Stamford, CT). DAQ-802 is a cost effective high speed data acquisition board that plug into ISA expansion slots in compatible personal computer. The DAQ-800 series circuit board provides 12-bit analog input, 32-bit digital input/output (I/O) and three 16-bit programmable timer/counters. The DAQ-802 is software programmable for gains 1, 2, 4 or 8 with the maximum sampling rate of 40 KHz. Quatech's Daq Ez is a software package which was specifically designed to support all Quatech's data acquisition adapter functions and is included with the hardware. Daq Ez is an easy to use application that requires no programming knowledge and allows the user to graphically acquire and display time data using customized channel labels, charts and displays. In our experiments Daq Ez automatically acquire the output signal from the O_3 analyzer with a rate of 1 scan per second.

Appendix D

FORTRAN CODE

FORTRAN code for determining rate constants of O_3 reaction with individual antioxidants.

```
PROGRAM OPTIMIZATION

USE NUMERICAL_LIBRARIES
IMPLICIT NONE

INTEGER LDFJAC, M, N
PARAMETER (LDFJAC=24, M=24, N=1)

INTEGER IPARAM(7)
INTEGER ITP
INTEGER NOUT

REAL FJAC(LDFJAC,N)
REAL FSCALE(M)
REAL FVEC(M)
REAL RPARAM(7)
REAL X(N)
REAL XGUESS(N)
REAL XLB(N)
REAL XS(N)
REAL XUB(N)
REAL XSCALE(N)
REAL Sum

EXTERNAL MODEL1

REAL AR_O3_Exp1,AR_Ua_Exp1,AR_U_1,AR_O3_1
REAL AR_O3_Exp2,AR_Ua_Exp2,AR_U_2,AR_O3_2
REAL AR_O3_Exp3,AR_Ua_Exp3,AR_U_3,AR_O3_3

REAL AR_O3_Exp4,AR_Ua_Exp4,AR_U_4,AR_O3_4
REAL AR_O3_Exp5,AR_Ua_Exp5,AR_U_5,AR_O3_5
REAL AR_O3_Exp6,AR_Ua_Exp6,AR_U_6,AR_O3_6


REAL AR_O3_Exp7,AR_Ua_Exp7,AR_U_7,AR_O3_7
REAL AR_O3_Exp8,AR_Ua_Exp8,AR_U_8,AR_O3_8
REAL AR_O3_Exp9,AR_Ua_Exp9,AR_U_9,AR_O3_9


REAL AR_O3_Exp10,AR_Ua_Exp10,AR_U_10,AR_O3_10
REAL AR_O3_Exp11,AR_Ua_Exp11,AR_U_11,AR_O3_11
```

```
REAL AR_O3_Exp12,AR_Ua_Exp12,AR_U_12,AR_O3_12

REAL Time_5min,Time_10min,Time_15min
REAL Cua1,Cua2,Cua3,Cua4
REAL P1,P2,P3

OPEN(UNIT=60,FILE="OutputFile.xls",STATUS="REPLACE")

Time_15min=15.0
Time_10min=10.0
Time_5min=5.0

P1=1.49
P2=2.8
P3=5.05

!*************************************************
!Experimental Data

Cua1=45.13*1E-6

AR_O3_Exp1=16.47    !5min exp
AR_Ua_Exp1=58.78    !5min exp

AR_O3_Exp2=37.90    !10min exp
AR_Ua_Exp2=92.26    !10min exp

AR_O3_Exp3=54.22    !15min exp
AR_Ua_Exp3=113.07   !15min exp

!*************************************************

Cua2=94.83*1E-6


AR_O3_Exp4=21.50    !5min exp
AR_Ua_Exp4=89.52    !5min exp

AR_O3_Exp5=54.16     !10min exp
AR_Ua_Exp5=151.96   !10min exp

AR_O3_Exp6=81.25     !15min exp
AR_Ua_Exp6=201.01   !15min exp


!*************************************************

Cua3=146.14*1E-6


AR_O3_Exp7=29.88     !5min exp
AR_Ua_Exp7=130.03   !5min exp

AR_O3_Exp8=72.62     !10min exp
```

```
AR_Ua_Exp8=199.93    !10min exp

AR_O3_Exp9=108.96    !15min exp
AR_Ua_Exp9=279.58    !15min exp


!*************************************************

Cua4=201.97*1E-6


AR_O3_Exp10=37.12     !5min exp
AR_Ua_Exp10=116.35   !5min exp

AR_O3_Exp11=85.43     !10min exp
AR_Ua_Exp11=254.55   !10min exp

AR_O3_Exp12=129.24   !15min exp
AR_Ua_Exp12=343.31   !15min exp


!*************************************************
! Compute the least squares for the Rosenbrock function.


XGUESS(1)=1E5    !--> Kr

XS(1)=1.0E0
FSCALE(1)=1.0E0


XLB(1)=1E1
XUB(1)=1E20


! All the bounds are provided
ITP = 0
XSCALE=0

! Default parameters are used
IPARAM(1) = 0
IPARAM(6)=1


!Bounded Method

CALL BCLSF (ROSBCK,M,N,XGUESS,ITP,XLB,XUB,XS,FSCALE,IPARAM,
RPARAM,X,FVEC,FJAC,LDFJAC)

!Unbounded Method

!CALL UNLSF (ROSBCK,M,N,XGUESS,XSCALE,FSCALE,IPARAM,RPARAM
,X,FVEC,FJAC,LDFJAC)
```

```
CALL MODEL1(X(1),AR_U_1,AR_O3_1,Cua1,P2,Time_5min)
CALL MODEL1(X(1),AR_U_2,AR_O3_2,Cua1,P2,Time_10min)
CALL MODEL1(X(1),AR_U_3,AR_O3_3,Cua1,P2,Time_15min)

CALL MODEL1(X(1),AR_U_4,AR_O3_4,Cua2,P2,Time_5min)
CALL MODEL1(X(1),AR_U_5,AR_O3_5,Cua2,P2,Time_10min)
CALL MODEL1(X(1),AR_U_6,AR_O3_6,Cua2,P2,Time_15min)

CALL MODEL1(X(1),AR_U_7,AR_O3_7,Cua3,P2,Time_5min)
CALL MODEL1(X(1),AR_U_8,AR_O3_8,Cua3,P2,Time_10min)
CALL MODEL1(X(1),AR_U_9,AR_O3_9,Cua3,P2,Time_15min)

CALL MODEL1(X(1),AR_U_10,AR_O3_10,Cua4,P2,Time_5min)
CALL MODEL1(X(1),AR_U_11,AR_O3_11,Cua4,P2,Time_10min)
CALL MODEL1(X(1),AR_U_12,AR_O3_12,Cua4,P2,Time_15min)

!*************************************************
!Sum of Errors

Sum=0.5*((FVEC(1))**2+(FVEC(2))**2+(FVEC(3))**2+(FVEC(4))**2
+(FVEC(5))**2+(FVEC(6))**2+(FVEC(7))**2+(FVEC(8))**2+(FVEC(9))**2
+(FVEC(10))**2+(FVEC(11))**2+(FVEC(12))**2+(FVEC(13))**2+(FVEC(14))**2
+(FVEC(15))**2+(FVEC(16))**2+(FVEC(17))**2+(FVEC(18))**2+(FVEC(19))**2
+(FVEC(20))**2+(FVEC(21))**2+(FVEC(22))**2+(FVEC(23))**2+(FVEC(24))**2)

!*************************************************
! Print Results

WRITE (*,*) 'Kr(in-guess)=',XGUESS(1)
WRITE (*,*) 'Kr=',X(1)
WRITE (*,*) 'Uric Acid=',Cua1

WRITE (*,*) 'AR(model)-(t=5,UA=50)=',AR_O3_1
WRITE (*,*) 'UA(model)-(t=5,UA=50)=',AR_U_1

WRITE (*,*) 'AR(model)-(t=10,UA=50)=',AR_O3_2
WRITE (*,*) 'UA(model)-(t=10,UA=50)=',AR_U_2

WRITE (*,*) 'AR(model)-(t=15,UA=50)=',AR_O3_3
WRITE (*,*) 'UA(model)-(t=15,UA=50)=',AR_U_3

WRITE (*,*) 'AR(exp)-(t=5,UA=50)=',AR_O3_Exp1
WRITE (*,*) 'UA(exp)-(t=5,UA=50)=',AR_Ua_Exp1

WRITE (*,*) 'AR(exp)-(t=10,UA=50)=',AR_O3_Exp2
WRITE (*,*) 'UA(exp)-(t=10,UA=50)=',AR_Ua_Exp2

WRITE (*,*) 'AR(exp)-(t=15,UA=50)=',AR_O3_Exp3
WRITE (*,*) 'UA(exp)-(t=15,UA=50)=',AR_Ua_Exp3


WRITE (*,*) 'Uric Acid=',Cua2

WRITE (*,*) 'AR(model)-(t=5,UA=100)=',AR_O3_4
```

```
WRITE (*,*) 'UA(model)-(t=5,UA=100)=',AR_U_4

WRITE (*,*) 'AR(model)-(t=10,UA=100)=',AR_O3_5
WRITE (*,*) 'UA(model)-(t=10,UA=100)=',AR_U_5

WRITE (*,*) 'AR(model)-(t=15,UA=100)=',AR_O3_6
WRITE (*,*) 'UA(model)-(t=10,UA=100)=',AR_U_5

WRITE (*,*) 'AR(exp)-(t=5,UA=100)=',AR_O3_Exp4
WRITE (*,*) 'UA(exp)-(t=5,UA=100)=',AR_Ua_Exp4

WRITE (*,*) 'AR(exp)-(t=10,UA=100)=',AR_O3_Exp5
WRITE (*,*) 'UA(exp)-(t=10,UA=100)=',AR_Ua_Exp5

WRITE (*,*) 'AR(exp)-(t=15,UA=100)=',AR_O3_Exp6
WRITE (*,*) 'UA(exp)-(t=15,UA=100)=',AR_Ua_Exp6


WRITE (*,*) 'Uric Acid=',Cua3

WRITE (*,*) 'AR(model)-(t=5,UA=150)=',AR_O3_7
WRITE (*,*) 'UA(model)-(t=5,UA=150)=',AR_U_7

WRITE (*,*) 'AR(model)-(t=10,UA=150)=',AR_O3_8
WRITE (*,*) 'UA(model)-(t=10,UA=150)=',AR_U_8

WRITE (*,*) 'AR(model)-(t=15,UA=150)=',AR_O3_9
WRITE (*,*) 'UA(model)-(t=15,UA=150)=',AR_U_9

WRITE (*,*) 'AR(exp)-(t=5,UA=150)=',AR_O3_Exp7
WRITE (*,*) 'UA(exp)-(t=5,UA=150)=',AR_Ua_Exp7

WRITE (*,*) 'AR(exp)-(t=10,UA=150)=',AR_O3_Exp8
WRITE (*,*) 'UA(exp)-(t=10,UA=150)=',AR_Ua_Exp8

WRITE (*,*) 'AR(exp)-(t=15,UA=150)=',AR_O3_Exp9
WRITE (*,*) 'UA(exp)-(t=15,UA=150)=',AR_Ua_Exp9


WRITE (*,*) 'Uric Acid=',Cua4

WRITE (*,*) 'AR(model)-(t=5,UA=150)=',AR_O3_10
WRITE (*,*) 'UA(model)-(t=5,UA=150)=',AR_U_10

WRITE (*,*) 'AR(model)-(t=10,UA=150)=',AR_O3_11
WRITE (*,*) 'UA(model)-(t=10,UA=150)=',AR_U_11

WRITE (*,*) 'AR(model)-(t=15,UA=150)=',AR_O3_12
WRITE (*,*) 'UA(model)-(t=15,UA=150)=',AR_U_12

WRITE (*,*) 'AR(exp)-(t=5,UA=150)=',AR_O3_Exp10
WRITE (*,*) 'UA(exp)-(t=5,UA=150)=',AR_Ua_Exp10

WRITE (*,*) 'AR(exp)-(t=10,UA=150)=',AR_O3_Exp11
```

```
WRITE (*,*) 'UA(exp)-(t=10,UA=150)=',AR_Ua_Exp11

WRITE (*,*) 'AR(exp)-(t=15,UA=150)=',AR_O3_Exp12
WRITE (*,*) 'UA(exp)-(t=15,UA=150)=',AR_Ua_Exp12


WRITE (*,*) 'SUM=',sum


CONTAINS

!************************************************

SUBROUTINE ROSBCK (M, N, X, F)
INTEGER M, N
REAL X(N), F(M)

CALL MODEL1(X(1),AR_U_1,AR_O3_1,Cua1,P2,Time_5min)


F(1) = AR_O3_1 - AR_O3_Exp1
F(2) = AR_U_1 - AR_Ua_Exp1


CALL MODEL1(X(1),AR_U_2,AR_O3_2,Cua1,P2,Time_10min)

F(3) = AR_O3_2 - AR_O3_Exp2
F(4) = AR_U_2 - AR_Ua_Exp2


CALL MODEL1(X(1),AR_U_3,AR_O3_3,Cua1,P2,Time_15min)

F(5) = AR_O3_3 - AR_O3_Exp3
F(6) = AR_U_3 - AR_Ua_Exp3


CALL MODEL1(X(1),AR_U_4,AR_O3_4,Cua2,P2,Time_5min)


F(7) = AR_O3_4 - AR_O3_Exp4
F(8) = AR_U_4 - AR_Ua_Exp4

CALL MODEL1(X(1),AR_U_5,AR_O3_5,Cua2,P2,Time_10min)

F(9) = AR_O3_5 - AR_O3_Exp5
F(10) = AR_U_5 - AR_Ua_Exp5


CALL MODEL1(X(1),AR_U_6,AR_O3_6,Cua2,P2,Time_15min)

F(11) = AR_O3_6 - AR_O3_Exp6
F(12) = AR_U_6 - AR_Ua_Exp6
```

```
CALL MODEL1(X(1),AR_U_7,AR_O3_7,Cua3,P2,Time_5min)


F(13) = AR_O3_7 - AR_O3_Exp7
F(14) = AR_U_7 - AR_Ua_Exp7

CALL MODEL1(X(1),AR_U_8,AR_O3_8,Cua3,P2,Time_10min)

F(15) = AR_O3_8 - AR_O3_Exp8
F(16) = AR_U_8 - AR_Ua_Exp8


CALL MODEL1(X(1),AR_U_9,AR_O3_9,Cua3,P2,Time_15min)

F(17) = AR_O3_9 - AR_O3_Exp9
F(18) = AR_U_9 - AR_Ua_Exp9


CALL MODEL1(X(1),AR_U_10,AR_O3_10,Cua4,P2,Time_5min)


F(19) = AR_O3_10 - AR_O3_Exp10
F(20) = AR_U_10 - AR_Ua_Exp10

CALL MODEL1(X(1),AR_U_11,AR_O3_11,Cua4,P2,Time_10min)

F(21) = AR_O3_11 - AR_O3_Exp11
F(22) = AR_U_11 - AR_Ua_Exp11


CALL MODEL1(X(1),AR_U_12,AR_O3_12,Cua4,P2,Time_15min)

F(23) = AR_O3_12 - AR_O3_Exp12
F(24) = AR_U_12 - AR_Ua_Exp12

RETURN
END SUBROUTINE

!************************************************

END PROGRAM


!@@@@@@@@@@@@@@@@@@@@@@@@@@@@@@@


SUBROUTINE MODEL1(Kr,AR_Ua,AR_O3,CUa,P,Time_exp)

USE NUMERICAL_LIBRARIES
IMPLICIT NONE

INTEGER MXPARM, N,M
PARAMETER (MXPARM=50, N=3,M=2000)
```

```
INTEGER MABSE, MBDF, MSOLVE
PARAMETER (MABSE=1, MBDF=2, MSOLVE=1)

INTEGER IDO,NOUT,ISTEP,ICOUNT
REAL SSTEP,STEPSIZE
REAL A(1,1),PARAM(MXPARM),T,TEND,TOL,TIMME(M),C(N,M),Y(N)

REAL ARo3(M)
REAL R,TEMP,H,Q,Lamda
REAL CCin,Cs
REAL Vg,VL,Vr,Vt
REAL CUa5,CUa10,CUa15
REAL VL0,VL5,VL10
REAL aa,bb
INTEGER ii,jj

REAL,INTENT(IN) :: Kr       !lit/(mole.min)
REAL,INTENT(IN) :: CUa      !mole/lit
REAL,INTENT(IN) :: P        !O3 ppm
REAL,INTENT(IN) :: Time_exp  !min

REAL,INTENT(OUT):: AR_Ua
REAL,INTENT(OUT):: AR_O3
        R=0.0826            !atm.lit/(mole K)
        TEMP=(273+25)       !K
        Vg=4.653            !cm3
        VL=3.0              !cm3
        VL0=3.0             !cm3
        Vr=275.0            !cm3
        Q=528.6             !cm3/min
        CCin=P/(R*TEMP*1E6)   !mole/lit
        H=4570.0            !atm
        lamda=H/(R*TEMP*55.5)
        Vt=Vg+VL/Lamda

        aa=1.0              !Stoichiometery
        bb=2.5              !Stoichiometery

C=0.0
Y=0.0
ARo3=0.0
TIMME=0.0
TEND=0

!************************************************
! Set initial conditions

        T = 0.0
        Y(1) = 0.0
        Y(2) = 0.0
        Y(3) = CUa

        C(1,1)=0.0
        C(2,1)=0.0
```

```
        C(3,1)=CUa

        ARo3(1)=0
        TIMME(1)=0

        CUa5=0.0
        CUa10=0.0
        CUa15=0.0
        VL5=0.0
        VL10=0.0

!*************************************************
! Set error tolerance

        TOL = 1E-10

!*************************************************
! Set PARAM to defaults

        CALL SSET (MXPARM, 0.0, PARAM, 1)

        PARAM(10) = MABSE
        PARAM(12) = MBDF
        PARAM(13) = MSOLVE

!*************************************************
        ii=1
        jj=1
        ICOUNT=0
        IDO = 1
        SSTEP = 0.0
        STEPSIZE=0.5
10 CONTINUE
        SSTEP = SSTEP + STEPSIZE
        TEND = SSTEP
        ICOUNT=ICOUNT+1

! The array a(*,*) is not used.

IF ((SSTEP>5.0) .and. (jj==1)) THEN
        VL=3.0-0.25
        Vt=Vg+VL/Lamda
        VL5=3.0-0.25
        CUa5=Y(3)
        jj=jj+1
ENDIF

IF ((SSTEP>10.0) .and. (ii==1)) THEN
        VL=3-0.5
        Vt=Vg+VL/Lamda
        VL10=3-0.5
        CUa10=Y(3)
        ii=ii+1
ENDIF
```

```
        CALL IVPAG (IDO,N,FUNC,FUNCJ,A,T,TEND,TOL,PARAM,Y)

        C(1,ICOUNT)=R*TEMP*1E6*Y(1)
        C(2,ICOUNT)=R*TEMP*1E6*Y(2)
        C(3,ICOUNT)=1E6*Y(3)

        Cs=CCin*(1-exp(-(Q/Vr)*TEND))        !Saline concentration

        ARo3(ICOUNT)=Q*(Cs-Y(2))*1E6         !nmole/min
        TIMME(ICOUNT)=TEND                   !time (min)


IF (SSTEP <= Time_exp+STEPSIZE) THEN

        ! Final call to release workspace
        IF (SSTEP .EQ. Time_exp+STEPSIZE) IDO = 3
        GO TO 10
END IF

!************************************************
!Integration Subroutine for O3

CALL INTEG(ARo3(:),TIMME(:),ICOUNT-1,AR_O3)

AR_Ua=(VL0*(CUa-CUa5)+VL5*(CUa5-CUa10)+VL10*(CUa10-Y(3)))*1E6


CONTAINS

!************************************************
! Differential Equations

SUBROUTINE FUNC(N,T,Y,YPRIME)
INTEGER N
REAL T, Y(N), YPRIME(N)

YPRIME(1)=Q*CCin/Vt-(Q/Vt)*Y(1)-(Kr*VL/(Vt*(Lamda**aa)))*(Y(1)**aa)*(Y(3)**bb)
YPRIME(2)=(Q/Vr)*Y(1)-(Q/Vr)*Y(2)
YPRIME(3)=-(bb/aa)*(Kr/(Lamda**aa))*(Y(1)**aa)*(Y(3)**bb)

RETURN
ENDSUBROUTINE

!************************************************
!Jacobian Matrix

SUBROUTINE FUNCJ(N,T,Y,DYPDY)

INTEGER N
REAL T, Y(N), DYPDY(N,N)

DYPDY(1,1)=-(Q/Vt)-((Kr*VL/(Vt*(Lamda**aa)))*(aa)*(Y(1)**(aa-1))*(Y(3)**bb))
DYPDY(1,2)=0
DYPDY(1,3)=-(Kr*VL/(Vt*(Lamda**aa)))*(bb)*(Y(1)**aa)*(Y(3)**(bb-1))
```

```
DYPDY(2,1)=Q/Vr
DYPDY(2,2)=-Q/Vr
DYPDY(2,3)=0
DYPDY(3,1)=-(bb/aa)*(Kr/(Lamda**aa))*(aa)*(Y(1)**(aa-1))*(Y(3)**bb)
DYPDY(3,2)=0
DYPDY(3,3)=-(bb/aa)*(Kr/(Lamda**aa))*(bb)*(Y(1)**aa)*(Y(3)**(bb-1))

RETURN
END SUBROUTINE

!************************************************
END SUBROUTINE



!@@@@@@@@@@@@@@@@@@@@@@@@@@@@@@@@@@@@



SUBROUTINE INTEG(P,T,N,AR)

IMPLICIT NONE
INTEGER j,N

REAL HH
REAL,INTENT(IN):: P(N)
REAL,INTENT(IN):: T(N)
REAL,INTENT(OUT):: AR


        HH=(T(N)-T(1))/(N-1)
        AR=0.0

        DO j=1,N-2,2 ! Simpsons Rule

                AR=AR+(HH/3.0)*(P(j)+4.0*P(j+1)+P(j+2))

        ENDDO

RETURN
END SUBROUTINE
```

Appendix E

CALCULATIONS OF REACTION RATE CONSTANTS USING DATA OBTAINED FROM MUDWAY AND KELLY (1998)

Mudway and Kelly (1998) studied the reaction of O_3 with 1 ml samples of antioxidant solution placed in multi-well plates. The plates were housed in a 5.6 L chamber that was continuously flushed with ozonated air at a flow rate of 3 L/min. The chamber rested on an orbital shaker that promoted mixing of the antioxidant solutions. Changes in UA, AH_2 and GSH concentrations were reported during 720 minutes of exposure time for various concentrations of O_3 in the chamber air.

If each sample well can be modeled as a perfectly-mixed batch reactor, then the rate of change in substrate concentration (c_S) can be formulated by the following material balance:

$$\frac{dc_S}{dt} = -\dot{R}_S = -k_r c_{O3}^m c_S^n \qquad \textbf{(E.1)}$$

Assuming that O_3 concentration in the liquid samples (c_{O3}) were in equilibrium with the (constant) chamber air concentration (C_{O3}), we can also write that

$$c_{O3} = \lambda^{L,G} C_{O3} \qquad \textbf{(E.2)}$$

For the reaction of UA and AH_2 with O_3, we know that m=n=1 so that Equation **E.1** can be integrated between t=0 and t=T to obtain

$$\frac{1}{T}\ln\left[\frac{c_S(t=0)}{c_S(t=T)}\right] = \left(k_r\,\lambda^{L,G}\right)C_{O3} \qquad \textbf{(E.3)}$$

We selected UA and AH_2 data points from figure 1 of Mudway and Kelly's paper at C_{O3} values of 0.1 to 1.50 ppm using the criterion that $c_A(t=0)/c_A(t=T)\approx 2$. Employing a least square regression of these data to Equation **E.3**, we obtained k_r values of 11840 $M^{-1}s^{-1}$ for UA and 13650 $M^{-1}s^{-1}$ for AH_2.

For GSH, the stoichiometry obtained in our study (m=0.5 and n=1.25) was used to integrate Equation **E.1** between t=0 and t=T with the result that

$$\frac{\left[c_S(t=T)\right]^{-0.25} - \left[c_S(t=0)\right]^{-0.25}}{0.25T} = \left(\lambda^{L,G}\,C_{O3}\right)^{0.5} k_r \qquad \textbf{(E.4)}$$

We selected data points for GSH from figure 2 of Mudway and Kelly's paper at C_{O3} values from 0.25 to 1.50 ppm using the criterion that $c_A(t=0)/c_A(t=T)\approx 1.3$. Employing a least square regression of these data to Equation **E.4**, we obtained a k_r value of 4.94 $M^{-0.75}s^{-1}$ for GSH. Furthermore, to compare k_r value for GSH to values reported by other research groups we assumed that O_3 reaction with GSH has a 1:1 stoichiometry. Employing a least square regression of above data to Equation **E.3**, we obtained a k_r value of 4622 $M^{-1}s^{-1}$ for GSH.

Appendix F

Mass Transfer Study

As was discussed in Chapter 5, reaction rate constants obtained from simulating the experimental data were two to three orders of magnitude smaller than the previously reported reaction rate constants (Table **5-1**). Furthermore, it was shown in Chapter 5 that mass transfer resistances in both gas phase and liquid phase are negligible and therefore, to develop the mathematical model an interfacial equilibrium was employed. However, to verify that the discrepancy between our values and the values found in the previous studies was not due to neglecting the mass transfer resistance in the model, an alternative mathematical model was developed in which, the reaction rate constant for UA was adopted from Giamalva et al. (1985) and the overall mass transfer coefficient in the gas phase was determined.

Equation **4.2** which shows a material balance for O_3 in the gas phase may be written as follows:

$$V_G \frac{dC_{O3,1}}{dt} = \dot{V}\,(C_{O3,0} - C_{O3,1}) - KA(C_{O3,1} - \lambda\, C_{O3,L}) \qquad \textbf{(F.1)}$$

where KA is the overall mass transfer coefficient in the gas phase. In addition, the material balance for O_3 in the liquid phase (Equation **4.3**) can be written as follows:

$$V_L \frac{dC_{O3,L}}{dt} = KA(C_{O3,1} - \lambda\, C_{O3,L}) - V_L \dot{R}_{O3} \qquad \textbf{(F.2)}$$

The final model is an initial value problem consisting of five equations (Equations **4.1**, **4.10**, **4.11**, **F.1**, and **F.2**). KA was determined to be 325 liter/min using an optimization program in which the squared-error between the observed amounts of O_3 absorbed and UA consumed and their simulated values was minimized. Figures **F-1** and **F-2** show a comparison between model simulations and experimental data for the time course of outlet O_3 concentration and O_3 absorption rate, respectively. Furthermore, these figures compare the simulation results obtained from the above method with the results obtained in Chapter 5 where negligible mass transfer resistances in the gas and liquid phases were employed. As can be observed from these figures, simulation results obtained using above procedure is not capable of predicting the right trend of the experimental data. Simulations results demonstrated that outlet O_3 concentration and consequently O_3 absorption rate leveled off after few minutes. Very large reaction rate constant that was reported by Giamalva et al. (1985) and employed in the model may explain these findings.

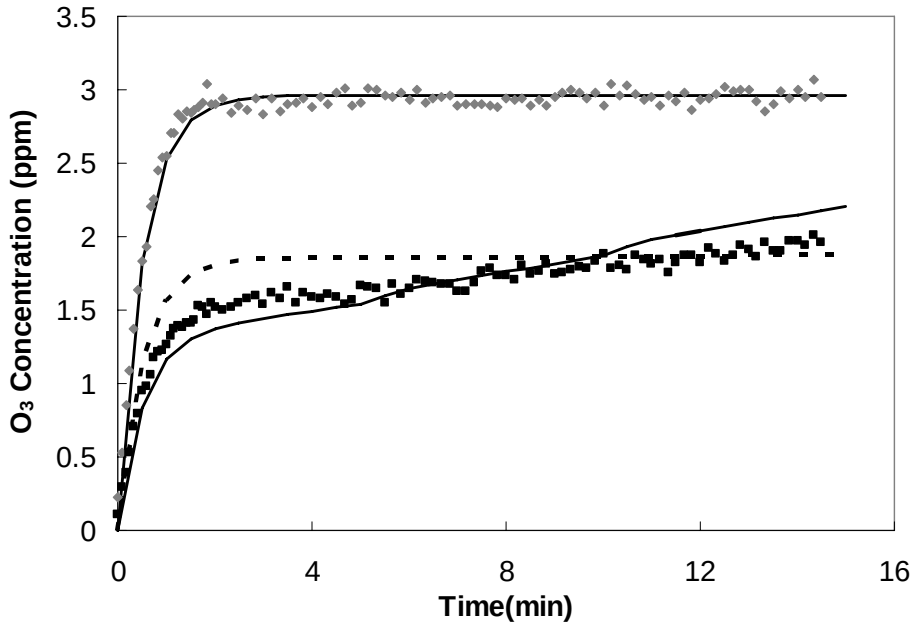

Figure **F-1**: Experimental Data and Model Simulations of Outlet O_3 Concentration

Representative data illustrate the model simulations (solid or dashed lines) and experimental data for a fixed flow of 500 ml/min, and a fixed O_3 concentration of 3.0 ppm. Experimental data of the time course of O_3 output concentration in saline control experiments (♦) and in the experiments with initial UA concentrations of 200 μM (■) are shown. Dashed line represents the simulation results obtained from the model discussed in the appendix F where $k_r = 1.4\times10^6\ M^{-1}\ \text{sec}^{-1}$ (Giamalva et al., 1985) and KA=325 liter/min, whereas solid line shows the simulation results obtained where negligible mass transfer resistances in both gas and liquid phases were considered.

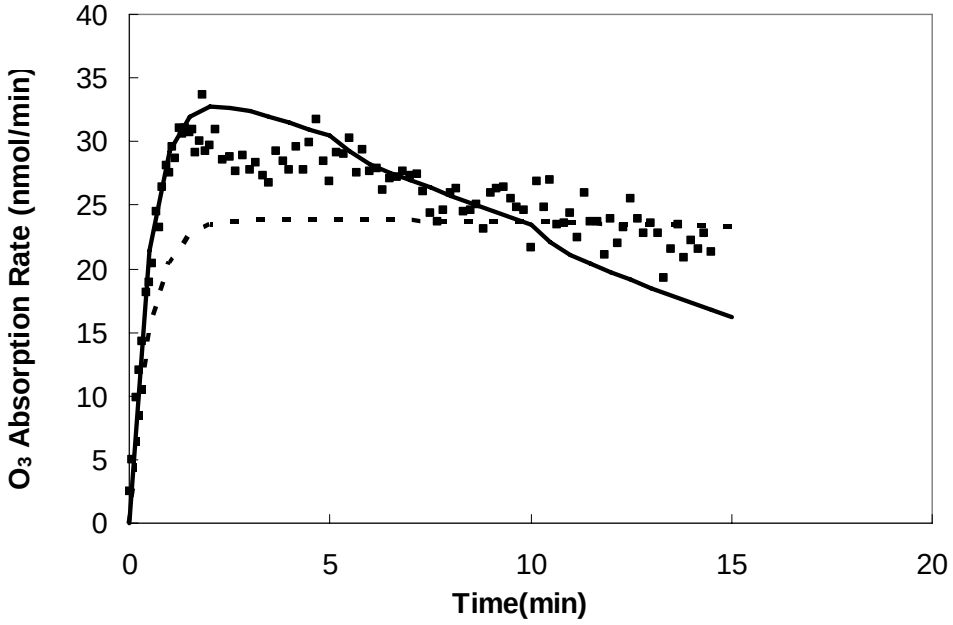

Figure **F-2**: Experimental Data and Model Simulations of O_3 Absorption Rate

Representative data illustrate the model simulations (solid or dashed lines) and experimental data for a fixed flow of 500 ml/min, and a fixed O_3 concentration of 3.0 ppm. Experimental data of O_3 absorption rate (■) is shown. Dashed line represent the simulation results obtained from the model discussed in the appendix F where $k_r = 1.4 \times 10^6 \, M^{-1} \sec^{-1}$ (Giamalva et al., 1985) and KA=325 liter/min, whereas solid line shows the simulation results obtained where negligible mass transfer resistances in both gas and liquid phases were considered.

SANAZ KERMANI

EDUCATION

- Ph. D. in Chemical Engineering, The Pennsylvania State University May 2007
- B.S. in Chemical Engineering, Sharif University of Technology, Iran Sept. 1999

RESEARCH EXPERIENCE

Graduate Assistant, Department of Chemical Engineering

- Developed an exposure system to study the kinetic parameters of the reaction between ozone and antioxidants under conditions that are similar to those encountered when polluted air is inhaled into the respiratory system
- Developed various assays to quantify substrate concentration using HPLC, spectrophotometer, and Spectrofluorometer
- Developed a mathematical model and a FORTARN code to obtain the reaction stoichiometries and rate constants for the reaction between ozone and biological substrates
- Developed a robust numerical simulation tool to determine the kinetics of spontaneous capillary penetration in a cylindrical capillary from an infinite liquid reservoir

TEACHING EXPERIENCE

- Teaching Assistant: Chemical Engineering Laboratory Fall 2003, 2004, and 2007
- Teaching Assistant: Advanced Mass Transfer Processes Fall 2006
- Teaching Assistant: Principles of Chemical Engineering Spring 2005

PUBLICATIONS and PRESENTATIONS

Kermani, S., A. Ben-Jebria and J.S. Ultman. Kinetics of ozone reaction with uric acid, ascorbic acid, and glutathione at physiologically relevant conditions. *Archives of Biochemistry and Biophysics.* 451, 8-16, 2006.

Kermani, S., A. Ben-Jebria and J.S. Ultman. Interaction of Antioxidants in Multi-component Mixtures. *Archives of Biochemistry and Biophysics.* (to be submitted)

Kermani, S., A. Ben-Jebria and J.S. Ultman. Kinetics of ozone reaction with Tryptophan Residues in Albumin and Study the Effectiveness of Glutathione in Sparing Tryptophan from Oxidation by Ozone. *Archives of Biochemistry and Biophysics.* (to be submitted)

Kermani, S. and A. Borhan. Numerical Simulations of Spontaneous Capillary Penetration of liquids. *Journal of Colloid and Interface Science.* (to be submitted)

Kermani, S., A. Ben-Jebria and J.S. Ultman. Reaction of Ozone with Nasal Antioxidants. *Annual Fall Meeting of the Biomedical Engineering Society*, *Philadelphia PA*, October 13, 2004.

Kermani, S., A. Ben-Jebria and J.S. Ultman. Kinetics of Ozone and antioxidants present in nasal lining fluid. *7th Annual Environmental Chemistry Student Symposium, University Park PA*, March 20, 2004. (Second Place, Poster Session I: Chemistry and Materials Sciences)